

University of Alberta

Hydraulics of the vertical slot fishway, a case study on the Vianney-
Legendre fishway in Quebec, Canada

by

Bryan Adam Marriner

A thesis submitted to the Faculty of Graduate Studies and Research
in partial fulfillment of the requirements for the degree of

Master of Science
in
Water Resources Engineering

Civil and Environmental Engineering

©Bryan Adam Marriner
Fall 2013
Edmonton, Alberta

Permission is hereby granted to the University of Alberta Libraries to reproduce single copies of this thesis and to lend or sell such copies for private, scholarly or scientific research purposes only. Where the thesis is converted to, or otherwise made available in digital form, the University of Alberta will advise potential users of the thesis of these terms.

The author reserves all other publication and other rights in association with the copyright in the thesis and, except as herein before provided, neither the thesis nor any substantial portion thereof may be printed or otherwise reproduced in any material form whatsoever without the author's prior written permission.

To my mom and dad, thank you for all the support.

Abstract

To follow is a case study on the hydraulics of the Vianney-Legendre vertical slot fishway on the Richelieu River in southwestern Quebec, Canada. This fishway is made up of three segments of linearly connected regular pools connected via two turning pools. It is known to pass multiple species of fish and is one of few worldwide to have documentation of successful passage of a species of sturgeon (lake sturgeons *Acipenser fulvescens*). The overall hydraulics of the fishway are characterized through field study and numerical modelling. A lack of hydraulic understanding coupled with recent links to high rates of fish passage failures are cause for study of turning pools. Consequently, numerical modeling is used to assess the hydraulic characteristics of seven turning pool design alternatives. It is hoped the results emanating from this study will act as reference to future fishway designs aimed at passing multiple species of fish.

Acknowledgements

To begin I would like to express the utmost gratitude to my supervisor Dr. David Z. Zhu. This has been an incredible period of growth for me, and it has been his excellent support and guidance throughout that has enabled me to succeed.

Secondly, I would like to thank my co-supervisor Dr. Steven J. Cooke for introducing me to fishways and for providing guidance, biological and otherwise, throughout the period of study. Experiencing firsthand the incredible work ethic of these two men has shown me what is required to excel in one's profession, and has inspired me to continuously improve my work ethic as I move forward in my career.

I would also like to extend my sincerest thank you to Abul Basar Baki and Jason D. Thiem for their collaborative contributions in the form of expert assistance in CFD modeling and ichthyology, respectively. My gratitude is also extended to the field work crew of Chris Krath and Travis Raison.

My appreciation goes out to Pierre Dumont and staff of Ministère des Ressources naturelles et de la Faune du Québec, and Parks Canada staff at the Saint Ours for the site access and logistical coordination of field work. Funding making this project possible was provided by the NSERC HydroNET research network.

Table of Contents

CHAPTER 1 Introduction	1
1.1 Fishways Background	1
1.2 Motivation for Research	3
1.3 Study Site Significance	4
1.4 Research Outline and Objectives	6
1.5 References	7
CHAPTER 2 Vianney-Legendre vertical slot fishway; study site and fishway description	10
2.1 Site Description	10
2.2 Fishway Design	11
2.3 References	13
CHAPTER 3 A case study on the overall hydraulics of the Vianney-Legendre vertical slot fishway in Quebec, Canada	19
3.1 Introduction	19
3.2 Study Outline	20
3.2.1 Field Methods and Instrumentation	20
3.2.2 CFD Model Study	27
3.3 Results and Discussion	29
3.3.1 Water Levels	29
3.3.2 Velocity and Flow Patterns	32
3.3.3 Kinetic Energy	37
3.3.4 Fishway Flow Rate	37
3.3.5 River Flow Rate	38
3.3.6 Tailrace Depths	39

3.4 Conclusions	41
3.5 References	43
CHAPTER 4 Field and numerical assessment of turning pool hydraulics in a vertical slot fishway	73
4.1 Introduction	73
4.2 Methods	76
4.2.1 Field Study	76
4.2.2 CFD Modeling	78
4.2.2.1 Governing Equations	78
4.2.2.2 Boundary Conditions and Computational Mesh	80
4.2.3 Design Modifications and Evaluation Criteria	82
4.3 Results	85
4.3.1 Field Results and CFD Model Validation	85
4.3.2 CFD Model Results	87
4.4 Discussion and Concluding Remarks	93
4.5 References	97
CHAPTER 5 Conclusions and Recommendations	115
5.1 Overall Conclusions	115
5.2 Recommendations for Future Study	117

List of Tables

Table 2-1 Fishway pool floor elevations.....	14
Table 3-1 Summary of regular pool geometry scenarios simulated using computational fluid dynamics modeling	47
Table 3-2 Velocity and flow rate field results at the Vianney-Legendre fishway recorded in July 2011	47
Table 3-3 Minimum normalized jet velocity u_{jm}/V_{sm} at distance $x_j/0.5b_0$ from the pool's slot entrance for Scenarios 1- 5	48
Table 3-4 Richelieu River flow rate measurements taken 250 – 300 m downstream of the Saint Ours Dam	48
Table 4-1 Summary of mesh properties as tested to assess the effect of mesh size on numerical modelling results	102
Table 4-2 Summary of turning pool vortex lengths and widths for Pools 8 and 13, and Designs 1, 3 4, 6, and 7	102

List of Figures

- Figure 2.1** The Vianney-Legendre vertical slot fishway (foreground), adjacent to the Saint Ours Dam spanning the Richelieu River (background) in southwestern Quebec; figure faces east 15
- Figure 2.2** The Vianney-Legendre vertical slot fishway (a) Fishway and the adjacent west bank of the river with a downstream (north) orientation and (b) Plan view diagram 16
- Figure 2.3** The Vianney-Legendre fishway entrance and exit (a) flow entering through the upstream entrance gate (b) flow exiting through the downstream exit gate 17
- Figure 2.4** Plan view schematic diagrams of (a) a regular pool (b) turning Pool 13 and (c) a baffle wall; in the Vianney-Legendre fishway 18
- Figure 3.1** A water level recording data logger housed in a steel cylinder suspended with airplane cable, prior to submergence for data gathering 49
- Figure 3.2** (a) A field constructed measurement frame mounted on Pool 15 of the Vianney-Legendre fishway recording velocities. (b) An acoustic Doppler velocimeter field probe submerged in Pool 15 recording velocity measurements 50
- Figure 3.3** Correlation of velocity measurements recorded in the Vianney-Legendre fishway with an Acoustic Doppler Velocimeter field probe ... 51
- Figure 3.4** Recording velocity measurements using an Acoustic Doppler Profiler 0.61 m downstream of the entrance to pool 5 52

Figure 3.5 Richelieu River water levels, upstream and downstream of the Vianney-Legendre fishway March 25 – August 7, 2011	53
Figure 3.6 Vianney-Legendre fishway water surface profiles measured on 07/22/2011 and predicted	54
Figure 3.7 Vianney-Legendre fishway water surface profiles measured on 06/06/2012 and predicted	55
Figure 3.8 Water levels upstream, downstream of the St. Ours Dam and in pools of the Vianney-Legendre fishway (a) July 18 – 29, 2011. (b) June 4 – July 30, 2012	56
Figure 3.9 Time-averaged field velocities 0.50 m below the water surface in Pool 5	57
Figure 3.10 Time-averaged field velocities 0.50 m below the water surface in Pool 15	58
Figure 3.11 Velocity profile at 0.61 m downstream of the slot in Pool 5 measured on June 6, 2012 and simulated in a CFD model	59
Figure 3.12 Velocity profile at 0.61 m downstream of the slot measured on June 6, 2012: (a) Pool 4; (b) Pool 8; (c) Pool 13; (d) Pool 14; (e) Pool 15; (f) Pool 16	60
Figure 3.13 Velocity distributions in regular pools at depths of $0.5h$: (a) Scenario 1, $L = 3.5\text{m} \times W = 3.0\text{m}$; (b) Scenario 2, $L = 4.87\text{m} \times W = 3.0\text{m}$; (c) Scenario 3, $L = 6.09\text{m} \times W = 3.0\text{m}$; (d) Senario 4, $L = 4.87\text{m} \times W = 4.87\text{m}$; (e) Scenario 5 $L = 6.09\text{m} \times W = 4.87\text{m}$	62

Figure 3.14 Normalized distribution of longitudinal mean velocity in Scenario 1 jet flow	64
Figure 3.15 Variation of normalized maximum velocity u_{im}/V_{sm} with $x_j/0.5b$ (Liu et al., 2006)	65
Figure 3.16 Time-averaged field velocities at a depth of 0.50 m below the water surface in Pool 13 of the Vianney-Legendre fishway	66
Figure 3.17 Time-averaged field velocities at a depth of 0.50 m below the water surface in Pool 8 of the Vianney-Legendre fishway	67
Figure 3.18 $K^{0.5}/V_{sm}$ in Pool 5 of the Vianney-Legendre fishway	68
Figure 3.19 $K^{0.5}/V_{sm}$ in Pool 15 of the Vianney-Legendre fishway	69
Figure 3.20 Acoustic Doppler Current Profiler Richelieu River flow rate measurement outputs 250 – 300 m downstream of the Saint Ours Dam: (a) Transect 1, (b) Transect 2, (c) Transect 3, (d) Transect 4	70
Figure 3.21 Tailrace of the Saint Ours Dam on the Richelieu River; (a) Contour map of water depths on June 7, 2012 (b) depth measurement point coordinates shown on satellite imagery	72
Figure 4.1 Plan view schematic diagram of a turning pool, Pool 13, in the Vianney-Legendre vertical slot fishway; this geometry is simulated using CFD modelling in Design 1	104
Figure 4.2 Results of the mesh independency test completed to determine the sensitivity of grid size on numerical results of Design 1	105

Figure 4.3 Plan view schematic diagrams of vertical slot turning pool designs: (a) Design 2, (b) Design 3, (c) Design 4, (d) Design 5, (e) Design 6, (f) Design 7	106
Figure 4.4 Velocity data points comparison between field measurements taken in Pool 13 of the Vianney-Legendre vertical slot fishway and results simulated in Design 1 for scenario 1 with CFD modelling	107
Figure 4.5 Velocity magnitudes and directions in turning pool Design 1: (a) at depth $z = 0.13h$, (b) at depth $z = 0.5h$, (c) at depth $z = 0.8h$	108
Figure 4.6 Velocity magnitudes and directions at depth $z = 0.5h$ in turning pool designs: (a) Design 3, (b) Design 4, (c) Design 6, (d) Design 7	109
Figure 4.7 Variation of maximum velocity, V_m , through the turning pool; where x_m is the path of V_m from the slot entrance to the slot exit: (a) Design 1 at depths of $z = 0.13h$, $z = 0.5h$, and $z = 0.8h$; (b) Designs 3, 4, 6, and 7 at depth of $z = 0.5h$	110
Figure 4.8 Maximum velocity, V_m , decay comparison of a single slot pool, a plane jet, and turning pool Designs 1, 3, 4, 6, and 7 at a depth of $z = 0.5h$	111
Figure 4.9 Radial velocity distributions of Designs 1, 3, 4, 6, and 7 at $z = 0.5h$: (a) $\theta = -27^\circ$, (b) $\theta = 67.5^\circ$, (c) $\theta = 112.5^\circ$	112
Figure 4.10 Turbulent kinetic energy levels at depth $z = 0.5h$ in turning pool designs: (a) Design 1, (b) Design 3, (c) Design 4, (d) Design 6, (e) Design 7	113

Figure 4.11 Vorticity levels at depth $z = 0.5h$ in turning pool designs: (a) Design 1, (b) Design 3, (c) Design 4, (d) Design 6, (e) Design 7 114

List of Symbols

Symbol	Definition
B	regular pool width
b_0	vertical slot width
b_t	turning pool width
C_d	discharge coefficient
b_v	vortex width
C_μ	$k - \varepsilon$ model constant
D_v	vortex diameter
G	acceleration due to gravity
H	depth of flow
I	turbulence intensity
K	kinetic energy
L	regular pool length
L_f	fish body length
l_t	turning pool length
l_v	vortex length
P	static pressure
Q	fishway average volumetric flow rate
r_t	radius of the turning pool's semi-circular back wall
R	radial distance
S_f	overall fishway slope
TKE	turbulent kinetic energy

TKE_{max}	maximum turbulent kinetic energy
u, v, w	longitudinal, transverse, and vertical velocities
$\bar{u}, \bar{v}, \text{ and } \bar{w}$	time-averaged components of u, v, w
u_j	time-averaged jet velocity
u_{jm}	maximum jet velocity at x_j
V	time-averaged velocity magnitude
V_m	maximum velocity
V_0	maximum simulated jet velocity in the slot
V_{sm}	maximum measured jet velocity in the slot
V_{theor}	maximum theoretical slot velocity
\bar{w}_{max}	maximum absolute vertical velocity measured in a pool
\bar{w}_{mean}	mean vertical velocity measured in a pool
x_j	distance along the curved jet centre line from the entrance slot
x_m	distance from the entrance slot along the flow path of V_m
x_r	radial distance from V_m at an angle of θ
x, y, z	longitudinal, transverse, and vertical Cartesian coordinates
y_j	distance from jet centre in the transverse direction orthogonal to x_j
h	difference in water level between adjacent pools
ε	turbulent kinetic energy dissipation
$\bar{\varepsilon}$	average volumetric energy dissipation
θ	angle measured from the centre of turning pool to the outer wall
ω_z	vorticity in the horizontal direction

List of Abbreviations

Acronym	Definition
ADP	acoustic Doppler profiler
ADV	acoustic Doppler velocimeter
CFD	computational fluid dynamics
CSF	continuum surface force
GPS	global positioning system
MAE	mean absolute error
m.a.s.l	metres above sea level
RTK	real time kinetic
SNR	signal to noise ratio

CHAPTER 1

Introduction

1.1 Fishways Background

Fishways are built on rivers all over the world. They restore connectivity to rivers that have been disconnected by hydraulics barriers. These barriers can be of natural or man-made origins and common examples include hydro-electricity producing facilities, water level controlling dams, and natural falls (Clay, 1961). Fishways are primarily designed to provide upstream swimming fish passage over hydraulic barriers. Fish enter the fishway through the downstream entrance below the hydraulic barrier, swim through a series of pools, and exit the fishway upstream of the hydraulic barrier.

There are a number of fishway designs used across North America. Designs are placed under two general categorizes; engineered structures and nature-like fishways. Engineered structures are built with hard construction materials (e.g., steel, reinforced concrete, and wood) and include the pool and weir, Denil, and vertical slot designs. Nature-like fishways are constructed using natural, also called soft, materials (e.g., boulders, gravel, and logs) and are designed to mimic the hydraulic, bed, and bank conditions of a natural stream (Katopodis et al., 2001).

The vertical slot is a commonly used design across North America. Canada alone has 37 documented vertical slot fishways, making it the second most common design in the country (Hatry et al., In press). They are made up of

regular pools connected to form linear segments (Rajaratnam et al., 1992B), are suitable for use in a large range of hydraulic and biologic environments, have several advantages over other designs, and are often the design of choice at relatively large fishway. In the vertical slot design fish pass from one to pool to the next by swimming through vertical slot openings in the baffle walls, whereas overflow design fishways (such as the pool and weir) require fish to jump out of the water to ascend pools. The vertical slot accommodates species who cannot or will not jump to pass between pools. It has been shown that even species that are capable of jumping prefer to stay submerged while ascending fishways (Warren and Beckman, 1993). A design goal of the vertical slot is to have low velocity areas for fish to rest during upstream passage (Rajaratnam et al., 1992B).

Turning pools can be added to fishways that are required to pass over relatively tall structures (Rajaratnam et al., 1997). For cases where the water level difference between the upstream and downstream ends of the fishway is greater than the maximum recommended design slope, turning pools are used to connect segments of regular pools. The primary functions of turning pools are to turn the flow direction and to provide resting area for fish (Marriner, Submitted; Rajaratnam et al., 1997). One of the more common types of fishway designs to incorporate turning pools is the vertical slot fishway. Examples of vertical slot fishways that utilize turning pools include the Vianney-Legendre fishway in Quebec, the Seton River dam in British Columbia, and the Torrumbarry in Australia (Pon et al., 2009; Thiem et al., In press; White et al., 2011).

1.2 Motivation for Research

Much of the existing fishways research focuses on hydraulics within individual regular pools (Liu et al., 2006; Rajaratnam et al., 1992B) as measured in laboratory or *in silico* settings. There are few documented field studies providing general observations and field measured data is limited (Rajaratnam et al., 1992A). Accordingly, a need exists to study the whole fishway to gain an understanding of its overall hydraulics as a system and to complete this study in a field setting.

Several biological studies have identified potential problems with turning pools (e.g., Bunt et al., 2000; Thiem et al., 2011; White et al., 2011). Thiem et al. (2011) studied the movements of 88 adult lake sturgeons *Acipenser fulvescens* as they attempted upstream passage at the Vianney-Legendre vertical slot fishway in Quebec. Of 56 individuals that failed passage, 20 failed in the two turning pools (out of a total of 18 pools); and fish spent disproportionately longer time in the turning pools than in the regular pools. Additionally, bony herring *Nematalosa erebi*, silver perch *Bidyanus bidyanus*, and golden perch *Macquaria ambigua* also appeared to have difficulty negotiating turning pools in a fishway in Australia (White et al., 2011). There are a number of potential explanations including confusion associated with complex flows, flow characteristics that exceed the swimming abilities of fish, or fish could actually be using such areas to rest. Although the delays may be associated with use of the turning pools to rest, the fact that a number of studies have found failures associated with turning pools is suggestive that there may be hydraulic challenges that impede passage.

There have been few attempts to characterize the hydraulic conditions within turning pools and relate flow characteristics to fish behaviour (Rajaratnam et al., 1997). Additionally, without any apparent investigation of the effects on hydraulics or fish passage, numerous styles of turning pools have been used in vertical slot fishways to achieve desired connection between the upstream and downstream ends of the fishway. These pools have an array of features including turning angles up to 180°, variable dimensions, baffles, square back and semi-circular back walls, etc. For example the Seton River dam fishway in British Columbia, the Torrumbarry fishway in Australia, the Dunnville dam fishway in Ontario, the Bonneville dam fishway on in Washington, and the Vianney-Legendre fishway in Quebec all have turning pools of various designs (Bunt et al., 2000; Rajaratnam et al., 1997; White et al., 2011).

Given the lack of existing hydraulic understanding, the variety of designs in use and the comparatively low passage success rates there is cause for further study to evaluate and improve turning pool hydraulics, relative to fish passage.

1.3 Study Site Significance

As the use of fishways changes from passing a target species to encompassing passage for whole fish communities, interest in fishway designs that are able to pass multiple species increases (Thiem et al., In press). In the spring of 2010 Thiem et al. (In press) documented the successful upstream passage of 18 species of fish and Desrochers (2009) indicated that annually over 35 species pass the Vianney-Legendre fishway, hereinafter called the site fishway. Included in this

list of species are lake sturgeons (*Acipenser fulvescens*) and copper redhorse (*Moxostoma hubbsi*). The Committee on the Status of Endangered Wildlife in Canada (COSEWIC) listed copper redhorses as 'endangered'. Copper redhorses are endemic to Quebec and are known to live in just three river systems. COSEWIC has categorized lake sturgeons based on populations throughout Canada. They have listed them as 'threatened', 'endangered' or of 'special concern' depending on the population (COSEWIC, 1, 2). This is one of few fishways worldwide to have documentation of successful passage of a species of sturgeon (Thiem et al., 2011).

The site fishway is one of few multi-species passing fishways to have quantitative passage documentation of number of species. It passes members of a number of fish families including the salmon (*Salmonidae*), sturgeon (*Acipenseridae*), perch (*Percidae*), sucker (*Catostomidae*), needlefish (*Belonidae*) and catfish (*Ictaluridae*) families. The number of species passing the site fishway demonstrates its ability to serve a diversity of species (Thiem et al., In press).

In addition to the diversity of fish passing, the site fishway differs from many vertical slot fishways in terms of design. Vertical slot fishways are most commonly constructed as a linear series of regular pools. The site fishway incorporates two 180°, which connect three linear segments of regular pools. The turning pools are twice the width of the regular pools and equal in length. They have semi-circular back walls to guide high velocity flow through the pools. The layout of the site fishway makes it more compact in comparison to many other vertical slot designs. The compact design economizes on space and facilitates a

more optimum location for the fish entrance, by placing it closer to the hydraulic barrier than would be obtainable with other designs. It is recommended that the downstream entrance be placed as close as possible to the hydraulic barrier as it makes it easier for fish to find (Bunt, 2001; Clay, 1961; Katopodis and Williams, 2012).

1.4 Research Outline and Objectives

The goal of this paper is to understand the hydraulics of the site fishway. A detailed account of the study site and fishway are provided in Chapter 2. Chapter 3 completes an overall assessment of the site fishway's hydraulics. Here the water level, flow, overall site and fishway design characteristics are analyzed through field measurements and numerical modeling. In Chapter 4 seven turning pool design geometry alternatives are assessed with respect to velocity, turbulent kinetic energy, vorticity, and flow structure in a numerical model study. It is hoped that this study along with concurrent ichthyology studies evaluating fish passage and behaviour at the site fishway will be tools to assist engineers and biologists to evaluate the site fishway's performance in terms of hydraulics and fish passage (Thiem et al., 2011; Thiem et al., In press). Additionally, this paper may serve reference, of a successful case study on a fishway passing multiple species, to future designers focusing on multi-species fish passage. The velocity and turbulence results presented on turning pools can provide a hydraulic understanding of turning pool hydraulics and hopefully will act as a foundation from which turning pool hydraulics and design can be developed.

1.5 References

- Bunt, C.M., 2001. Fishway entrance modifications enhance fish attraction. *Fish. Manag. and Ecol.* 8, 95-105.
- Bunt, C.M., Cooke, S.J., McKinley, R.S., 2000. Assessment of the Dunnville fishway for passage of walleyes from Lake Erie to the Grand River, Ontario. *J. Great Lakes Res.* 26, 482-488
- Clay, C.H., 1961. Design of fishways and other fish facilities. Dept. of Fisheries of Canada, Ottawa, 301 pp.
- COSEWIC (Committee on the Status of Endangered Wildlife in Canada). Wildlife Species search. Government of Canada. Updated: 2012/08/03, accessed: 2012/12/05.
- (1)http://www.cosewic.gc.ca/eng/sct1/SearchResult_e.cfm?commonName=lake+sturgeon&scienceName=&Submit=Submit.
- (2)http://www.cosewic.gc.ca/eng/sct1/SearchResult_e.cfm?commonName=copper+redhorse&scienceName=&Submit=Submit.
- Hatry, C., Binder, T.R., Thiem, J.D., Hasler, C.T., Smokorowski, K.E., Clarke, K.D., Katopodis, C., Cooke, S.J., In press. The status of fishways in Canada: trends identified using the national CanFishPass database. *Rev. Fish Biol. Fish.*
- Katopodis, C., Kells, J.A., Acharya, M., 2001. Nature-like and conventional fishways; alternative concepts?. *Can. Water Resour. J.* 26, 211-232.
- Katopodis, C., Williams, J.G., 2012. The development of fish passage research in a historical context. *Ecol. Eng.* 48, 8-18.

- Liu, M., Rajaratnam, N., Zhu, D.Z., 2006. Mean flow and turbulence structure in vertical slot fishways. *J. Hydraul. Eng.* 132(8), 765-777.
- Marriner, B.A., Baki, A.B., Zhu, D.Z., Thiem, J.D., Cooke, S.J., Katopodis, C. Submitted for publication. Field and numerical assessment of turning pool hydraulics in a vertical slot fishway. *Ecol. Eng.*
- Pon, L.B., Hinch, S.G., Cooke, S.J., Patterson, D.A., Farrell, A.P., 2009. Physiological, energetic and behavioural correlates of successful fishway passage of adult sockeye salmon *Oncorhynchus nerka* in the Seton River, British Columbia. *J. Fish Biol.* 74, 1323-1336.
- Rajaratnam, N., Katopodis, C., Paccagnan, R. 1992A. Field studies of fishways in Alberta. *Can. J. Civ. Eng.* 19, 627-638.
- Rajaratnam, N., Katopodis, C., Solanki, S., 1992B. New designs for vertical slot fishways. *Can. J. Civ. Eng.* 19, 402-414.
- Rajaratnam, N., Katopodis, C., Wu, S., Saburm, M.A., 1997. Hydraulics of resting pools for denil fishways. *ASCE J. Hydraul. Eng.* 123 (7), 632-638.
- Thiem, J., Binder, T., Dawson, J., Dumont, P., Hatin, D., Katopodis, C., Zhu, D.Z., Cooke, S., 2011. Behaviour and passage success of upriver-migrating lake sturgeon *Acipenser fulvenscens* in a vertical slot fishway on the Richelieu River, Quebec, Canada. *Endanger. Species Res.* 15, 1-11.
- Thiem, J.D., Binder, T.R., Dumont, P., Hatin, D., Hatry, C., Katopodis, C., Stamplecoskie, K.M., Cooke, S.J. In press. Multispecies fish passage behaviour in a vertical slot fishway on the Richelieu River, Quebec Canada. *River Res. Appl.*

White, L.J., Harris, J.H., Keller, R.J., 2011. Movement of three non-salmonid fish species through a low-gradient vertical-slot fishway. *River Res. Appl.* 27, 499-510.

CHAPTER 2

Vianney-Legendre vertical slot fishway; study site and fishway

description

2.1 Site Description

The Richelieu River flows north from its headwaters of Lake Champlain, situated along the state border of New York and Vermont in USA, to Sorel-Tracey in southwestern Quebec, Canada where it empties into the St. Lawrence River. The site fishway is on the Richelieu River 18 km upstream of the confluence with the St. Lawrence River and is situated just outside of Saint-Ours, Quebec. The fishway sits on the west bank of the river adjacent to the Saint Ours dam. The dam is 180 m wide, 3.4 m high, and separated into 5 equally sized submersible gates. The dam starts on the west bank, spans across the river connecting to the upstream end of a large island (Ile Darvard) on the east side of the river. On the east side of Ile Darvard is a separate canal channel to allow boat passage across the dam. Ile Darvard is 430 m long and 95 m wide. Upstream of the dam the river is 315 m wide, downstream of Ile Darvard the river is 270 m wide. The Richelieu River's average annual discharge is 362 m³/s (Thiem et al, 2011). The study site is shown in Figure 2.1.

Constructed in 2001-2002, the site fishway is a staircase style vertical slot design. It is constructed of reinforced concrete, with baffles made of steel. The current dam, built in 1967, did not include fish passage facilities. The site

fishway's construction represented a renewal of fish passage facilities as they were present prior to 1967 (Parks Canada, 2011).

2.2 Fishway Design

The site fishway, see Figure 2.2, has 18 pools total; 12 regular pools, 2 turning pools, entrance and exit pools, and two pools with slot openings in the centre of the pool. It is formed of three segments of linearly connected regular pools attached via two 180° turning pools, with entrance and exit pools at the upstream and downstream ends of the fishway, respectively.

Water enters the upstream end of the fishway into Pool 1 through the entrance pool, flows through Pools 1 – 7, turns 180° in Pool 8, flows through Pools 9 – 12, turns 180° in Pool 13, flows through Pools 14 – 16 and then enters the river downstream of the dam through the exit pool. The fishway length is 48.5 m and width is 9.60 m. The elevation change in the fishway is 2.55 m, resulting in an overall fishway slope of 2.8%. The pool floor depth at the upstream entrance is 4.85 m.a.s.l (m.a.s.l = metres above sea level), and the pool floor depth is 2.3 m.a.s.l at the downstream exit. Table 2-1 summarizes floor elevations at the upstream and downstream ends of the fishway's pools. The top of fishway walls were level at 6.85 m.a.s.l or 7.2 m.a.s.l, corresponding to 2.4 m – 4.55 m above the pool floor.

Flow enters the fishway through a 0.85 m wide gate, see Figure 2.3a. The upstream entrance and Pool 1 are a combined 15.65 m long, 3.0 m wide. The

downstream exit pool is 12.50 m long, with flow exiting the fishway through a 3.50 m wide gate, see Figure 2.3b.

Regular pools (Pools 3, 4, 5, 6, 7, 9, 10, 11, 12, 14, 15, 16) are 3.50 m ($5.83b_0$) long, 1, and 3.00 m ($5.0b_0$) wide, b , see Figure 2.4a. The slot width, b_0 , is 0.609 m in pools 2 - 16. The regular pools ratios of length and width to slot width are less than $l = 10b_0$ and $b = 8b_0$, recognized across North America and Europe as the recommended design dimensions for regular pools (Bell, 1973; Larinier et al, 1999; Rajaratnam et al., 1992). Regular pool floors are sloped 0.075 m lengthwise.

Turning pools (Pools 8 and 13) are 6.30 m wide, b_t . The back wall is semi-circular with a radius, r_t , of 3.15 m. Pool 13 has a maximum length, l_t , of 3.50 m from centre wall to back wall, see Figure 2.4b, while Pool 8 is shorter with $l_t = 3.35$ m. The pool floor is stepped, with a 0.075 m elevation change at the pool's centre. There is an elevation change of 0.075 m across the slot area between adjacent pools from Pool 3 – 16, resulting in a 3.95% slope.

The long baffle is 2.12 m long, attached its end is a 1.0 m x 0.5 m guide extending upstream into the pool. The short baffle is 0.46 m long. Both baffles are 0.30 m thick. The slot angle is 57° , see Figure 2.4c. The baffle design used throughout the fishway is similar in shape to the baffle used in Design 1, as described by Rajaratnam et al. (1992), and follows the recommended design.

2.3 References

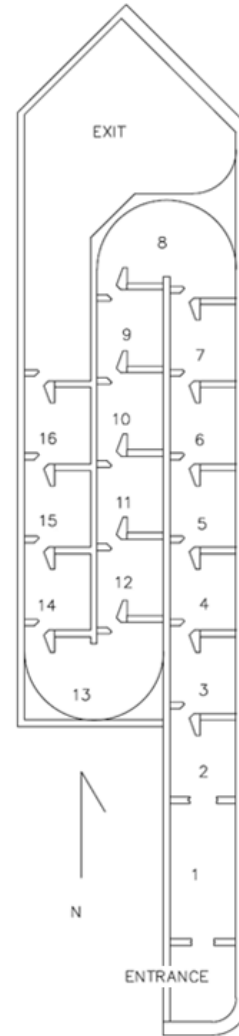
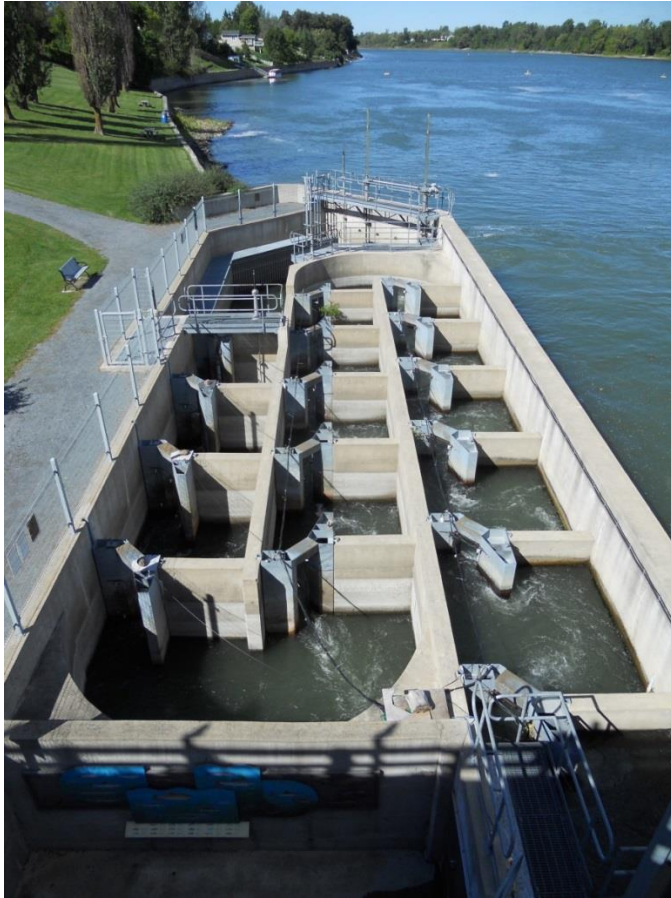
- Bell, M.C. 1973. Fisheries handbook of engineering requirements and biological criteria. U.S. Army Corps of Engineers, North Pacific Division, Portland, Ore.
- Larinier, M., Gosset, C., Porcher, J.P., Travade. 1999. Passes à poissons : Expertises et conception des ouvrages de franchissement. Paris, France: La Documentation Française.
- Parks Canada. Vianney-Legendre Fishway at the Saint-Ours Canal National Historic Site of Canada. Updated: 18/08/2010, accessed: 05/2011.
<http://www.pc.gc.ca/lhn-nhs/qc/saintours/ne.aspx>.
- Rajaratnam, N., Katopodis, C., Solanki, S. 1992. New designs for vertical slot fishways. *Can. J. Civ. Eng.* 19, 402-414.
- Thiem, J., Binder, T., Dawson, J., Dumont, P., Hatin, D., Katopodis, C., Zhu, D.Z., Cooke, S. 2011. Behaviour and passage success of upriver-migrating lake sturgeon *Acipenser fulvenscens* in a vertical slot fishway on the Richelieu River, Quebec, Canada. *Endanger. Species Res.* 15, 1-11.

Table 2-1 Fishway pool floor elevations

Pool No.	Pool floor elevation – Upstream end (m.a.s.l)	Pool floor elevation – Downstream end (m.a.s.l)
Entrance	4.85	-
1	4.85	4.795
2	4.7	4.625
3	4.55	4.475
4	4.4	4.325
5	4.25	4.175
6	4.1	4.025
7	3.95	3.875
8	3.8	3.8
9	3.65	3.725
10	3.5	3.575
11	3.35	3.425
12	3.2	3.275
13	3.05	3.125
14	2.9	2.975
15	2.75	2.825
16	2.6	2.675
Exit	2.45	2.525



Figure 2.1 The Vianney-Legendre vertical slot fishway (foreground), adjacent to the Saint Ours Dam spanning the Richelieu River (background) in southwestern Quebec; figure faces east.



(a)
Figure 2.2 The Vianney-Legendre vertical slot fishway (a) Fishway and the adjacent west bank of the river with a downstream (north) orientation and (b) Plan view diagram.



(a)



(b)

Figure 2.3 The Vianney-Legendre fishway entrance and exit (a) flow entering through the upstream entrance gate (b) flow exiting through the downstream exit gate.

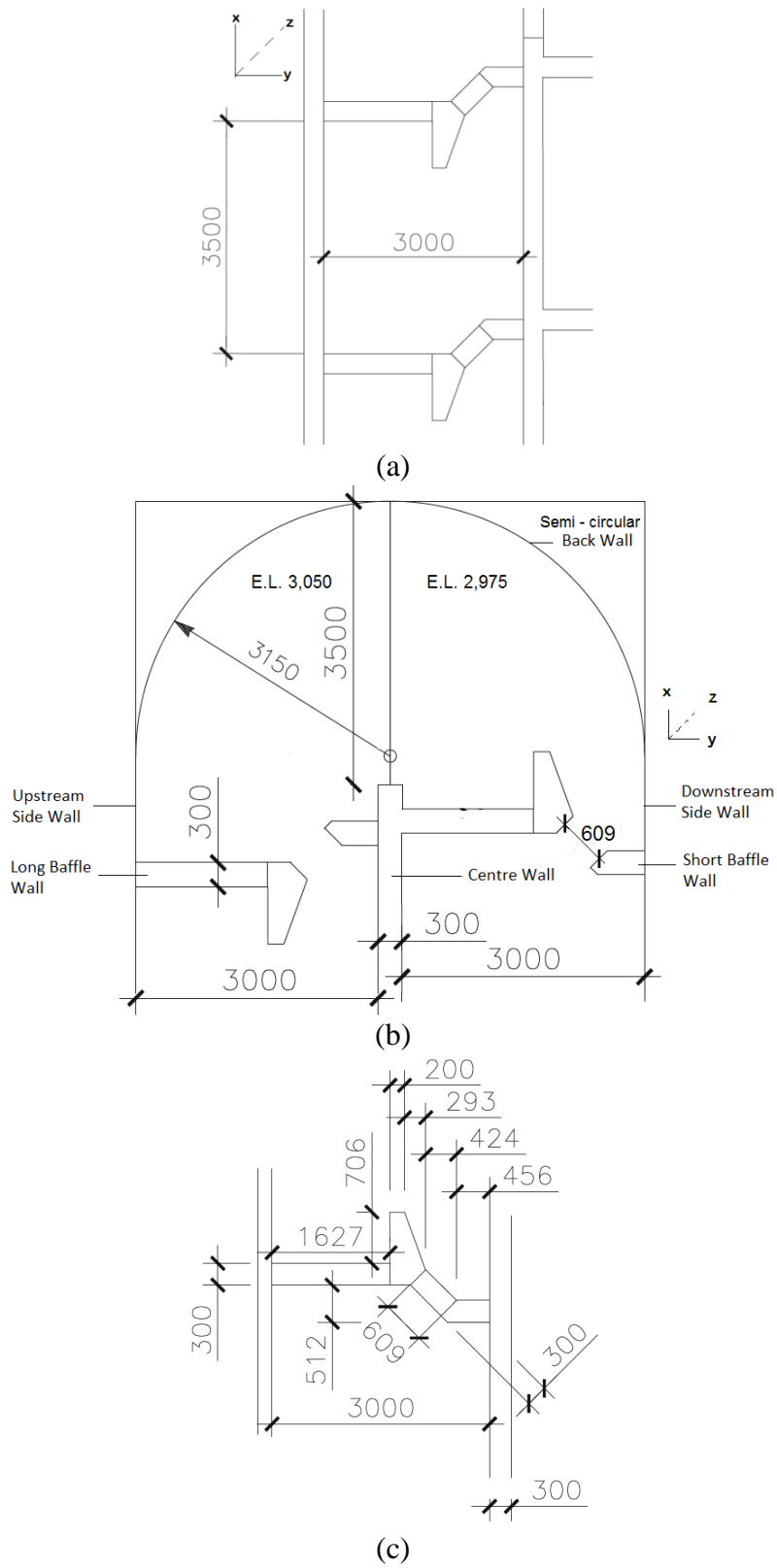


Figure 2.4 Plan view schematic diagrams of (a) a regular pool (b) turning Pool 13 and (c) a baffle wall; in the Vianney-Legendre fishway.

CHAPTER 3

A case study on the overall hydraulics of the Vianney-Legendre vertical slot fishway in Quebec, Canada

3.1 Introduction

This study aims to understand the hydraulics of the Vianney-Legendre vertical slot fishway, hereinafter called the site fishway, on the Richelieu River in Quebec. Laboratory and numerical studies have developed a good understanding of the hydraulics of regular pools. Recommended design dimensions of pool length, $l = 10b_0$, and width, $b = 8b_0$, where b_0 represents the slot width, have been adopted in North America and Europe (Bell, 1973; Larinier et al., 1999; Rajaratnam et al., 1992B). Guidelines also exist for baffle and baffle wall geometries (Rajaratnam et al., 1992B). Recently, studies have focused on flow patterns, velocity distribution, energy dissipation rates, and turbulent kinetic energy levels within fishway pools (Wu, et al., 1999; Puertas, et al., 2004; Liu, et al., 2006).

Much of the existing fishways research focuses on hydraulics within individual regular and turning pools (Liu et al., 2006; Marriner et al., Submitted; Rajaratnam et al., 1992B) as measured in laboratory or *in silico* settings. There are few documented field studies providing general observations and limited field

The content of this chapter has been submitted for publication in Journal of Hydraulic Engineering as: Marriner et al. (Submitted). "A case study on the overall hydraulics of the Vianney-Legendre vertical slot fishway in Quebec, Canada".

measured data (Rajaratnam et al., 1992A). Accordingly, a need exists to study the whole fishway to gain an understanding of its hydraulics as a system. The current study does this by assessing the site fishway's overall hydraulics and design.

Here we use water level, velocity and flow measurements taken in the field to understand the fishway's flow type, allowing the water surface profile to be predicted. The flow characteristics in both regular and turning pools are investigated in the field. A CFD model is used to compare the jet velocity decay in the site fishway's regular pools to other designs. Vertical velocity profiles are measured in the field providing an understanding of velocities through the height of the water column. The dam and fishway tailrace is contour mapped for water depth, and the river's flow rate is measured to display the conditions fish searching for the fishway's entrance will encounter.

An understanding of the overall hydraulics and design of the site fishway may allow engineers and biologists to make recommendations to improve the site fishway's design in the future. Additionally, this case study may serve as a reference for future designers of a fishway that successfully passes multiple species of fish (Thiem et al., In press).

3.2 Study Outline

3.2.1 Field Methods and Instrumentation

Field data was collected in 2011 and 2012. In 2011, fieldwork was conducted from July 18 – 29. Detailed point velocity measurements were taken in 4 pools and water levels were collected in 5 pools. In 2012, field data was gathered from

June 4 – 8. Depth measurements were recorded immediately downstream of the dam in the tailrace area, the river's flow rate was measured, water levels were recorded in 9 pools, and velocity measurements were taken in all pools. Water levels immediately upstream and downstream of the dam were recorded in both 2011 and 2012.

The Mini-Diver model pressure and temperature measuring dataloggers manufactured by Schlumberger Water Services were used to record water level measurements in the fishway pools. The divers are accurate to ± 0.005 mH₂O, with a resolution of 0.002 mH₂O (Schlumberger Water Services, 2010). For the purpose of this study water level data is presented to 0.01 m, with an accuracy of ± 0.01 m. Divers were housed in perforated steel cylinders hung from 1" diameter airplane cable, see Figure 3.1. The cable was fastened to the top of the pool wall with a C-clamp. The steel cylinders protected the divers from potential damage caused by hitting the concrete walls while submerged. Perforations in the steel cylinders allowed for accurate diver readings. When deployed in single slot pools divers were placed in the upstream corner at the intersection of the longitudinal and long baffle walls. In turning pools divers were placed on the downstream side of the centre wall, at the intersection with the long baffle wall. In Pool 1 the diver was mounted along the west wall on a metal walkway crossing the pool 2.65 m downstream of the entrance opening. It was important to place divers in low velocity, and turbulence areas. This allowed the divers to suspend with little movement. High velocity and turbulence areas would cause the divers to swing and hit the pool walls. Swinging of the diver changes disrupts depth

measurements because it changes the diver position and depth. Hitting the pool walls can damage the steel cylinder, airplane cable or the diver itself.

In 2011 divers were deployed from July 18 – 29 in pools 5, 8, 11, 13, and 15; measurements were taken at a frequency of 1 minute. In 2012 divers were deployed from June 5 – July 30 in Pools 1, 6, 7, 8, 9, 12, 13, 14 and 15; measurements were taken at a frequency of 4 minutes. An additional diver, recording barometric temperature and pressure, was attached to the entrance gate above Pool 16 in 2011 and 2012. Parks Canada records water levels immediately upstream and downstream of the St. Ours Dam. Water levels upstream and downstream of the dam were provided by them.

The water depths in Pools 3 – 16 were using a staff gauge on July 22, 2011 from 5 – 5:30 pm EST. Measurements were taken in the centre of regular pools $x = 1.50$ m on the upstream and downstream sides of the long baffle wall $y = 0$ m and $y = 3.50$ m. Turning pool measurements were taken at the upstream and downstream long baffle walls, in the centre of adjacent single pool widths $x = 1.50$ m and $x = 4.8$ m. Each measurement was recorded and averaged over one minute and is accurate to ± 0.01 m.

To assess the conditions facing fish trying to find the downstream entrance to the fishway, river depth measurements were recorded immediately downstream to 250 m downstream of the dam on June 7, 2012. Water depths were recorded with a sonar unit and position was simultaneously recorded using a Trimble R8 real time kinetic (RTK) global positioning system (GPS). Both units were mounted on the stern of a 15' flat bottom aluminum boat to take measurements.

Measurement transects were completed longitudinal and transverse to the river. Depth and position were simultaneously recorded at an interval of 5 seconds. A total of 738 points were recorded. Depth and position measurements are accurate to ± 0.1 m.

Instantaneous velocity point measurements were recorded with a three-dimensional (3D) Acoustic Doppler Velocimeter (ADV) (Nortek AS, 2011). Puertas et al. (2004) and Liu et al. (2006) used ADVs to measure 3D point velocities in recent fishway studies. The ADV uses the Doppler effect to measure velocity. The ADV field probe was mounted on a frame to record velocity measurements. The frame was constructed on-site with modular T-slotted aluminum framing. It was designed to be completely adjustable in order to mount on the various wall heights and pool sizes. In Figure 3.2 the frame is mounted on Pool 15 and the field probe submerged recording a velocity measurement.

Measurements were taken in both turning pools (Pools 8 and 13) and two regular pools (Pools 5 and 15). Pool 15 is the second most downstream standard pool. It is in the most downstream ladder which was affected by high tail water levels in the river during the 2011 fieldwork trip. Pool 5 is in the upstream ladder of the fishway, it was selected because it was not impacted by high tail water levels and had fully developed flow. Pool 5 is in the middle of the upstream column and had minimal flow effects from the upstream fishway entrance and the downstream turning pool. A grid spacing of 0.50 m x 0.50 m was used for measurements, with increased densities in areas of importance (e.g., slot and jet flow areas). 58, 83, 106, and 58 measurements were taken in pools 5, 8, 13, and

15, respectively. A physical barrier in Pool 8 prevented velocity measurements from being taken from $x = 5.655 \text{ m} - 6.30 \text{ m}$. Measurements were taken at a fixed elevation. The field probe was submerged 0.50 m below the water surface and fixed at that elevation for all measurements within the pool. Initially, measurements were also taken 1.50 m below the water surface. However, at that depth of submergence the vertical arm had large vibrations which producing low data quality. The data quality was less than the minimum quality acceptable for measuring accurate time-averaged velocities. The manufacturer specifies that the velocity data collected with the ADV is accurate to $\pm 0.5\%$ of the measured value, with a maximum accuracy of $\pm 0.001 \text{ m/s}$ (Nortek, 2011). The maximum velocity recorded was 1.40 m/s, with a theoretically accuracy $\pm 0.007 \text{ m/s}$. Velocity in this study is expressed to 0.01 m/s, and an accuracy of $\pm 0.01 \text{ m/s}$.

Prior to data collection preliminary testing was done to determine the required ADV sampling period for accurate time-averaged velocity measurements. Sample test periods of 30 – 120 s were taken. Velocity became nearly constant after 45 s. All point measurements were recorded for 180 s at a sampling frequency of 25Hz. In total 4,500 instantaneous velocity readings were recorded at each point. Measurements were taken in the x, y, z coordinate system. Longitudinal, transverse, and vertical velocities ($u, v,$ and w) were averaged over the sampling period to produce time-averaged velocities ($\bar{u}, \bar{v},$ and \bar{w}).

When using acoustic devices to conduct field measurements data correlation is an important quality control parameter. A high correlation value confirms the measurement recorded is of high quality, whereas a low correlation

value indicates potential measurement errors. The ADV used to measure water velocities uses a linear correlation scale of 0 – 100%. The linear scale ranges from no correlation at 0% to 'perfect' correlation at 100% (Nortek, 2011). For time averaged velocity values a minimum correlation of 40% is acceptable. 70% or better correlation is needed to provide accurate turbulent velocities, as the correlation drops below 70% the data becomes too noisy to provide accurate turbulence parameters. Low data correlation can be caused by environmental and procedural factors. Highly turbulent flow, aerated or 'bubbly' flow, clear water with small amounts of particulate matter, and vibrations in the measurement set-up all can cause data correlation values to be poor.

A second measure of data quality used in ADV field measurements is the signal to noise ratio (SNR). It is used to determine if the water has an adequate amount of suspended particulate matter to reflect the acoustic signal and deliver accurate measurements. Low SNR values can be problematic in extremely clear water systems, such as the open ocean or large mountain reservoirs, and result in inaccurate measurements. The Richelieu River has a relatively large amount of suspended particulate matter. The water depth visibility in the fishway was less than 0.10 m. The poor depth visibility was caused by the large amounts of suspended particulate matter in the river water and consequently SNR values were deemed adequate and not investigated further.

Data correlation was highest in low velocity measurements and decreased as velocity increased. The correlation values presented represent time averaged correlation values in the same fashion as the velocity measurements which they

are taken for. The values are averaged in the x, y, z - plane and represent a correlation magnitude. The correlation range was 42.5% - 94.5% across the four pools, see Figure 3.3. For velocities less than 0.5 m/s the average correlation was 82%, and for velocities greater than 0.5 m/s the average correlation was 63%. There is a visible transition from higher to low correlations occurring from approximately 0.5 – 0.6 m/s. All velocity measurements taken had a correlation value above 40% and therefore can be deemed accurate for time average velocity.

The Sontek River Surveyor model acoustic Doppler profiler (ADP) was used to measure the river's flow rate downstream of the dam. The ADP was mounted on a trimaran mounted on the alongside the boat to complete measurements. 4 transects were taken 250 m – 300 m downstream of the dam on June 7, 2012, where bin size = 0.3 m and blanking distance = 0.2 m. The advantage of an ADP over an ADV is they measure velocities over the full height of the water column. As such the ADP was also used to record velocity profiles 0.61 m downstream of and perpendicular to the slot as flow entered Pools 4, 5, 8, 13, 14, 15 and 16, where bin size = 0.15 m and blanking distance = 0.2 m. Figure 3.4 shows the field team recording a velocity measurement in Pool 5. Additionally it was used to measure water depths in pools 3 – 16 from June 5 – 6, 2012.

3.2.2 CFD Model Study

The site fishway's regular pool dimensions are shorter and narrower than recommended. Accordingly, CFD modeling was used to assess the effect of dimensions on flow structure and jet velocity decay in five different regular pool geometries. The geometric scenarios are summarized in Table 3-1. Scenario 1 represents the site fishway's regular pool and has dimensions of $l = 5.75b_0$ and $b = 4.9b_0$. b in Scenarios 2 and 3 are equal to Scenario 1, and l is increased to 8 and $10b_0$, respectively, where $10b_0$ is the recommended length for regular pools. Scenarios 4 and 5 are wider than Scenarios 1 – 3 with $b = 8b_0$, where $8b_0$ is the recommended width for regular pools. Scenarios 4 and 5 have lengths of 8 and $10b_0$, respectively. The five scenarios simulated provide a to demonstrate hydraulic effects of using shorter and narrower dimensions..

... Scenario 5 represents the recommended design and has dimensions of $l = 10b_0$, $b = 8b_0$. (Bell, 1973; Larinier et al., 1999; Rajaratnam et al., 1992B)....

The model was validated previously in a study focusing on the hydraulics in the site fishway's turning pools. A complete outline of the model and validation used is provided in Chapter 4. To ensure the CFD model was simulating field conditions Δh between Pools 4 and 5, and Pool 5 V_{sm} in Scenario 1 were set equal to the velocity measurements taken in the field. The isometric contours method, with the water volume fraction equal to 0.5, was used to measure $\Delta h = 0.185$ m in the model; $\Delta h = 0.18$ m in field measurements. At $(x, y) = (2.025, 2.84)$, where x is the distance from the river side longitudinal wall and y is the distance from the downstream long baffle wall; V_{sm} was 1.36 m/s in the

field and 1.38 m/s in the cfd model. The Δh and V_{sm} parameters show strong agreement between the field measurements and the CFD model simulations and providing confidence in the accuracy of results produced with the model.

3.3 Results and Discussion

3.3.1 Water Levels

Figure 3.5 shows water levels in the Richelieu River typically peak in late April to early May during spring freshet. Upstream of the dam water levels fluctuate naturally until June or July, depending on levels, then are maintained at $6.85 \text{ m} \pm 0.1 \text{ m}$ during the summer months to support recreational boater traffic.

Downstream of the dam water levels decrease naturally until September when it reaches its annual minimum (MDDEP 1 and 2, 2013). During the spring and summer of 2011 abnormally high water levels were present throughout the Richelieu River system. Water levels in 2012 were less extreme and closer to historical averages (MDDEP 1 and 2, 2013).

The flow in a vertical slot fishway can be uniform, where the depth, h , of flow in each pool is approximately the same; or non-uniform, with M1 or M2 type backwater curves (Chow, 1959; Rajaratnam et al., 1986). In a M1 type backwater curve h increases towards the downstream end of the fishway, this is caused by high tailwater levels in the river at the exit of the fishway. In a M2 type backwater curve h decreases towards the downstream end of the fishway. Under uniform flow conditions the head drop per pool, Δh , which is the change in water level across the slot, will be equal in all pools. For non-uniform flow Δh will decrease towards the downstream end of the fishway in M1 type backwater curve, and increase towards the downstream end of fishway in M2 type backwater curve. The effect of tailwater is not always over the full length of the fishway. Accordingly, the extent affected by tailwater is treated as gradually varied flow

and the remainder can be considered as uniform flow. For both the uniform and non-uniform sections flow rate Q through a slot can be predicted following the equation proposed by Clay (1961):

$$Q = C_d \sqrt{2g\Delta h} * (b_0 h) \quad (3.1)$$

where $V_{theor} = \sqrt{2g\Delta h}$ is the maximum theoretical velocity, C_d is a discharge coefficient, b_0 is the slot width, and h is the flow depth at the slot up to the water surface on the upstream side. Rajaratnam et al. (1986) in their laboratory experiments predicted values of $C_d = 0.3 - 1.3$ for a variety of vertical slot designs tested. $C_d = 0.6 - 0.8$ for a Design 1 type pool; the baffle design in Design 1 closely resembles the design of the site fishway's baffle geometry. Using $V_{theor} = \sqrt{2g\Delta h}$ as a method of predicting maximum velocity in a vertical slot fishway has been previously used by Rajaratnam et al (1986), Wu et al. (1999), and Liu et al. (2006) with good accuracy.

Equation 3.1 was used to determine C_d for the site fishway. Assuming a known $Q = 1.63 \text{ m}^3/\text{s}$ from measurements taken in July 2011, see section 2.4.4 Fishway Flow Rate for further details, and a known h measured in slot 3, an iterative solver was used to calculate h in slots 3 – 16, where the slot number represents the pool jet flow is entering. Predicted h values were then compared to h values measured in the field on July 7, 2011 and June 6, 2012. The solver was repeated increasing or decreasing C_d until there was strong agreement between the predicted and measured data sets. h measurements on July 7, 2011 were recorded at the centre of the downstream long baffle wall in the pool upstream of the slot,

and h measurements on June 6, 2012 were recorded 0.61 m downstream of the slot. In both cases h measured is assumed to be approximately equal to h in the slot and therefore is acceptable for comparison to h predicted in Equation 3.1.

Flow in the site fishway was found to be non-uniform with a M1 type backwater curve, and h increased towards the downstream end of the fishway. Figures 2.10 and 2.11 show the comparison of h predicted against h measured on July 7, 2011 and June 6, 2012, respectively. As shown in Figures 3.6 and 3.7 there are two different flow sections in the fishway. From the entrance of the fishway downstream to pool 8 $C_d = 0.86$, in Pool 8 and downstream of pool 8 to pool 16 $C_d = 0.95$. In Pool 8, which is the upstream turning pool, a transition in the flow occurs. There is strong agreement between predicted and measured h values, with mean absolute error (MAE) equal to 0.01 m on July 7, 2011 and 0.04 m on June 6, 2012 (excluding measured values in Pools 8 and 13). On June 6, 2012 the measured values in turning pools is approximately 0.4 m less than predicted, the reason for this is unknown.

C_d in Equation 3.1 at the site fishway is greater than previously calculated in a Design 1 type pool by Rajaratnam et al. (1986). The shorter regular pools in the site fishway have less jet velocity decay through the pool which results in higher velocities and a correspondingly higher C_d in comparison to a regular pool of recommended dimensions. Further analysis of jet velocity decay is provided section 2.4.2 Velocity and Flow Patterns.

Figure 3.8 shows the variation in water levels upstream, downstream and throughout the fishway from July 18 – 29, 2011 and June 4 -16, 2012. The

upstream of the fishway water levels are maintained at approximately 6.85 ± 0.1 m.a.s.l during both periods of measurement. Downstream water levels decreased during both periods, ranging from 4.5 – 5.24 m.a.s.l. Further investigation is needed to assess the fishway's flow type over a large range of discharges to determine the effects that of various upstream and downstream water level pairings.

3.3.2 Velocity and Flow Patterns

Pools 5, 8, 13 and 15 had maximum measured slot velocity vectors, V_{sm} , of 1.36 m/s, 1.40m/s, 1.12m/s and 1.00 m/s, respectively, see Table 3-2. The greater V_{sm} values in pools 5 and 8 than in pools 13 and 15 were caused by larger water level changes between adjacent pools in the upstream portion of the fishway than downstream.

V_{sm} was compared to V_{theor} . The water levels measured on July 22, 2011 from 5 – 5:30 pm EST were compared to the water levels recorded by the data diver at the time V_{sm} was recorded, in order to determine the suitability of July 22, 2011 measurements for use as Δh in V_{theor} calculations. In Pools 5, 13, and 15 suitable data was available and the comparison of V_{sm} to V_{theor} was made. The comparison could not be completed for Pool 8 because the water levels measured on July 22, 2011 did not match the water levels recorded on the data diver at the time V_{sm} was measured in that pool. There were an insufficient number of data divers available to record water levels in all pools and therefore cannot be used to calculate Δh . V_{theor} is 34% greater than V_{sm} in Pool 5, 17% greater in Pool 13, and

V_{theor} is equal to V_{sm} in Pool 15, see Table 3-2. These results are consistent with other studies done on vertical slot fishways without turning pools which found V_{sm} and V_{theor} to be nearly equal (Liu *et al.*, 2006; Wu *et al.*, 1999). This data suggests V_{theor} can be used in vertical slot fishways with turning pools to estimate V_{sm} in both regular and turning pools.

The maximum vertical velocity magnitude, \bar{w}_{max} , was 0.29 m/s and 0.26 m/s in pools 5 and 15, respectively. The maximum upward velocities were downstream of the slot, after the jet entered the pool, and in the low velocity area adjacent to the longitudinal wall between the two short baffles. Maximum downward velocity was located upstream of the slot entrance. The mean vertical velocity, \bar{w}_{mean} , was 0.12 m/s and 0.091 m/s in pools 5 and 15, respectively.

Pools 5 and 15 share a flow pattern. Flow enters the pool through the upstream slot as a jet. The jet travels in the direction of the downstream corner, at the intersection of the long baffle and longitudinal walls. As the jet reaches the centre of the pool it turns, arcing in the direction of the slot, and flows downstream out of the pool. A large resting area, characterized by low velocities and flow recirculation, is situated between the two short baffles. Low velocities also occur adjacent to the longitudinal wall between the two long baffles. These two areas provide resting spaces for fishes ascending the ladder. The flow pattern in pools 5 and 15 is similar to Pattern 2 type flow described by Wu *et al.* (1999) in a previous study done on a Design 18 laboratory model (Rajaratnam *et al.*, 1992B). Figures 3.9 and 3.10 show the velocity field diagrams in the x, y – plane at 0.5 m below water surface for Pools 5 and 15.

The velocity measurements recorded in Pools 4, 5, 8, 13, 14, 15, and 16 using the ADP are shown in Figures 3.11 and 3.12. Each bin's average velocity is plotted as a single point at the mid height of the bin. Figure 2.15 shows strong agreement between the velocities measured with the ADP and simulated in the CFD model in pool 5, further strengthening the confidence in results from both data sets. Velocity in the measured pools is fairly uniform at depths of 0.2 – 1.0 m below the water surface, then at approximately 1.2 m depth velocities begin to decrease with increasing depth towards the pool floor. At 0.2 m – 1.0m below the water surface the highest velocities measured were 1.30 m/s in Pool 4 and 1.32 m/s in Pool 5 at the upstream end of the fishway. In the same depth range the lowest measured velocities were at the downstream end of the fishway, 0.98 m/s in Pool 15 and 0.95 m/s in Pool 16. These results show highest velocities measured at the upstream end and decreased towards the downstream end, where lowest velocities were measured. This is in agreement with ADV measured velocity results which showed higher velocities in Pools 5 and 8, than further downstream in Pools 13 and 15. It also agrees with M1 type backwater curve from the water level measurements which showed that Δh is highest at the upstream end of the fishway, which would cause velocities to be highest there as well.

The velocity distributions at depths of $z = 0.5h$ for the five scenarios simulated using CFD modeling are shown in Figure 3.13. Figure 3.14 shows jet velocity, u_j , distributions for Scenario 1 in the y_j direction. y_j represents the distance from the jet centre in the transverse direction orthogonal to x_j , x_j is the

distance along the curved jet center line from the entrance slot, and u_j is the time-averaged longitudinal velocity in the x_j direction (Liu et al., 2006). The flow is similar to the Gaussian distribution of a plane turbulent jet (Rajaratnam, 1976). However, the structure is not symmetric about the x_j axis because the jet doesn't enter through the pool's center and there are flow recirculation regions on either side of the jet. The velocity u_j is made dimensionless by dividing it by V_{sm} .

The dissipation of jet velocity for Scenarios 1 – 5 is shown in Figure 3.15. The normalized maximum jet velocity u_{jm}/V_{sm} is plotted against $x_j/0.5b_0$, where u_{jm} represents the maximum jet velocity at a distance x_j from the entrance slot. Corresponding curves are plotted for a plane turbulent jet and the mean curve from a previous study of a Design 18 (Liu et al., 2006; Rajaratnam et al., 1992B) regular pool. Measurements are taken starting at $x_j/0.5b_0 = 0.7$. Scenario 1 has the shortest length of jet velocity decay $8.7x_j/0.5b_0$ and correspondingly the largest minimum jet velocity $0.69u_{jm}/V_{sm}$, see Table 2-3. The jet in Scenario 5 has the longest length velocity decay and the smallest minimum jet velocity. The jet velocity decays less than 0.48 the length and the minimum normalized jet velocity is 2.09 times larger in Scenario 1 as compared to Scenario 5. The rate of jet velocity decay in all scenarios is similar to the rate found by Liu et al. (2006):

$$\frac{u_{jm}}{V_{sm}} = 1 - 0.035 \frac{x_j}{0.5b_0} \quad r^2 = 0.77 \quad (3.2)$$

It can be concluded that less jet velocity dissipation occurs in the shorter regular pool design used in the site fishway (Scenario 1) than the longer recommended design geometry (Scenario 5), which results in larger jet velocities through the pool. The jet velocity decay in all five scenarios is more rapid than in

a plane turbulent jet. The rapid velocity decay is attributed to the flow entrainment and recirculation zones surrounding the jet flow caused by the longitudinal pool walls.

Turning Pools 8 and 13 have a common flow pattern. Flow enters the pool through the upstream slot as a jet, flows with high velocity towards the back wall, turns flowing along the semi-circular back wall, and flows out through the downstream slot. A large recirculation area, or vortex, forms in the centre of the pool. A second, smaller recirculation area is located in the upstream corner of the pool between the long baffle and side walls. These two areas are characterized by low velocities and recirculating flow. The large vortex is 3.0 m long, l_v , and 2.5 m wide, b_v , in pools 8 and 13. Figures 3.16 and 3.17 show the velocity field diagrams in the x, y – plane at 0.5 m below water surface for Pools 13, and 8, respectively.

The vertical velocities in both turning pools were low in relation to transverse and longitudinal velocities. Pools 8 and 13 had a \bar{w}_{mean} of 0.03 m/s. \bar{w}_{max} was 0.07 m/s and 0.14 m/s in pools 8 and 13, respectively. The low vertical velocities indicate turning pool velocities are primarily in the x, y – plane. This in addition to pools 8 and 13 having very similar velocity field diagrams shows that the x, y – plane velocity pattern is consistent throughout the water column, less the small height adjacent to the pool bottom where velocities will be affected by the pool's concrete bottom and riprap. A CFD model study was completed to further investigate the hydraulics of turning pools, full hydraulic analysis can be seen in Chapter 3.

3.3.3 Kinetic Energy

The mean flow kinetic energy per unit mass is described as;

$$K = \frac{1}{2}(u^2 + v^2 + w^2) \quad (3.2)$$

where K is the mean flow kinetic energy per unit mass, u is the average x - directional velocity, v is the average y - direction velocity, and w is the average z - direction velocity.

As shown in Figures 3.18 and 3.19 the non-dimensional kinetic energy dissipation in Pools 5 and 15 is maximum downstream of the slot entrance. Kinetic energy then dissipates rapidly as jet velocity decays as it travels through the pool. The rapid decay is caused by entrainment of recirculating flow on either side of the jet. Away from the jet area $K^{1/2}$ is typically less than 35% of V_{sm} in the rest of the pool. The pools at the site fishway have less kinetic energy dissipation as compared to results found by Liu et al. (2006) in a laboratory study of regular pools. This is because the regular pools at the site fishway are shorter and narrower than pools following the recommended design dimensions. As described in section 3.3.2 the shorter and narrower pools have higher jet velocities, this leads to higher kinetic energy than in pools of recommended design.

3.3.4 Fishway Flow Rate

The fishway's volumetric flow rate, Q , was calculated in pools 5, 8, 13, and 15 using the following equation:

$$Q = V_{sm}b_0h \quad (3.4)$$

where V_{sm} is the maximum measured slot velocity (measured in July 2011), b_0 is the slot width, and h is the pool's water depth at the time of V_{sm} was recorded. An average Q equal to $1.63 \text{ m}^3/\text{s}$ was calculated, see Table 3-4. In addition to Q , $6.5 \text{ m}^3/\text{s}$ of attraction flow is released through the floor of the Entrance pool. This combines for a total of $8.13 \text{ m}^3/\text{s}$ of flow being released through the entrance and into the river downstream of the fishway.

3.3.5 River Flow Rate

A goal of this study was to measure the attraction flow immediately downstream of the fishway entrance. Velocity transects were to be measured from a 15' aluminum boat with an ADP mounted on a trimaran. The flow conditions downstream of the dam were characterized by high turbulence, large and strong recirculation zones, and large waves. As transects were attempted the boat would pass through a range of flow speeds and directions. This pulled the boat in changing directions, forcing the captain to change the engine speed and direction accordingly. The large recirculation zones also caused the boat to rotate. Due to complicated flow conditions the slow and linear transects required to record flow measurements could not be completed. The flow pulled the front end of the trimaran under water, causing it to overturn. The tendency to overturn put the field team at risk of losing the unit and interrupted measurement recording. The large waves also lifted the ADP unit out of the water interrupting measurements.

Additionally, the high flow turbulence caused the ADP to produce flawed measurements.

Overall the flow conditions immediately downstream of the dam and fishway were both unsuitable for recording measurements and unsafe for the field team. Attempts to quantify attraction flow were unsuccessful. New techniques and further study are required to take successful measurements in these conditions.

The highly turbulent flow immediately downstream of the dam forced the field team to record transects measuring the Richelieu River's volumetric flowrate 250 – 300 m downstream of the dam on June 7, 2012, where conditions were suitable for measurement recording. The average volumetric flow rate taken over four transects was $406 \text{ m}^3/\text{s}$. Flow rates are shown in Table 3-4, and the ADP data output is displayed in Figure 3.20.

3.3.6 Tailrace Depths

Figure 3.21a shows the contour map of water depths in the tailrace area immediately downstream of the Saint Ours dam, measurement points are shown as white dots on the contours. Figure 3.21b shows the measurement point coordinates as black dots over top of satellite imagery to serve as a frame of reference for the contour map of Figure 3.21a. Note in Figure 3.21b data points have been shifted to the left bank a small amount in reference to the satellite imagery. This is caused by a slight disagreement between the satellite imagery and GPS data. Immediately downstream of the dam, a large area in the centre of

the river has been eroded by flow undergoing hydraulic jump as it passes over the dam. The tailrace area is more than 15.0 m deep at the deepest points measured. Comparatively, the depth range is typically 2 – 5 m deep at 200 m and greater downstream of the dam. The flow over the dam has created a deep water pool in the tailrace area, see Figure 3.21. The hydraulic jump at the dam creates a large area immediately downstream of the dam where flow was highly turbulent. Between the dam and the most upstream data points, depth measurements were attempted, but flow was too turbulent for successful measurements. It is thought the depth in the unmeasured area is not greater than the depth recorded at the deepest point of measurement.

3.4 Conclusions

This paper presents the results of a study investigating the overall hydraulics of the Vianney-Legendre vertical slot fishway on the Richelieu River in Quebec, Canada. The site was selected because it is a vertical slot fishway with turning pools that passes annually more than 35 species and is one of few fishways worldwide to pass a species of sturgeon (Thiem et al., 2010).

The fishway's layout, with two turning pools connecting three segments of regular pools together, forms a staircase or fold-back pattern that is more compact than an equivalent fishway without turning pools. This design is more cost efficient with respect to construction and places the fishway closer to the hydraulic barrier making it easier for fish to find the entrance (Bunt, 2001; Clay, 1961; Katopodis and Williams, 2012). The fishway's regular pool geometry is shorter and narrower than is recommended (Rajaratnam et al., 1992B). The turning pools are twice the width of the attaching two regular pools; have semi-circular back wall and a maximum length from centre wall to back wall of just over half the width. The fishway releases over $8 \text{ m}^3/\text{s}$ of flow into the Richelieu River through the fishway exit. For comparison the Richelieu River was $406 \text{ m}^3/\text{s}$ on June 12, 2012. The river's flow rate and corresponding water levels reach annual maximums in late April and early May, and then decrease reaching annual minimums in September. Upstream of the fishway the water levels are maintained at $6.85 \text{ m} \pm 0.1 \text{ m}$ over the summer months to allow for recreational boater traffic in the river. Downstream of the fishway water levels fluctuate naturally.

The fishway was found to have non-uniform flow with an M1 type backwater curve, which is characterized by increasing water levels towards the downstream end of the fishway. The flow rate and water surface profile were predicted using $Q = C_d \sqrt{2g\Delta h} * (b_0 h)$ which was developed to describe the flow in a vertical slot fishway (Clay, 1961). C_d for the site fishway was higher than in comparable vertical slot fishways studied by Rajaratnam et al. (1986). The shorter and narrower regular pool dimensions in the site fishway resulted less jet velocity decay as compared to the recommended design geometry. This led to larger jet velocities through the pool explaining the higher C_d value. Consequently, the regular pool design dimensions of $l = 10 b_0$ and $b = 8 b_0$ are recommended over the site fishway's dimensions of $l = 5.83 b_0$ and $b = 5 b_0$.

Regular pools 5 and 15 showed a common flow pattern similar to Pattern 2 type flow (Rajaratnam et al., 1992B; Wu et al., 1999). Turning pools 8 and 13 also had a common flow pattern. In turning pools flow entered the pool through the upstream slot as a jet, flowed with high velocity towards the back wall, turned flowing along the semi-circular back wall, and flowed out through the downstream slot. A large recirculation area formed in the centre of the pool, and a second, smaller recirculation area was located in the upstream corner of the pool. Velocity in both turning pools was primarily in the x, y – plane.

3.5 References

Bell, M.C. 1973. Fisheries handbook of engineering requirements and biological criteria. U.S. Army Corps of Engineers, North Pacific Division, Portland, Ore.

Bunt, C.M., 2001. Fishway entrance modifications enhance fish attraction. *Fish. Manag. and Ecol.* 8, 95-105.

Chow, V.T. 1959. Open-channel hydraulics. McGraw-Hill Book Co., New York, N.Y., 680 pp.

Clay, C.H., 1961. Design of fishways and other fish facilities. Dept. of Fisheries of Canada, Ottawa, 301 pp.

COSEWIC (Committee on the Status of Endangered Wildlife in Canada).

Wildlife Species search. Government of Canada. Updated: 2012/08/03, accessed: 2012/12/05.

(1)http://www.cosewic.gc.ca/eng/sct1/SearchResult_e.cfm?commonName=lake+sturgeon&scienceName=&Submit=Submit.

(2)http://www.cosewic.gc.ca/eng/sct1/SearchResult_e.cfm?commonName=copper+redhorse&scienceName=&Submit=Submit.

Hatry, C., Binder, T.R., Thiem, J.D., Hasler, C.T., Smokorowski, K.E., Clarke, K.D., Katopodis, C., Cooke, S.J., In press. The status of fishways in Canada: trends identified using the national CanFishPass database. *Rev. Fish Biol. Fish.*

Katopodis, C., Kells, J.A., Acharya, M., 2001. Nature-like and conventional fishways; alternative concepts?. *Can. Water Resour. J.* 26, 211-232.

Katopodis, C., Williams, J.G., 2012. The development of fish passage research in a historical context. *Ecol. Eng.* 48, 8-18.

Larinier, M., Gosset, C., Porcher, J.P., Travade. 1999. Passes à poissons : Expertises et conception des ouvrages de franchissement. Paris, France: La Documentation Française.

Liu, M., Rajaratnam, N., Zhu, D.Z., 2006. Mean flow and turbulence structure in vertical slot fishways. *J. Hydraul. Eng.* 132(8), 765-777.

Marriner, B.A., Baki, A.B., Zhu, D.Z., Cooke, S.J. Submitted for publication. A case on the overall hydraulics of the Vianney-Legendre vertical slot fishway in Quebec, Canada. *J. Hydraul. Eng.*

Marriner, B.A., Baki, A.B., Zhu, D.Z., Thiem, J.D., Cooke, S.J., Katopodis, C. Submitted for publication. Field and numerical assessment of turning pool hydraulics in a vertical slot fishway. *Ecol. Eng.*

MDDEP (Ministere du Developpement durable, de l'Environnement, de la Faune et des Parcs). Centre D'expertise hydrique. Updated: 18/03/2013, accessed: 18/03/2013.

(1)

<http://www.cehq.gouv.qc.ca/suivihydro/graphique.asp?NoStation=030401>

(2)

<http://www.cehq.gouv.qc.ca/suivihydro/graphique.asp?NoStation=000116>

Nortek AS. 2009. Vectrino velocimeter user guide. Nortek AS, Vangkroken, Norway.

- Parks Canada. Vianney-Legendre Fishway at the Saint-Ours Canal National Historic Site of Canada. Updated: 18/08/2010, accessed: 05/2011.
<http://www.pc.gc.ca/lhn-nhs/qc/saintours/ne.aspx>.
- Pon, L.B., Hinch, S.G., Cooke, S.J., Patterson, D.A., Farrell, A.P., 2009. Physiological, energetic and behavioural correlates of successful fishway passage of adult sockeye salmon *Oncorhynchus nerka* in the Seton River, British Columbia. *J. Fish Biol.* 74, 1323-1336.
- Puertas, J., Pena, L., Teijeiro, T., 2004. Experimental approach to the hydraulics of vertical slot fishways. *ASCE J. Hydraul. Eng.* 130, 10-23.
- Rajaratnam, N., 1976. *Turbulent Jets*, Amsterdam, The Netherlands.
- Rajaratnam, N., Van der Vinne, G., Katopodis, C. 1986. Hydraulics of vertical slot fishways. *J. Hydraul. Eng.* 112, 909-927.
- Rajaratnam, N., Katopodis, C., Paccagnan, R. 1992A. Field studies of fishways in Alberta. *Can. J. Civ. Eng.* 19, 627-638.
- Rajaratnam, N., Katopodis, C., Solanki, S., 1992B. New designs for vertical slot fishways. *Can. J. Civ. Eng.* 19, 402-414.
- Rajaratnam, N., Katopodis, C., Wu, S., Saburm, M.A., 1997. Hydraulics of resting pools for denil fishways. *ASCE J. Hydraul. Eng.* 123 (7), 632-638.
- Schlumberger Water Services. 2011. Mini-Diver product manual. Schlumberger Water Services, Delft, The Netherlands.
- Thiem, J., Binder, T., Dawson, J., Dumont, P., Hatin, D., Katopodis, C., Zhu, D.Z., Cooke, S., 2011. Behaviour and passage success of upriver-

migrating lake sturgeon *Acipenser fulvenscens* in a vertical slot fishway on the Richelieu River, Quebec, Canada. *Endanger. Species Res.* 15, 1-11.

Thiem, J.D., Binder, T.R., Dumont, P., Hatin, D., Hatry, C., Katopodis, C., Stamplecoskie, K.M., Cooke, S.J., In press. Multispecies fish passage behaviour in a vertical slot fishway on the Richelieu River, Quebec Canada. *River Res. Appl.*

Warren, J.J., Beckman, L.G., 1993. Fishway use by white sturgeon on the Columbia River. Washington Sea Grant Program; Marine Advisory Services.

White, L.J., Harris, J.H., Keller, R.J., 2011. Movement of three non-salmonid fish species through a low-gradient vertical slot-fishway. *River Res. Appl.* 27, 499-510.

Wu, S., Rajaratnam, N., Katopodis, C., 1999. Structure of flow in vertical slot fishway. *J. Hydraul. Eng.* 125(4), 351-360.

Table 3-1 Summary of regular pool geometry scenarios simulated using computational fluid dynamics modeling.

Scenario	Length (m)	Width (m)	Slot width (m)	$L:b_0$	$b:b_0$	Slope (%)
1	3.5	3	0.609	5.75	4.9	2
2	4.87	3	0.609	8	4.9	2
3	6.09	3	0.609	10	4.9	2
4	4.87	4.87	0.609	8	8	2
5	6.09	4.87	0.609	10	8	2

Table 3-2 Velocity and flow rate field results at the Vianney-Legendre fishway recorded in July 2011.

Parameter	Pool 5	Pool 8	Pool 13	Pool 15
V_{sm} (m/s)	1.36	1.40	1.14	1.00
V_{theor} (m/s)	1.74	N/A	1.29	0.99
Q (m ³ /s)	1.54	1.79	1.62	1.57
h (m) Note: at time V_{sm} was recorded.	1.89	2.09	2.34	2.58
b_0 (m)	0.609	0.609	0.609	0.609

Table 3-3 Minimum normalized jet velocity u_{jm}/V_{sm} at distance $x_j/0.5b_0$ from the pool's slot entrance for Scenarios 1- 5.

Scenario	$x_j/0.5b_0$	u_{jm}/V_{sm}
1	8.7	0.69
2	12.2	0.43
3	16.1	0.41
4	17.0	0.59
5	18.1	0.33

Table 3-4 Richelieu River flow rate measurements taken 250 – 300 m downstream of the Saint Ours Dam.

Transect	Flow Rate (m^3/s)
1	412
2	412
3	406
4	395
Mean	406



Figure 3.1 A water level recording data logger housed in a steel cylinder suspended with airplane cable, prior to submergence for data gathering.



(a)



(b)

Figure 3.2 (a) A field constructed measurement frame mounted on Pool 15 of the Vianney-Legendre fishway recording velocities. (b) An acoustic Doppler velocimeter field probe submerged in Pool 15 recording velocity measurements.

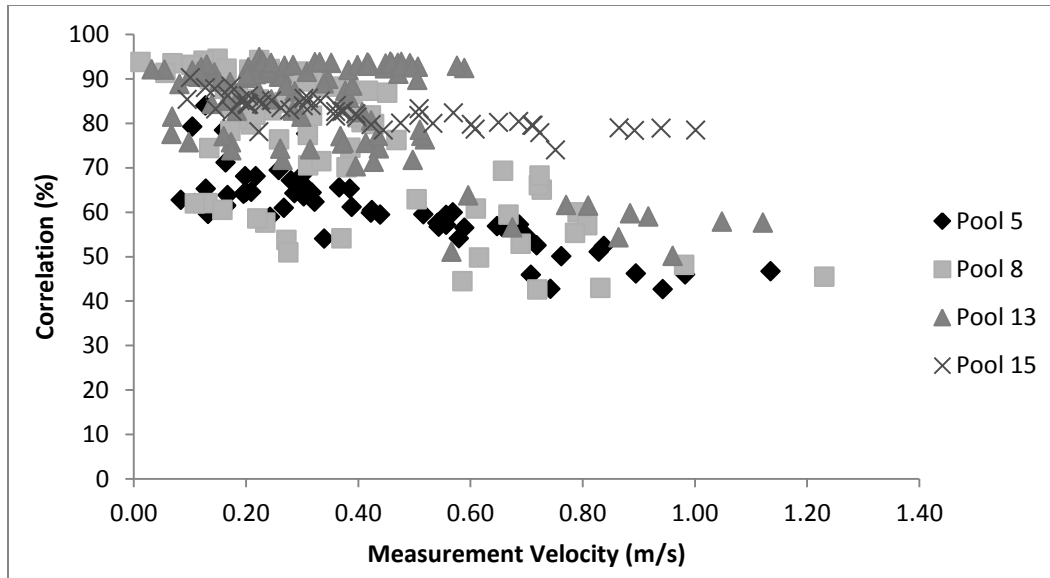


Figure 3.3 Correlation of velocity measurements recorded in the Vianney-Legendre fishway with an Acoustic Doppler Velocimeter field probe.



Figure 3.4 Recording velocity measurements using an Acoustic Doppler Profiler
0.61 m downstream of the entrance to pool 5.

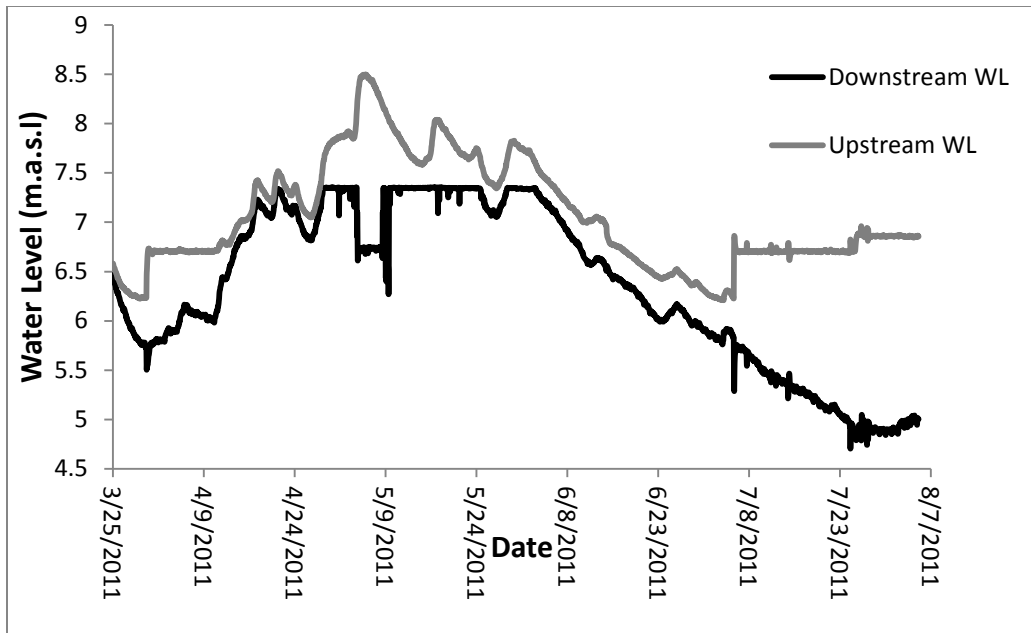


Figure 3.5 Richelieu River water levels, upstream and downstream of the Vianney-Legendre fishway March 25 – August 7, 2011.

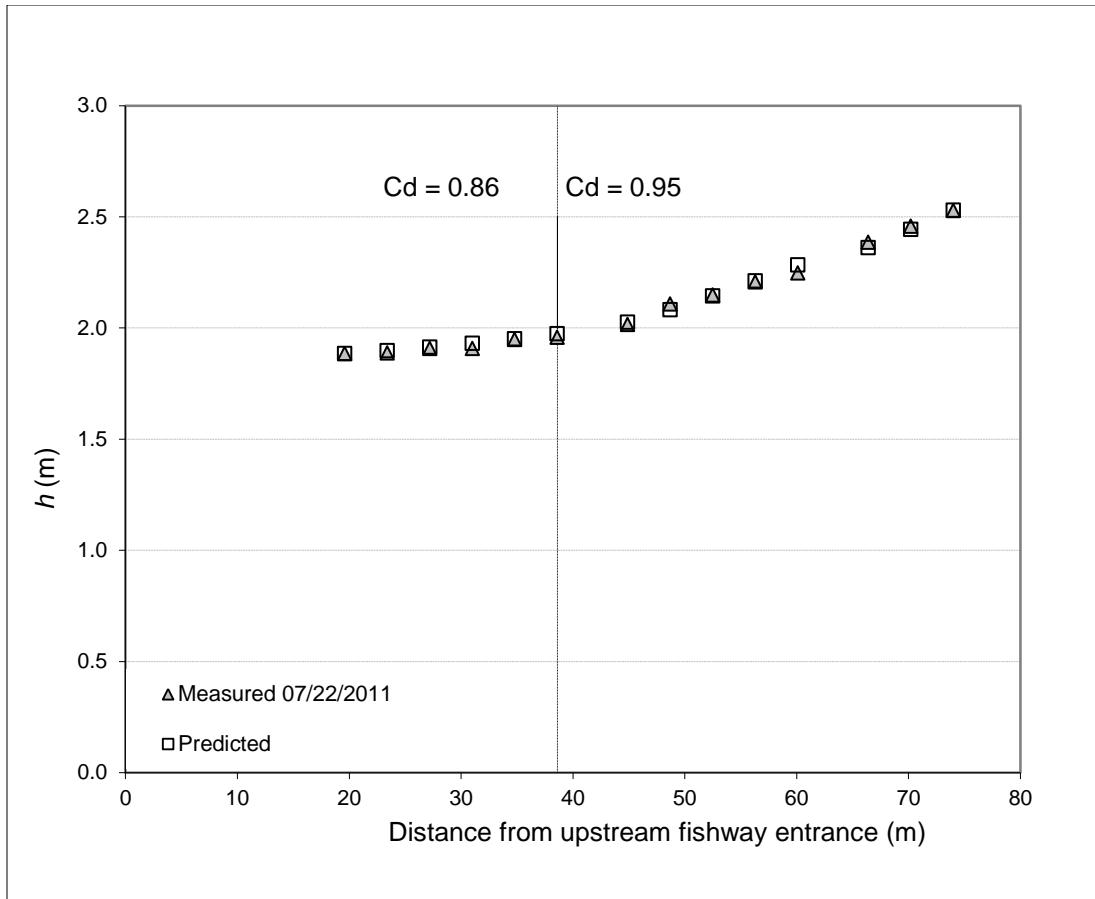


Figure 3.6 Vianney-Legendre fishway water surface profiles measured on 07/22/2011 and predicted.

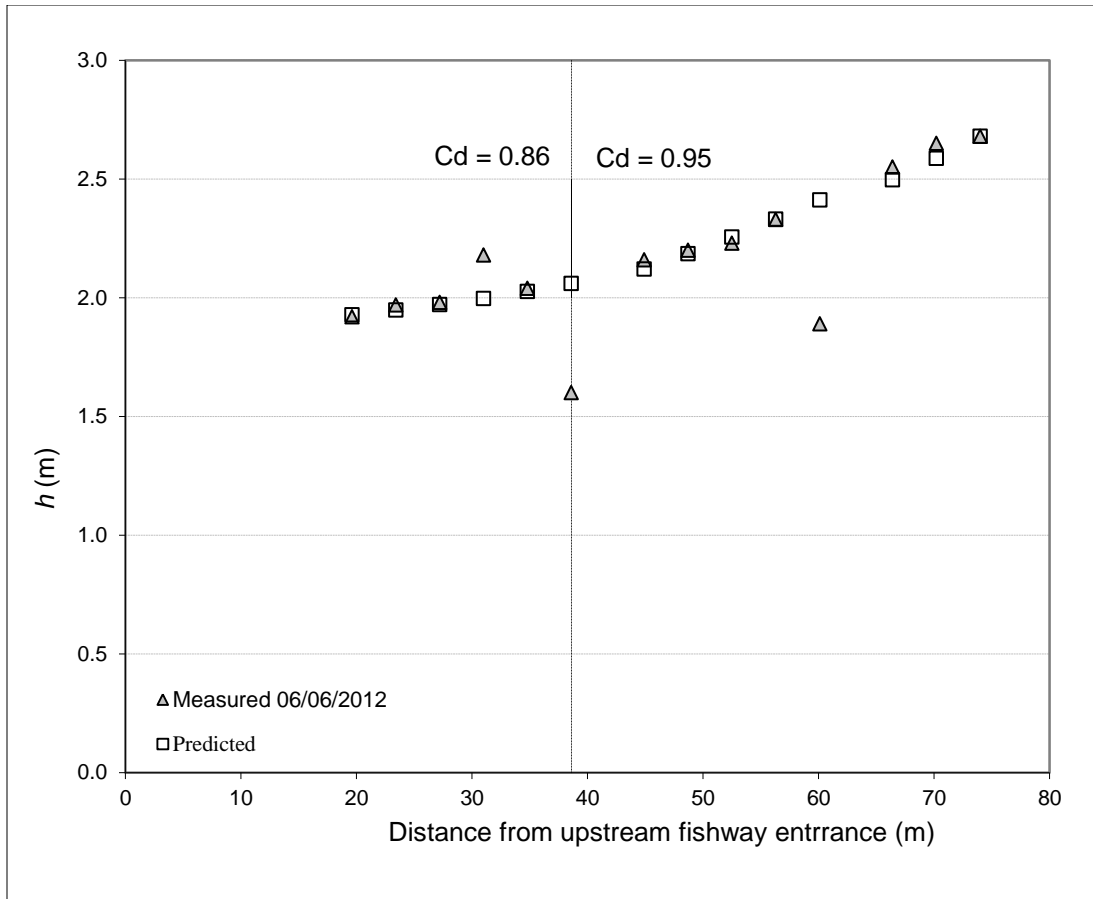
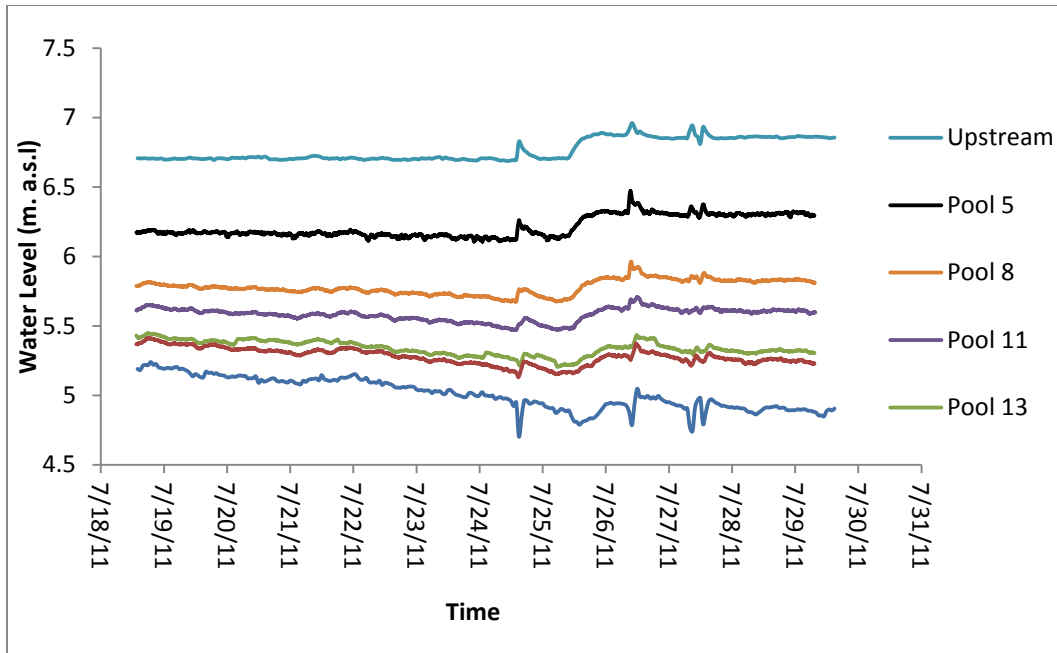
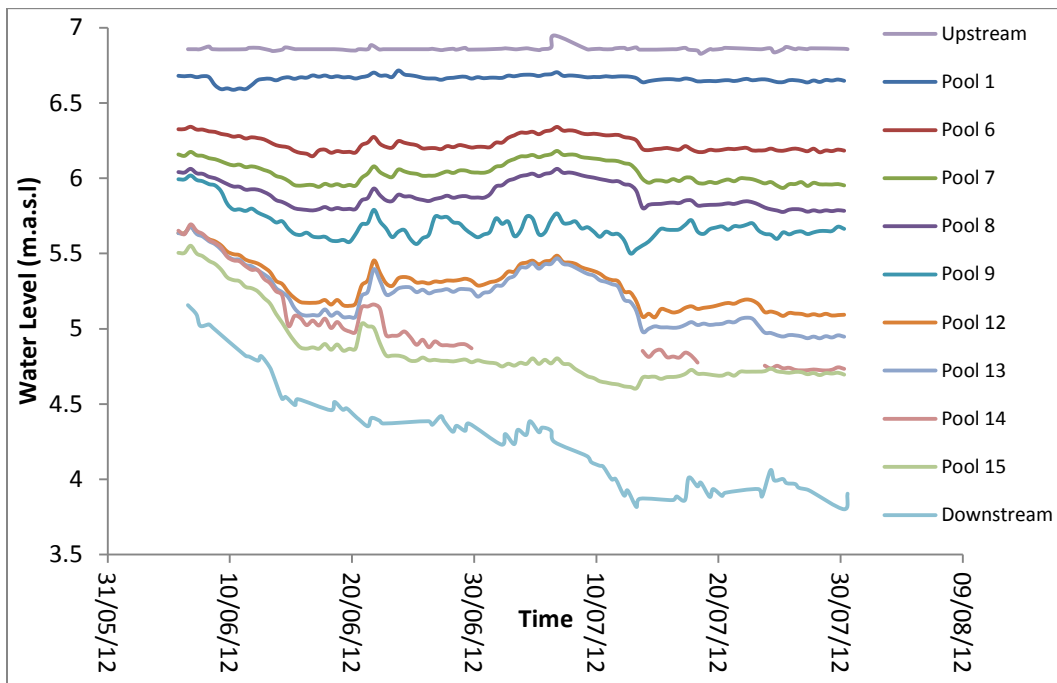


Figure 3.7 Vianney-Legendre fishway water surface profiles measured on 06/06/2012 and predicted.



(a)



(b)

Figure 3.8 Water levels upstream, downstream of the St. Ours Dam and in pools of the Vianney-Legendre fishway (a) July 18 – 29, 2011. (b) June 4 – July 30, 2012.

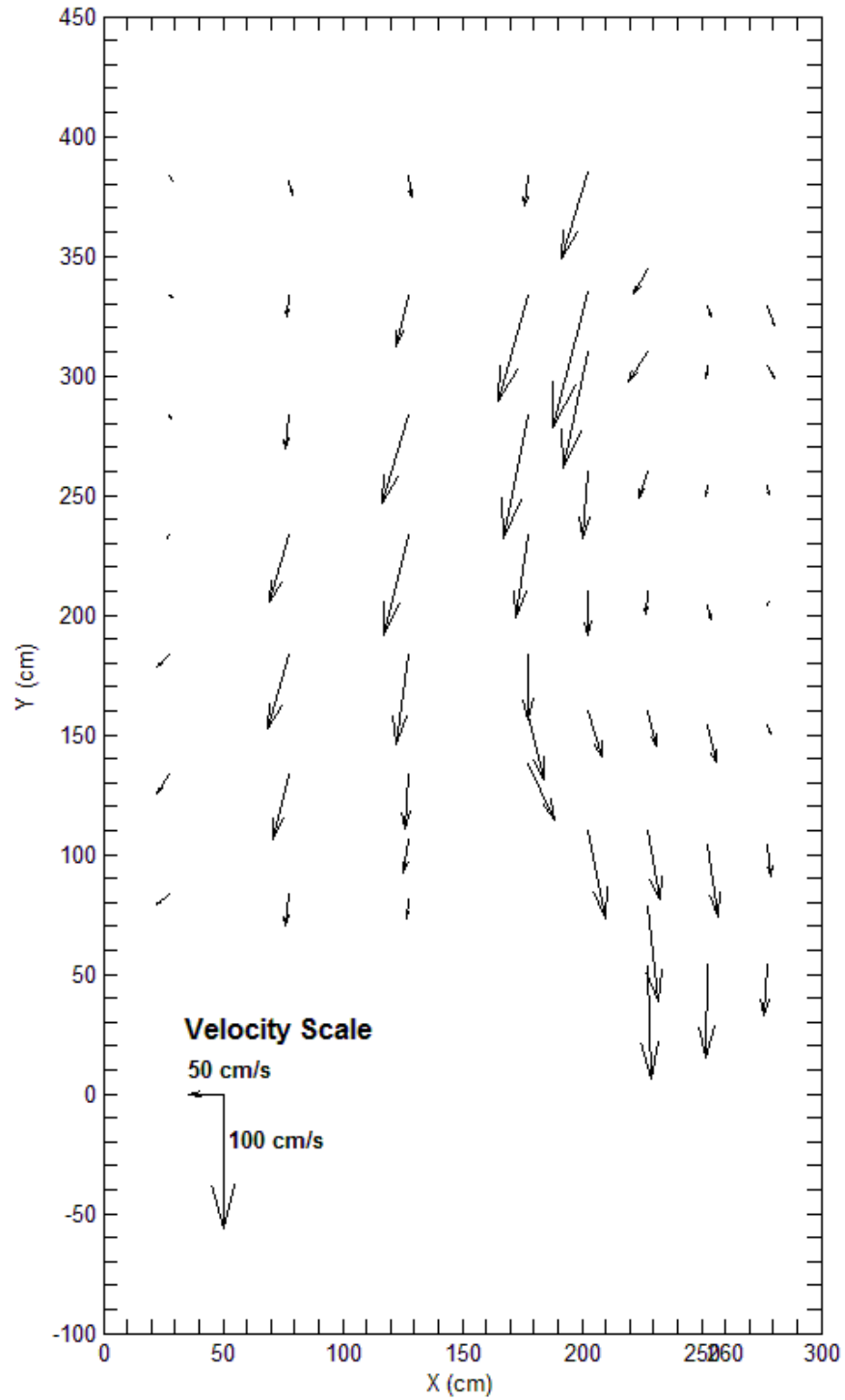


Figure 3.9 Time-averaged field velocities 0.50 m below the water surface in Pool

5.

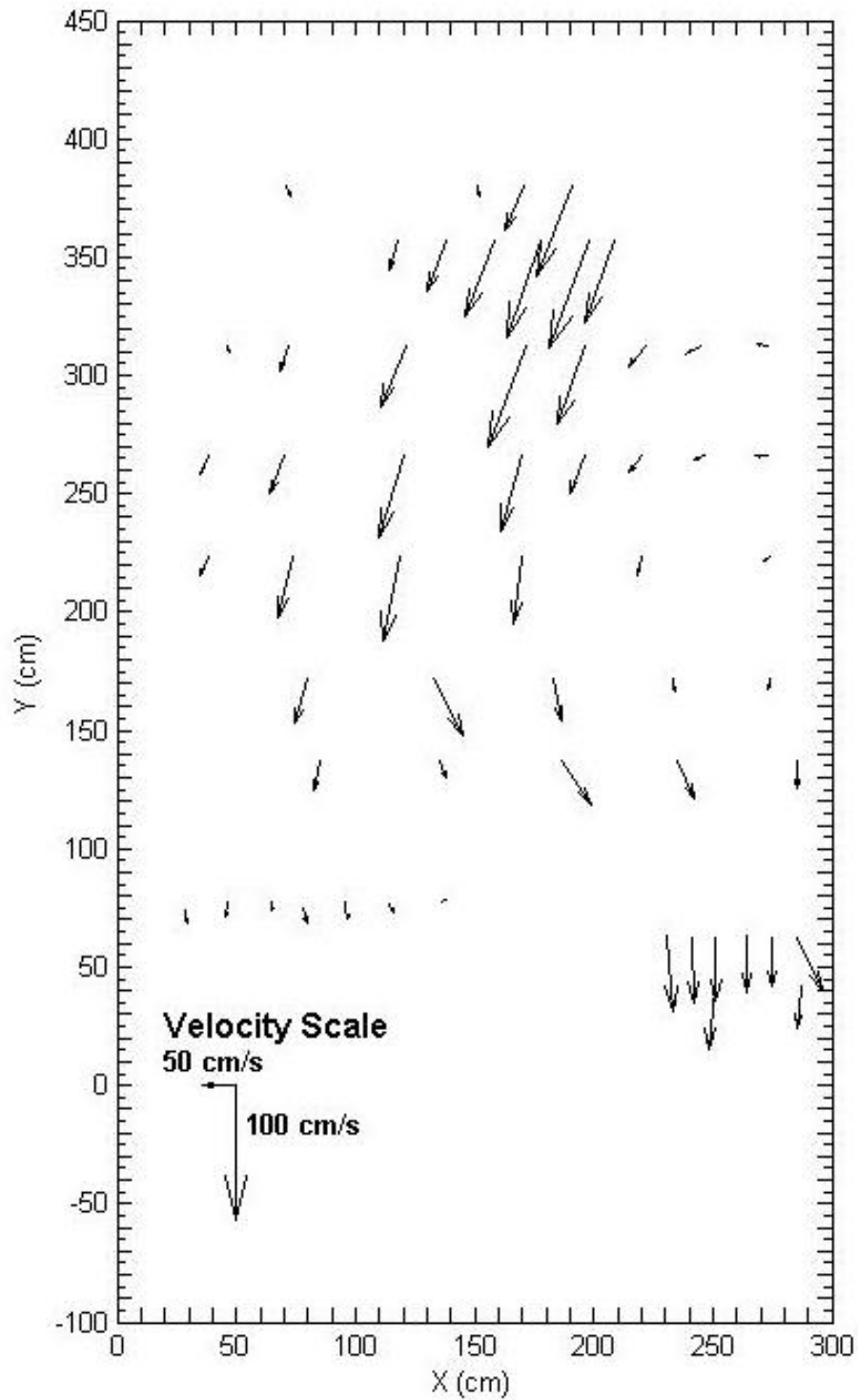


Figure 3.10 Time-averaged field velocities 0.50 m below the water surface in Pool 15.

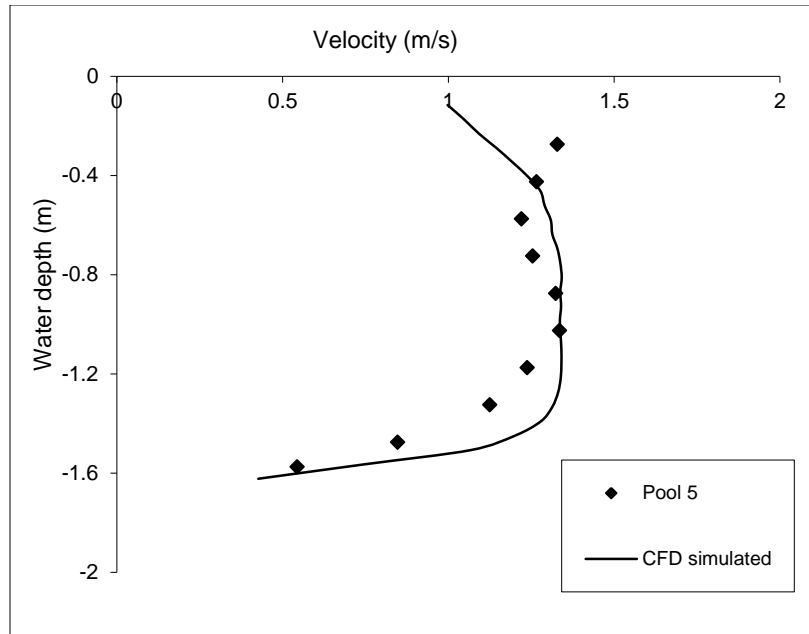
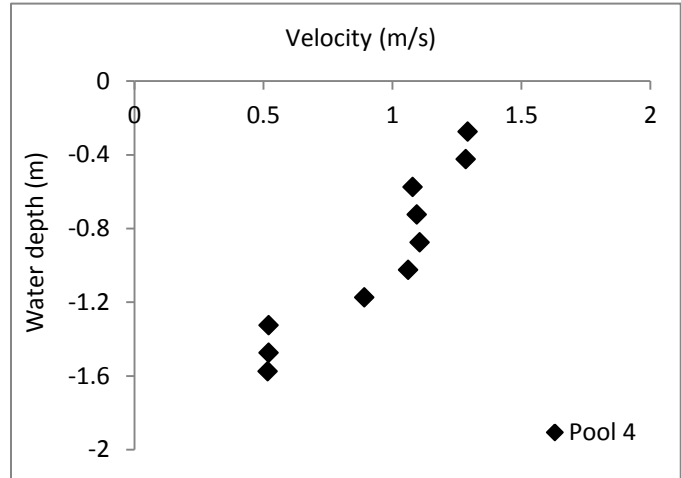
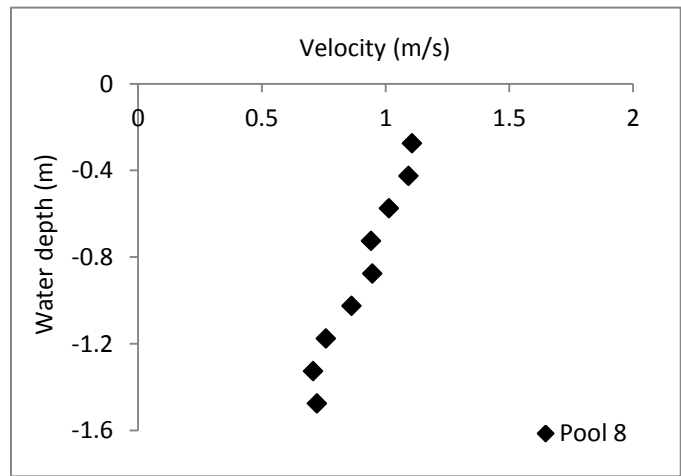


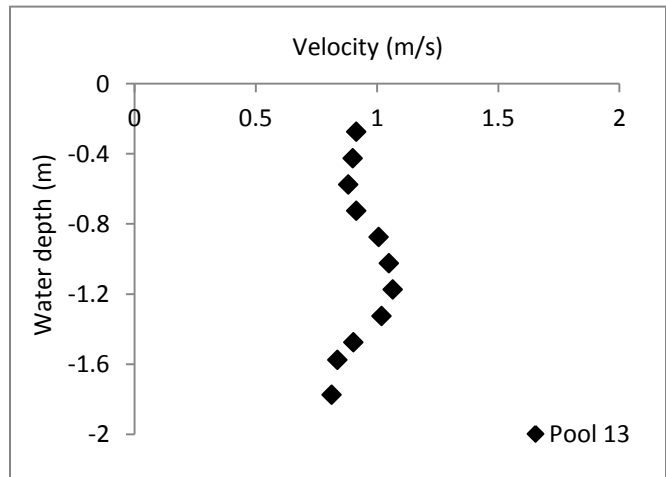
Figure 3.11 Velocity profile at 0.61 m downstream of the slot in Pool 5 measured on June 6, 2012 and simulated in a CFD model.



(a)

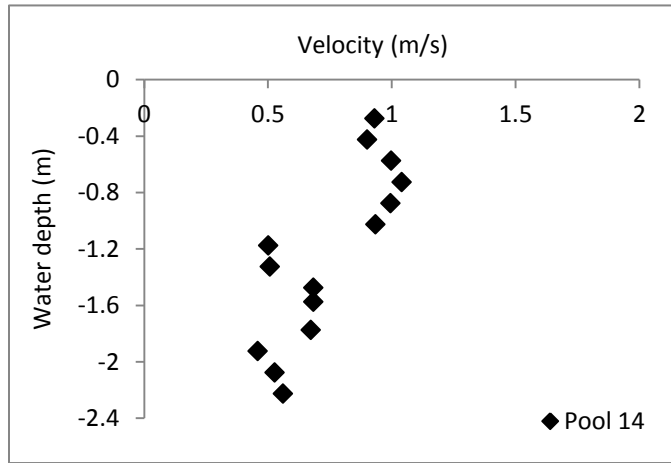


(b)

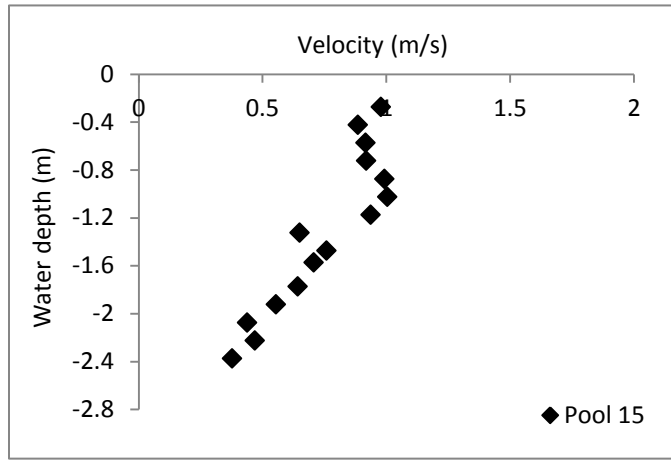


(c)

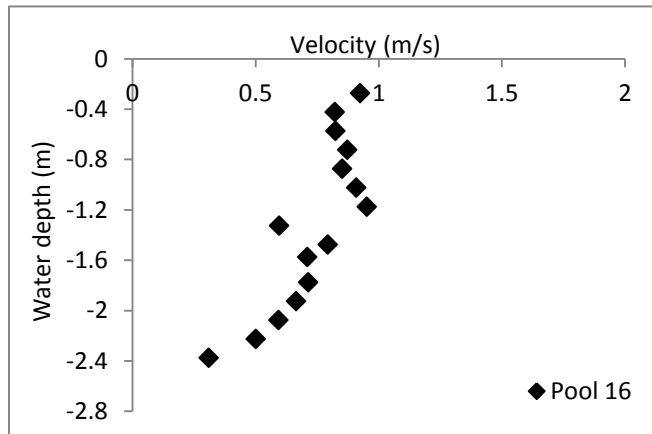
Figure 3.12 Velocity profile at 0.61 m downstream of the slot measured on June 6, 2012: (a) Pool 4; (b) Pool 8; (c) Pool 13; (d) Pool 14; (e) Pool 15; (f) Pool 16.



(d)



(e)



(f)

Figure 3.12 - Continued

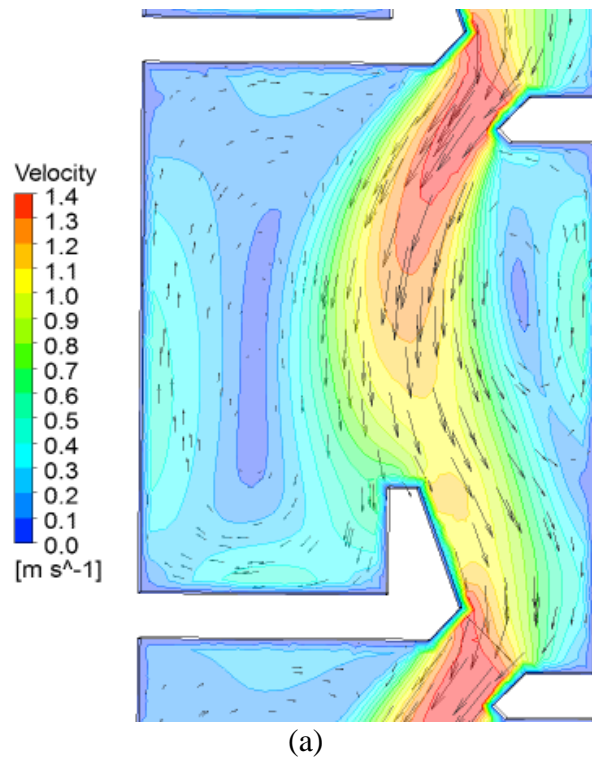


Figure 3.13 Velocity distributions in regular pools at depths of $0.5h$: (a) Scenario 1, $l = 3.5\text{m} \times b = 3.0\text{m}$; (b) Scenario 2, $l = 4.87\text{m} \times b = 3.0\text{m}$; (c) Scenario 3, $l = 6.09\text{m} \times b = 3.0\text{m}$; (d) Scenario 4, $l = 4.87\text{m} \times b = 4.87\text{m}$; (e) Scenario 5 $l = 6.09\text{m} \times b = 4.87\text{m}$.

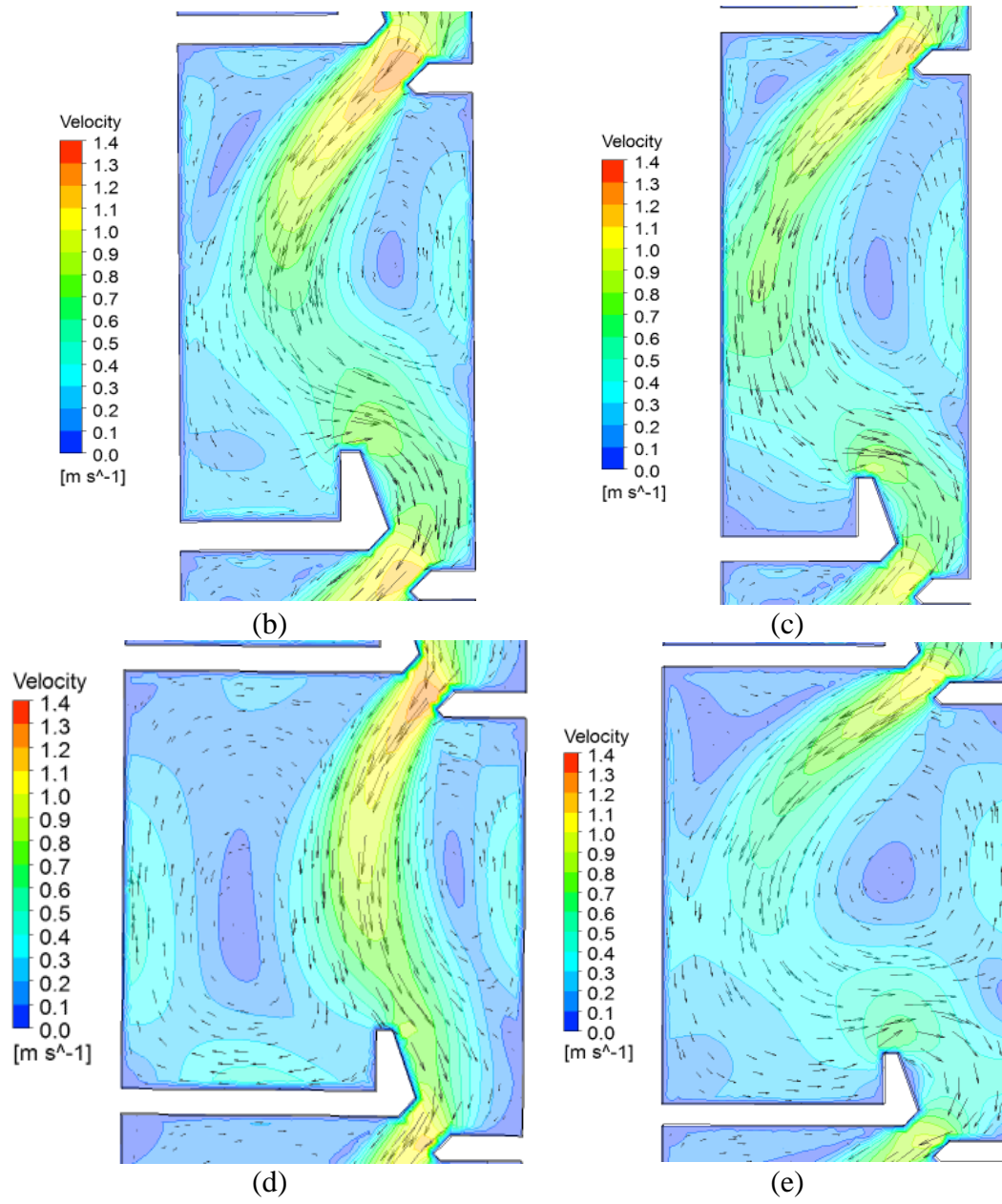


Figure 3.13 - Continued

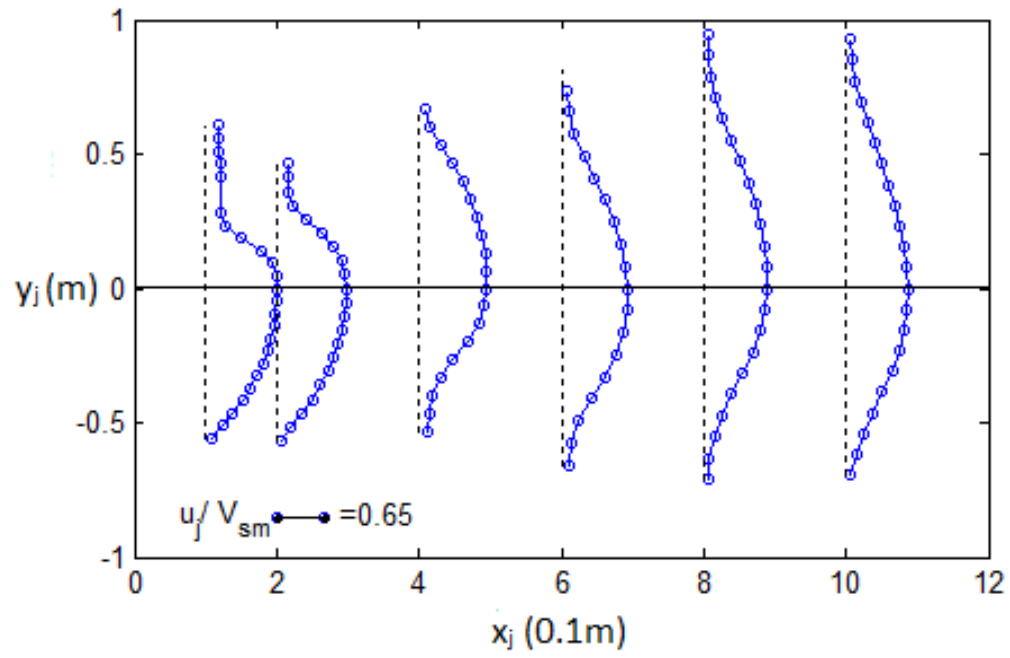


Figure 3.14 Normalized distribution of longitudinal mean velocity in Scenario 1 jet flow.

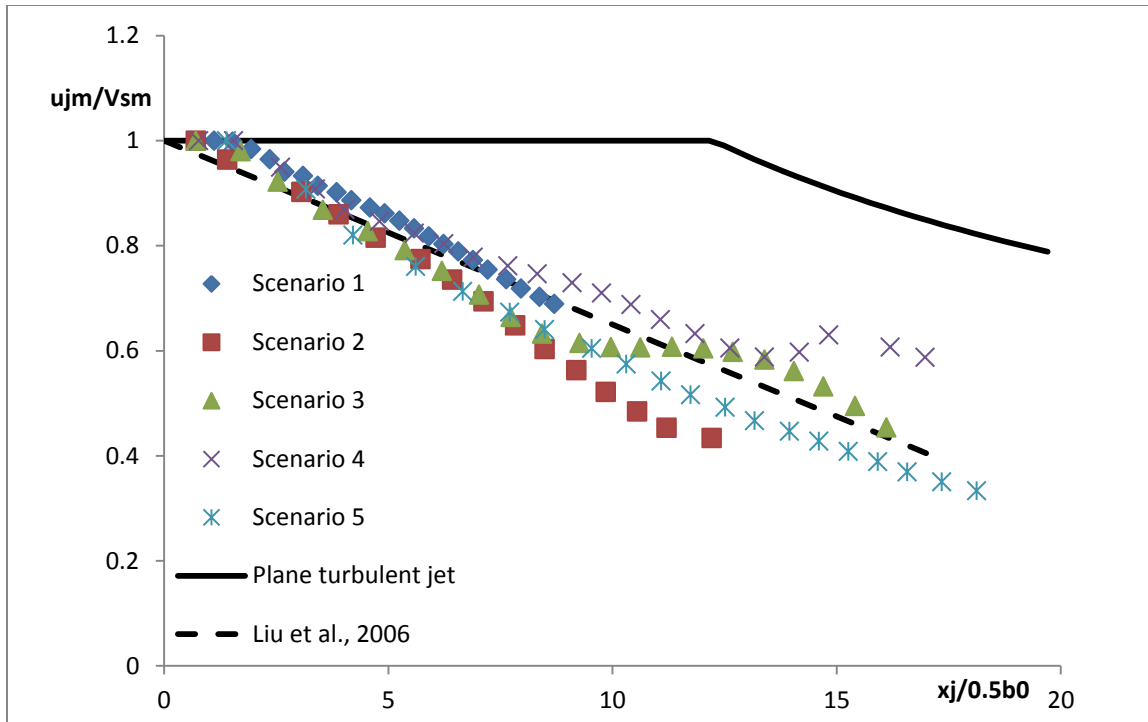


Figure 3.15 Variation of normalized maximum velocity u_{jm}/V_{sm} with $x_j/0.5b_0$ (Liu et al., 2006).

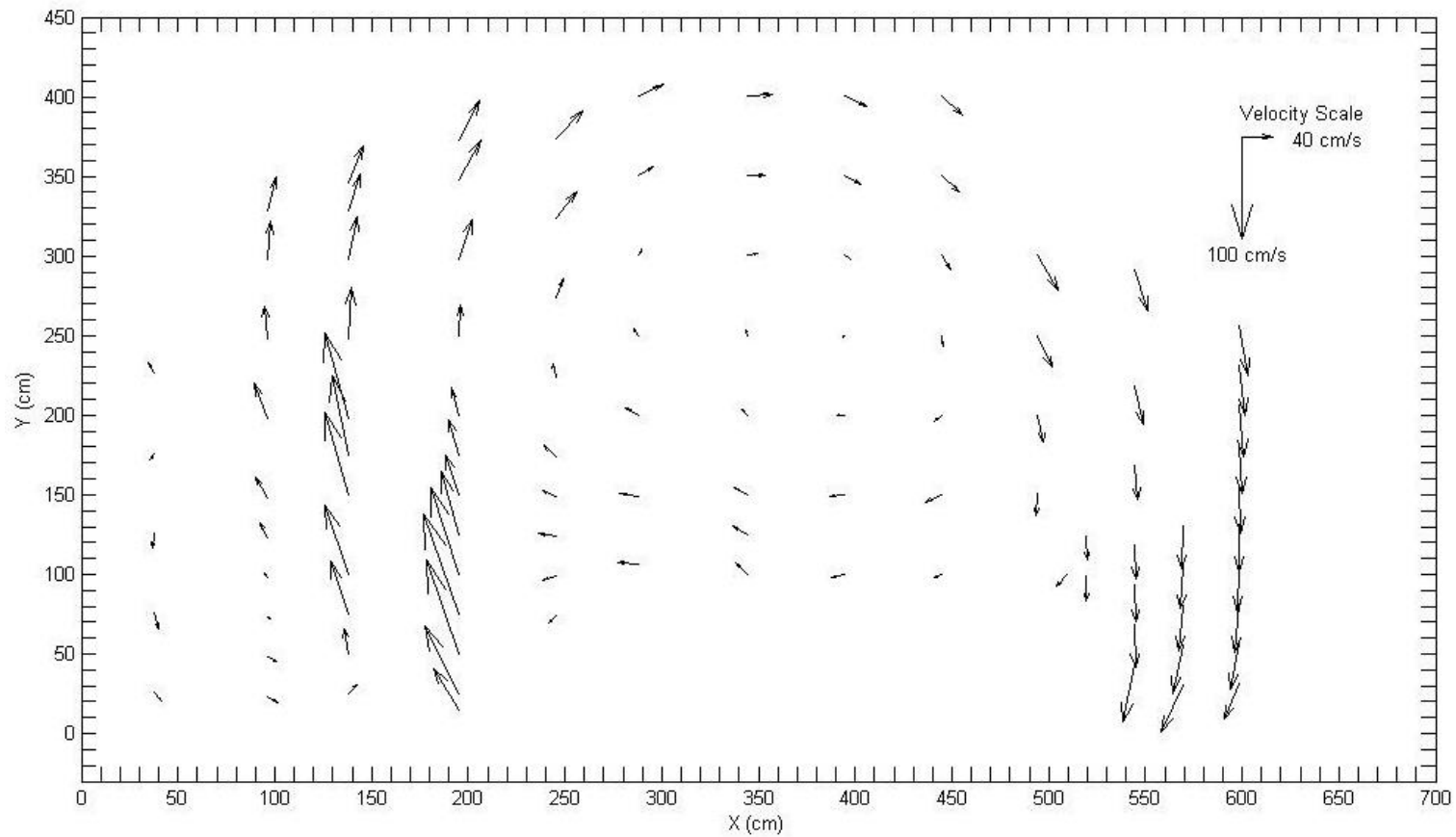


Figure 3.16 Time-averaged field velocities at a depth of 0.50 m below the water surface in Pool 13 of the Vianney-Legendre fishway.

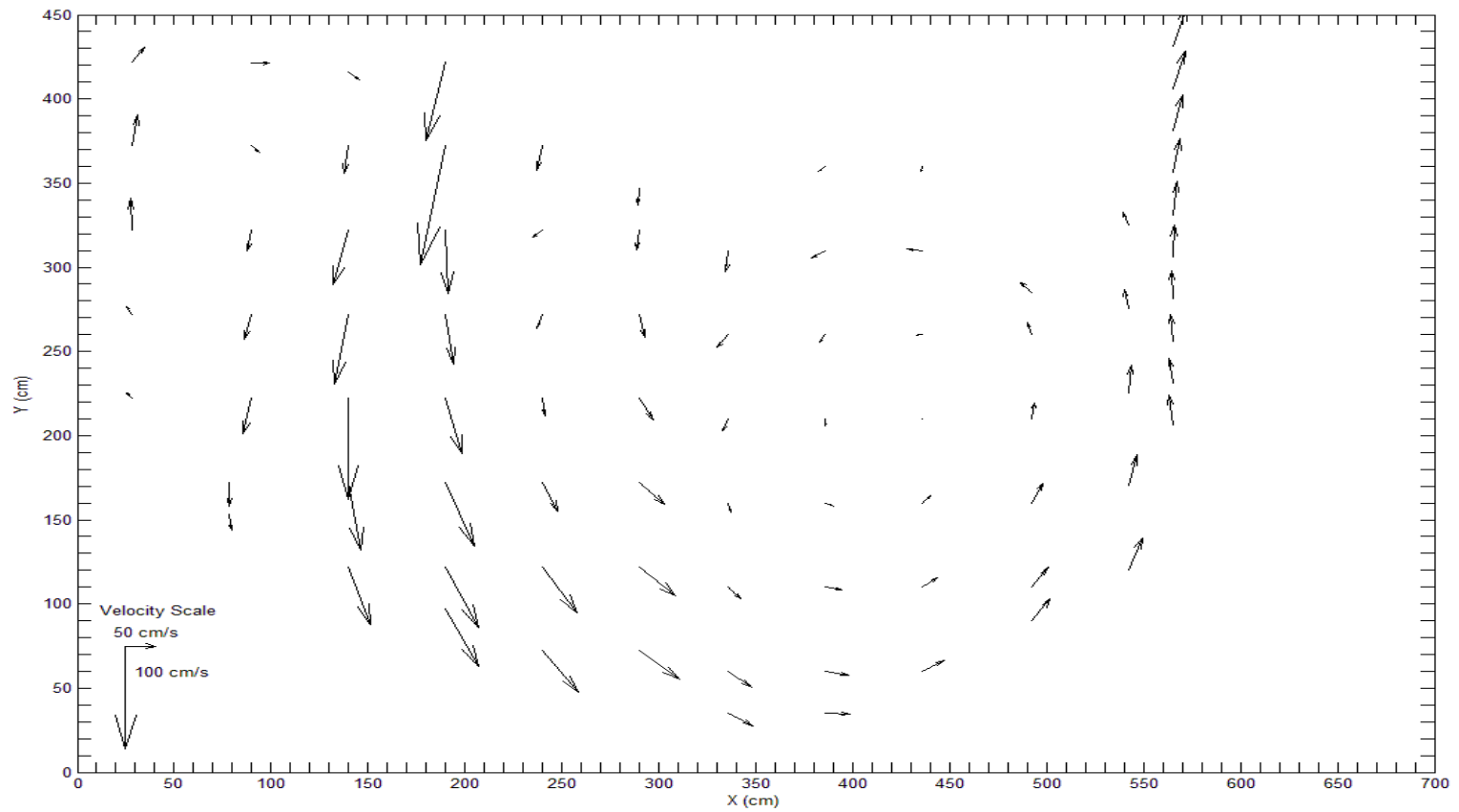


Figure 3.17 Time-averaged field velocities at a depth of 0.50 m below the water surface in Pool 8 of the Vianney-Legendre fishway.

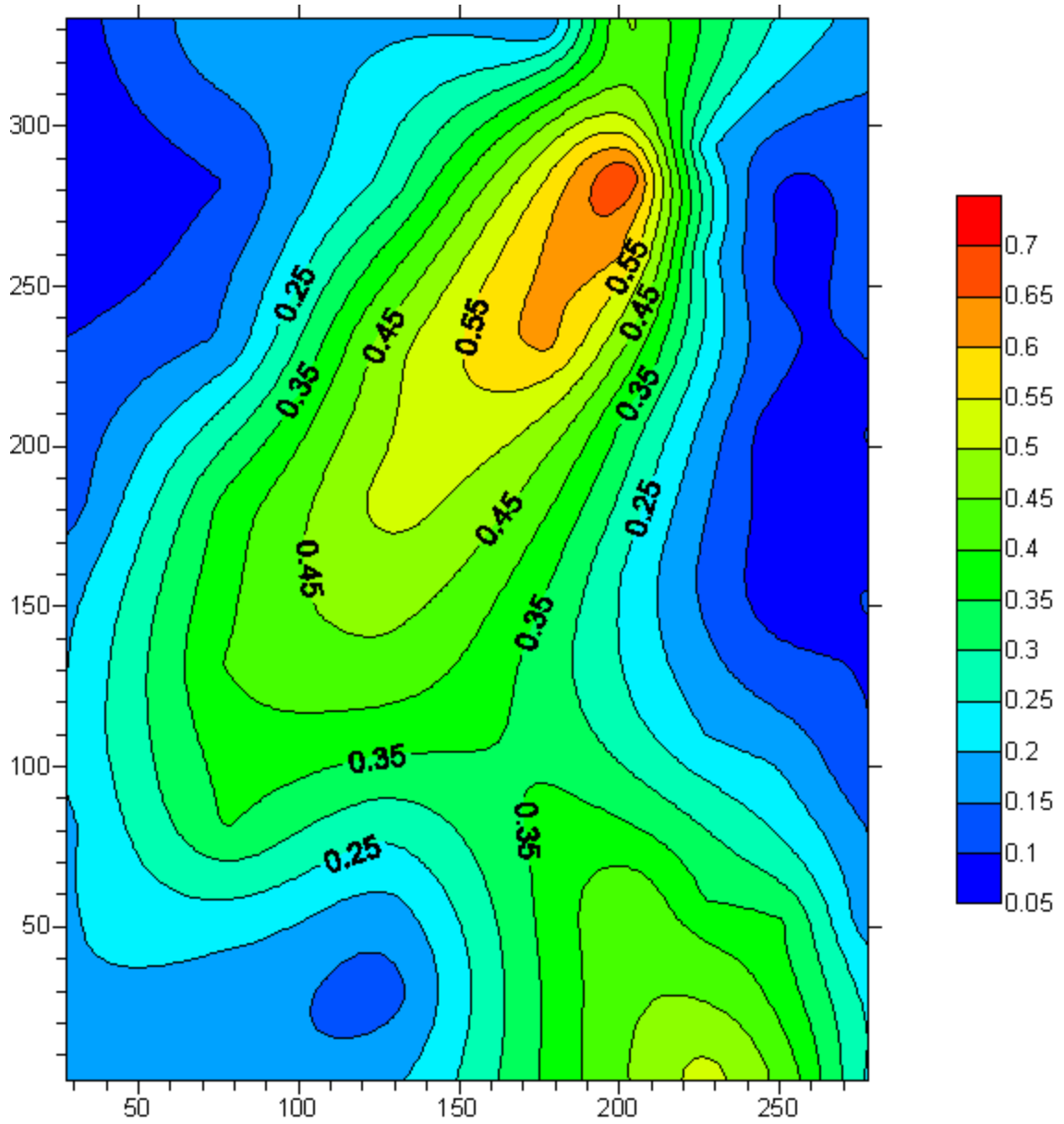


Figure 3.18 $K^{0.5}/V_{sm}$ in Pool 5 of the Vianney-Legendre fishway.

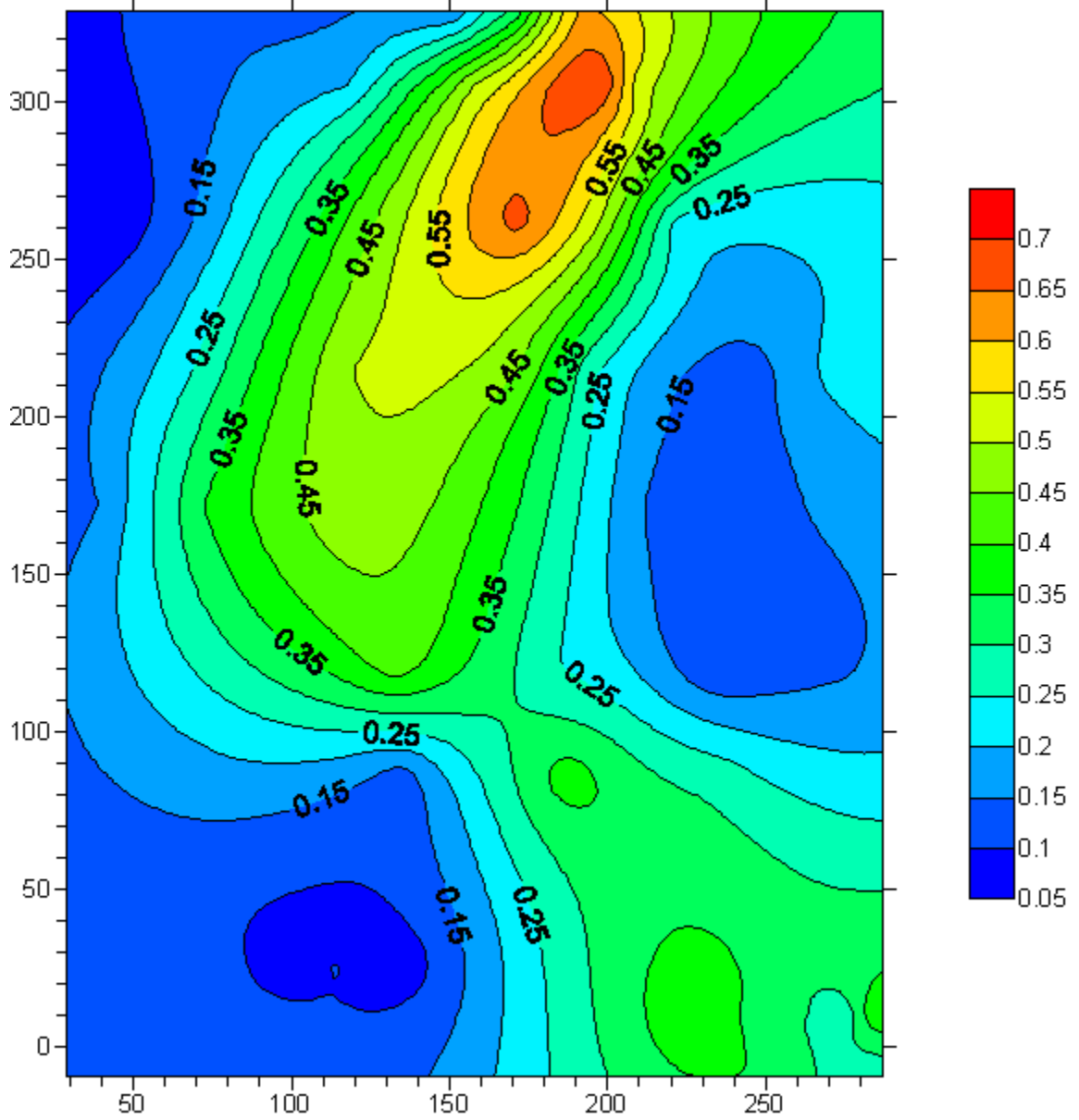
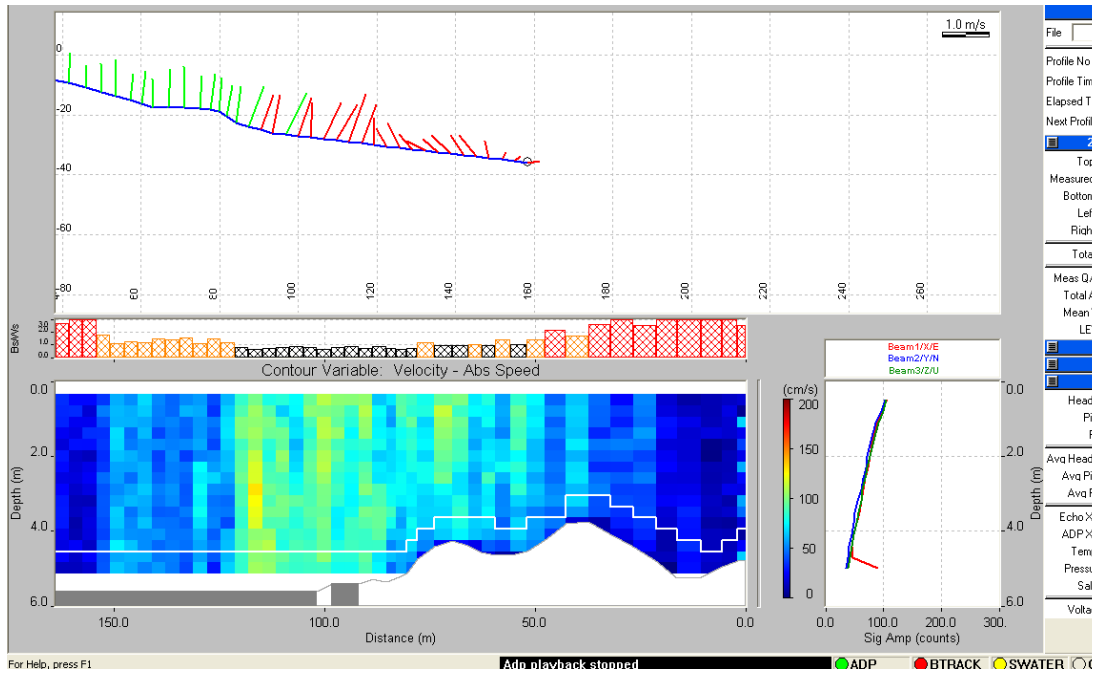
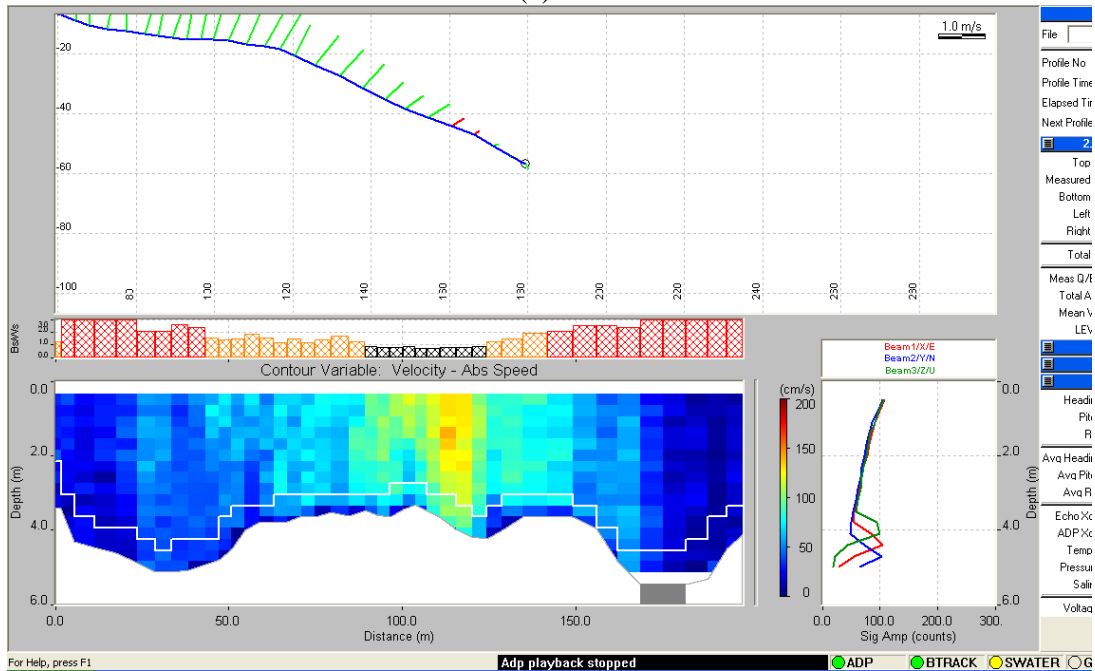


Figure 3.19 $K^{0.5}/V_{sm}$ in Pool 15 of the Vianney-Legendre fishway.

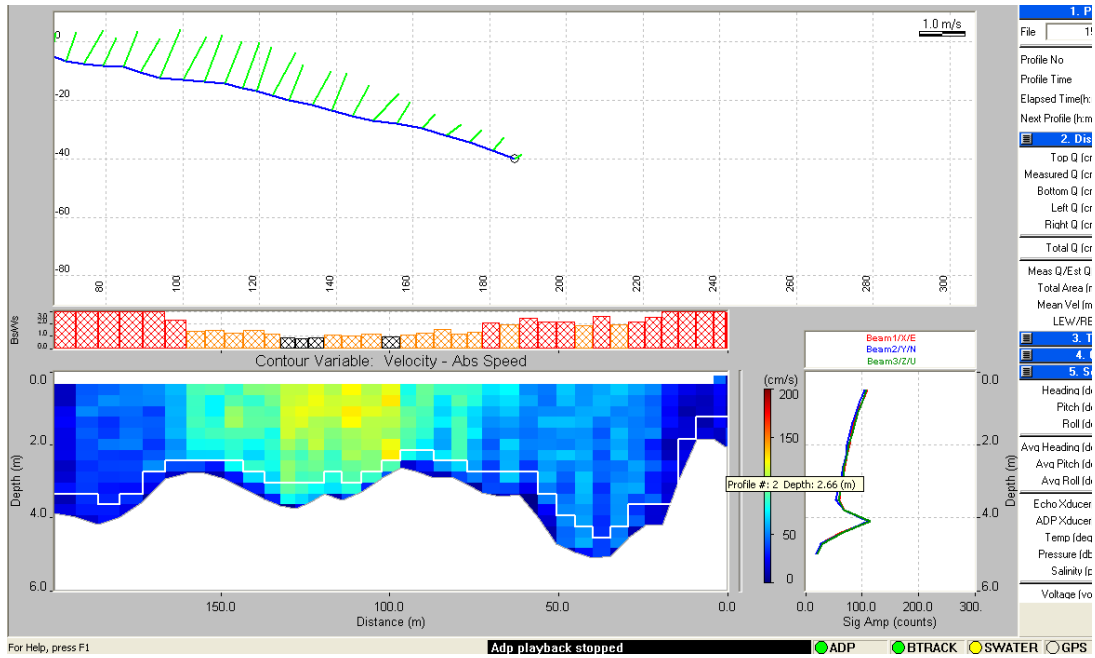


(a)

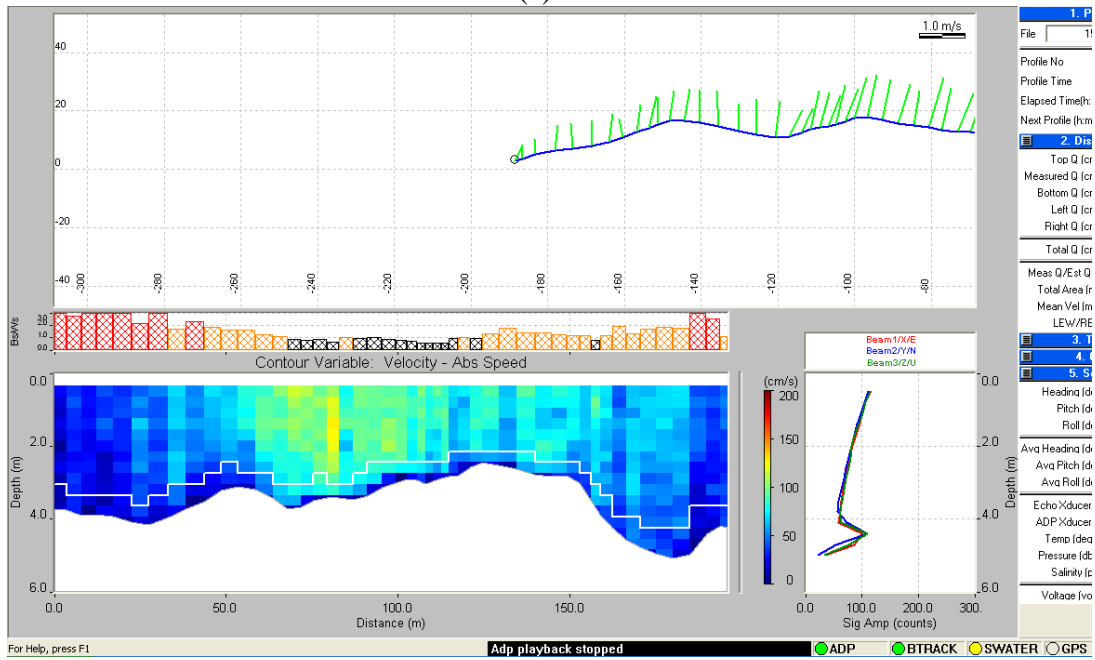


(b)

Figure 3.20 Acoustic Doppler Current Profiler Richelieu River flow rate measurement outputs 250 – 300 m downstream of the Saint Ours Dam: (a) Transect 1, (b) Transect 2, (c) Transect 3, (d) Transect 4.



(c)



(d)

Figure 3.20 - Continued

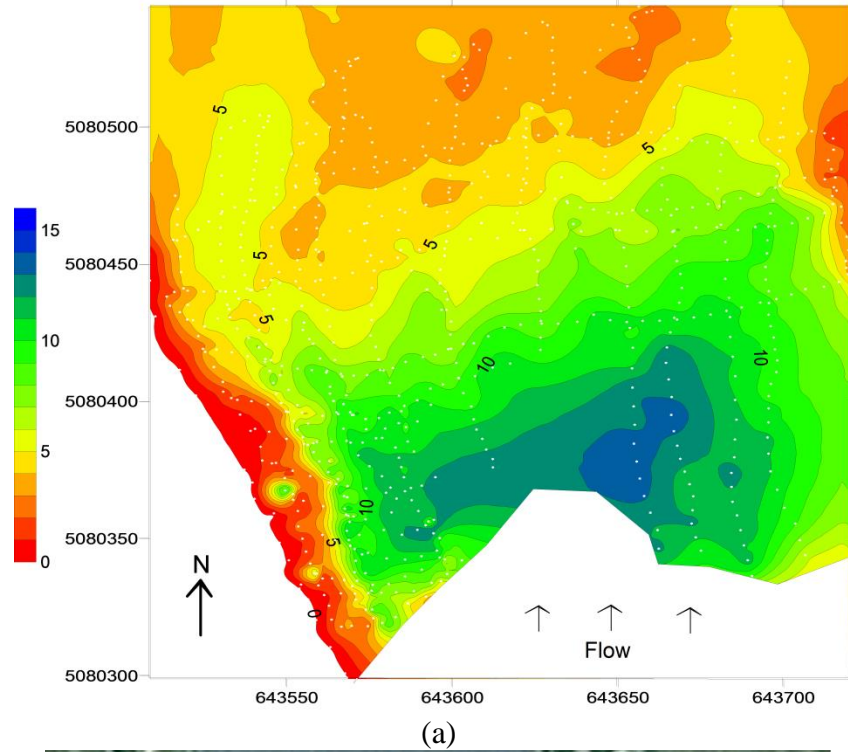


Figure 3.21 Tailrace of the Saint Ours Dam on the Richelieu River; (a) Contour map of water depths on June 7, 2012 (b) depth measurement point coordinates shown on satellite imagery.

CHAPTER 4

Field and numerical assessment of turning pool hydraulics in a vertical slot fishway.

4.1 Introduction

Fishways have been subject to much study to understand their biological effectiveness and to identify opportunities for refining their design to improve passage (reviewed in Bunt et al., 2012; Katopodis and Williams, 2012; Noonan et al., 2012; Roscoe and Hinch, 2010; Williams et al., 2012). However, one aspect of fish passage that has received little study is the hydraulics and passage efficiency of turning pools.

In cases where the difference between upstream and downstream water levels is greater than the maximum allowable design slope, more than one segment of linearly connected regular pools is required, leading to the use of turning pools. The primary functions of turning pools are to turn the flow, to minimize flow energy carry over between turning and regular pools, and to provide resting space for fish (Rajaratnam et al., 1997). Fishways with turning pools are more compact than equivalent fishways without turning pools as they economize on space and facilitate a more optimum location for the fish entrance (flow exit). Design guidelines recommend and field studies have confirmed that

The content of this chapter has been submitted for publication in Ecological Engineering as: Marriner et al. (Submitted). "Field and numerical assessment of turning pool hydraulics in a vertical slot fishway".

the fish entrance in a fishway be placed as close as possible to the hydraulic barrier, making it easier for fish to find (Bunt, 2001; Clay, 1961; Katopodis and Williams, 2012). The Seton River dam fishway in British Columbia, the Vianney-Legendre fishway in Quebec, and the Torrumbarry fishway in Australia are a few examples of vertical slot fishways with turning pools (Pon et al., 2009; Thiem et al., 2011; White et al., 2011).

Several biological studies have identified potential problems with turning pools (e.g., Bunt et al., 2000; Thiem et al., 2011; White et al., 2011). In a companion study of fish migration, Thiem et al. (2011) studied the movements of 88 adult lake sturgeons *Acipenser fulvescens* as they attempted upstream passage at the Vianney-Legendre vertical slot fishway in Quebec, Canada. Of 56 individuals that failed passage, 20 failed in the two turning pools (out of a total of 18 pools); and fish spent disproportionately longer time in the turning pools than in the regular pools. Additionally, bony herring *Nematalosa erebi*, silver perch *Bidyanus bidyanus*, and golden perch *Macquaria ambigua* also appeared to have difficulty negotiating turning pools in a fishway in Australia (White et al., 2011). There are a number of potential explanations including confusion associated with complex flows, flow characteristics that exceed the swimming abilities of fish, or fish could actually be using such areas to rest. Although the delays may be associated with use of the turning pools to rest, the fact that a number of studies have found failures associated with turning pools is suggestive that there may be hydraulic challenges that impede passage.

There have been few attempts to characterize the hydraulic conditions within turning pools and relate flow characteristics to fish behaviour. Rajaratnam et al. (1997) completed a laboratory scale model study of a turning pool in a Denil fishway, but no hydraulic studies have been conducted for turning pools in vertical slot fishways. Given the lack of existing hydraulic data accompanied by the comparatively low passage success rates there is cause for further study to evaluate and improve turning pool hydraulics, relative to fish passage.

Here we characterize turning pool hydraulics of the Vianney-Legendre vertical slot fishway, hereinafter called the site fishway, using field based measurements and computational fluid dynamics (CFD) modeling. In the spring of 2010 Thiem et al. (In press) tagged 18 species of fish during their successful upstream passage and Desrochers (2009) indicated that annually 36 species pass the fishway. It is one of few fishways worldwide to successfully pass a species of sturgeon, although delays and failures were noted for the species at turning pools (Thiem et al., 2011). In the case of the site fishway, three segments of regular pools are placed in series connected via two turning pools, creating a more compact design using a fold-back or staircase pattern, and thus making it a suitable model for a turning pool study.

We first describe the site fishway, and present the methods used to obtain velocity results from measurements taken in the two turning pools. We then present a CFD model study which assesses seven turning pool design geometry alterations with respect to velocity, turbulent kinetic energy, vorticity, and flow structure. Design 1 simulates the site fishway's downstream turning pool, Designs

2 – 7 have design elements altered from Design 1. Field results are used to validate the CFD model study findings. Results are discussed in the context of what the turning pool hydraulic conditions may mean to fish behaviour. It is hoped that the findings emanating from this study will help to supplement general fishway design guidelines and help to inform the design of turning basins that minimize delays and facilitate passage of fish.

4.2 Methods

4.2.1 Field Study

Fieldwork was conducted from July 18 – 29, 2011. Velocity point measurements were recorded in turning Pools 8 and 13 with a three-dimensional (3D) Acoustic Doppler Velocimeter (ADV). The ADV uses the Doppler shift to measure 3D point velocities (Nortek AS, 2009). Many recent fishway studies have used ADVs to measure 3D point velocities (e.g., Liu et al., 2006; Puertas et al., 2004, Silva et al., 2012). A grid spacing of 0.50 m x 0.50 m was used, with increased point densities in slot and jet flow areas. A total of 83 and 106 measurements were taken in Pools 8 and 13, respectively. The ADV field probe was submerged 0.50 m and fixed at that elevation for all points within the pool. The probe was mounted on a rigid frame constructed of modular t-slotted aluminum. The frame was mounted on pool walls to record measurements, see Chapter 3 for further details.

Velocity measurements were recorded for 180 seconds at a sampling frequency of 25Hz. Prior to data collection preliminary testing was done to

determine the required ADV sampling period for accurate time-averaged velocity measurements. Sample test periods of 30-120 seconds were taken; velocity became nearly constant after 45 seconds. Longitudinal, transverse, and vertical velocities (u , v , and w), corresponding to x , y , and z in the Cartesian coordinate system, were averaged over the sampling period to produce time-averaged velocities (\bar{u} , \bar{v} , and \bar{w}), see Figure 4.1. The manufacturer specifies that the velocity data collected with the ADV is accurate to $\pm 0.5\%$ of the measured value, with a maximum accuracy of ± 0.001 m/s (Nortek AS, 2009). The maximum velocity recorded was 1.4 m/s, with an accuracy of ± 0.007 m/s. Velocity data for this study is expressed to 0.01 m/s. The ADV used in this study has a correlation scale of 0-100% (Nortek AS, 2009). The scale ranges from no correlation at 0% to perfect correlation at 100%. For time-averaged velocity values a minimum correlation of 40% is generally taken as acceptable. All measurements had a correlation value above 40% and therefore are deemed accurate for time-averaged velocity calculations. A minimum correlation value of 80% is required to produce accurate turbulence values. Correlation of field measurements was less than 80% and therefore not suitable for turbulence calculations. A water level measuring data logger was used to record water levels in Pool 13 (Schlumberger Water Services, 2011). The loggers are accurate to ± 0.01 mH₂O, with a resolution of 0.002 mH₂O. Water level data presented to 0.01 m, with an accuracy of ± 0.01 m in this study. Measurements were taken on July 22, 2011 to assess the change in water levels between adjacent pools, Δh . These

measurements were recorded by hand, and are accurate to ± 0.01 m, see Chapter 3 for further details.

4.2.2 CFD Modeling

4.2.2.1 Governing Equations

A commercial software program was used to create a numerical model simulating Pools 11 – 15 (ANSYS, 2009). The model uses the finite volume method to solve the Reynolds averaged Navier-Stokes equation in three-dimensions. It models the *free surface*, the interface between air and water, following the volume of fluid (VOF) method. The VOF method solves a set of momentum equations through the domain, while maintaining a record of the volume of the two phases in each computational cell. The software program solves the continuity and momentum equations (in tensor form) as follows:

$$\begin{aligned} \frac{\partial \rho}{\partial t} + \frac{\partial \rho u_j}{\partial x_j} &= 0 \\ \frac{\partial \rho u_i}{\partial t} + \frac{\partial \rho u_j u_i}{\partial x_j} &= -\frac{\partial p}{\partial x_i} + \frac{\partial}{\partial x_j} \left\{ (\mu + \mu_t) \left(\frac{\partial u_i}{\partial x_j} + \frac{\partial u_j}{\partial x_i} \right) - \frac{2}{3} \rho TKE \delta_{ij} \right\} + (\rho - \rho_a) g_i \end{aligned} \quad (4.1)$$

where δ_{ij} is the Kronecker delta, g is the gravitational force, TKE is the turbulent kinetic energy, μ is the molecular viscosity of fluid, μ_t is the turbulent viscosity of fluid, p is the static pressure, ρ is the fluid density, and ρ_a is the density of air. The standard $TKE - \varepsilon$ model, where ε is the turbulent kinetic energy dissipation rate, was used to determine the turbulent viscosity (Launder and Spalding, 1974). Previously, Khan et al. (2006) used this model for a vertical slot fishway and

Kirkgoz et al. (2009) showed this model performed better than the $TKE - \omega$ model for predicting the velocity field over a chute spillway.

Equation 4.1 uses the volume fraction of air and water phases in the physical properties of density and viscosity. The phase-averaged density and viscosity are as follows:

$$\rho = \alpha_w \rho_w + \alpha_a \rho_a \quad (4.2)$$

$$\mu = \alpha_w \mu_w + \alpha_a \mu_a \quad (4.3)$$

where α is the volume fraction, with subscripts a and w representing the air and water phases. When modelling the free surface the transport equation is used to represent the water phase and is defined by:

$$\frac{\partial \alpha_w}{\partial t} + u_j \frac{\partial \alpha_w}{\partial x_j} = 0 \quad (4.4)$$

In this case the air phase volume fraction is determined from the constraint and the transport equation is simplified to:

$$\alpha_a = 1 - \alpha_w \quad (4.5)$$

Equation 4.5 is solved across the entire domain and the volume fraction is computed for all cells within the domain. In the main flow region cells are filled with water and $\alpha_w = 1$. In cells filled with air $\alpha_w = 0$. Interface tracking occurs in cells where $0 < \alpha_w < 1$. These cells contain a combination of air and water and are located on the *free surface*.

In a homogeneous model the mass transfer terms between phases are neglected (Fernandes et al., 2008 and 2009). Comparatively, the VOF model takes into account the surface tension along the phases interface. The simulations

ran in this experiment use the surface tension model continuum surface force (CSF) (Brackbill et al., 1992). CSF models the surface tension force as a volume force concentrated at the interface, as opposed to a surface force.

4.2.2.2 Boundary Conditions and Computational Mesh

The model's pool geometries match the dimensions of the field fishway. Boundary conditions are applied to all faces of the domain (pool walls and floor). The mass flow rate was specified at the upstream inlet boundary and atmospheric pressure was applied at the downstream boundary of the domain. At the upstream boundary the turbulence intensity (I) was set to 10% to take into account the effect of strong turbulence and recirculation in the flow field. However, it has been shown that the predicted velocities are graphically indistinguishable for 5, 10, and 20% turbulence intensities (Ma et al., 2002).

Given a known intensity the software program uses the following expressions to compute k and ε at the boundary inlet (ANSYS, 2009):

$$k_{in} = \frac{3}{2} I^2 u_{in}^2 \quad (4.6)$$

and

$$\varepsilon_{in} = \rho C_{\mu} \frac{k^2}{100 I \mu_t} \quad (4.7)$$

For the $k - \varepsilon$ turbulence model C_{μ} is the constant and has a value of 0.09. The no-slip condition and roughness heights of 0.00014m were applied to all of the model's surfaces. Roughness height values are representative of smooth concrete.

The top surface is an open boundary and is a pressure boundary allowing both inflow and outflow.

The model was simulated for two different scenarios. In the first scenario Δh between Pools 12 and 13 was set equal to 0.09 m which was measured in the field. V_{sm} in the field is equivalent to the CFD simulated value. The first is used for the purpose of comparing CFD simulated data to the field measured values in Pool 13. The second scenario has a larger Δh (0.11 m) and a 15% higher volumetric flow rate. This scenario produced larger velocities and represents spring conditions. Spring conditions were chosen because the site fishway is most frequently used in the spring months (Thiem et al., 2012). All results and discussion in this paper focus on the values simulated in the second scenario. In both scenarios at the inlet boundary an initial longitudinal velocity was fixed while transverse and vertical velocities were set to zero. At the outlet boundary, the initial pressure was assumed to be hydrostatic in the water region and zero in the air region. In addition to the velocity and hydrostatic pressure water levels were fixed at the inlet and outlet to specify the water volume fraction at the boundary.

The model uses an upwind scheme for advection. It also uses an unstructured tetrahedral mesh in the solution domain. The typical relative error between two successive iterations is 0.0001. For modeling purposes all fluids are assumed to be Newtonian, isothermal and incompressible. This allows model to keep their properties constant during simulations. All simulations were run under steady state conditions and the model converged after less than 600 iterations.

To determine the result's sensitivity to simulation grid size a mesh independency study was conducted using the simulation of Pool 13 (Design 1). Three mesh sizes were tested to assess the effect of mesh size on numerical results. The meshes are summarized in Table 4-1. Two points were selected to test the mesh independency. The first point was at (4.04, 2.86) and the second at (1.54, 1.86). The combined average velocity difference for both points is 0.014, 0.021 and 0.031 m/s when comparing mesh 1 to 2, mesh 2 to 3, and mesh 1 to 3, respectively. Figure 4.2 shows the results of the mesh independency test. After the test was completed all simulations were run with Mesh 3.

4.2.3 Design Modifications and Evaluation Criteria

CFD modeling was used to simulate the hydraulics of the existing conditions in Pool 13 (Design 1), see Figure 4.1. Six additional designs were simulated, Designs 2-7, each having geometric elements differing from Design 1, see Figure 4.3. A baffle wall is added to the pool's centre in Designs 2, 3, and 4. It is 0.30 m x 1.50 m in Designs 2 and 3, and 0.3 m x 2.0 m in Design 4. The purpose of adding a baffle wall is to reduce the size of the large vortex in Design 1 (see 4.3 Results) and to provide fish with resting space in the turning pools. The position is altered in these three designs to assess the influence position has on hydraulics. Alterations to the pool floor are made in Designs 5 and 6. In Design 5 the floor is sloping at 3.5%, a 0.225 m elevation drop from the upstream side wall to the downstream side wall. This is the maximum slope allowable given the restrictions of the connecting pools (Pools 12 and 14). The pool floor ramps from

the outer wall radially inward about the end of the centre wall at 10% in Design 6. These geometry alterations to the pool floor were tested to encourage flow in the downstream direction, and to reduce flow recirculation. Design 7 has a straight back wall; different from the semi-circular back wall in Designs 1-6. The straight back wall is less expensive to construct than a semi-circular back wall, making Design 7 a more cost effective alternative to the other designs. Design 7 turning pools have been constructed at vertical slot fishways (e.g., Seton River dam fishway, British Columbia (Pon et al., 2009)). Anecdotally, in the past where little assessment has been given to their hydraulics, designers may have defaulted to Design 7 turning pools because of cost savings, and limited hydraulic information available for alternatives.

Designs simulated in this study are evaluated on velocity, and two turbulence parameters, turbulent kinetic energy and vorticity. Velocity is typically the major consideration in fishways. To allow fish to ascend through the pool the maximum flow velocity must be less than the maximum attainable swimming speed. Typically, burst or prolonged modes are considered, a positive ground speed is required for successful passage (swimming speed must be greater than water velocity), and the combination of distance and velocity should not exceed endurance (Peake et al., 1997). Turbulent kinetic energy represents one turbulence parameter that could potentially affect fish passage through a fishway. Fish typically expend more energy swimming in comparatively high turbulent flows than in low turbulent flows (Enders et al., 2003, 2005), and have significantly lower swimming capabilities in turbulent flows as compared to

laminar flows (Pavlov et al., 2000). In fishways, preferences to areas with 'low' turbulent kinetic energy levels over areas of 'high' turbulent kinetic energy levels have been demonstrated, and a negative correlation exists between fish transit time (the length of time a fish requires to successfully ascend a fishway pool) and turbulent kinetic energy levels (Silva et al., 2012). Vorticity was used in design evaluation as recent studies assessing the effects of vortex size on the swimming capabilities of fish have found that when the diameter of a flow vortex oriented in the horizontal plane, D_v , exceeded 0.5 – 0.75 of fish body length, L_f , fishes swimming capabilities were challenged. Fish spun in an orientation consistent with the rotational axis of the vortices and translated downstream. To combat the loss of balance fish used their pectoral fins to restore spatial balance control, forcing them to expend more energy to maintain spatial balance control and leaving less energy to swimming speeds (Lupandin, 2005; Tritico and Cotel, 2010; Webb et al., 2010).

Time-averaged velocity magnitude, V , is defined as:

$$V = \sqrt{\bar{u}^2 + \bar{v}^2 + \bar{w}^2} \quad (4.8)$$

where \bar{u} , \bar{v} , and \bar{w} represent the longitudinal (x), transverse (y), and vertical (z) components of time-averaged velocity, respectively. Turbulent kinetic energy, TKE , is defined as:

$$TKE = \frac{1}{2} (u'^2_{rms} + v'^2_{rms} + w'^2_{rms}) \quad (4.9)$$

where u' , v' and w' are the stream-wise, cross-stream and vertical fluctuating velocities, respectively. TKE levels are categorized as 'low' for $TKE \leq 0.05 \text{ m}^2/\text{s}^2$

and 'high' for $TKE > 0.05 \text{ m}^2/\text{s}^2$ (Silva et al., 2012). Vorticity in the horizontal (x , y) plane, ω_z , is the magnitude of rotation about the z -axis and is defined as:

$$\omega_z = \frac{1}{2} \left(\frac{\partial \bar{u}}{\partial y} - \frac{\partial \bar{v}}{\partial x} \right) \quad (4.10)$$

where $\frac{\partial \bar{u}}{\partial y}$ and $\frac{\partial \bar{v}}{\partial x}$ are components of angular velocity in along the x -axis and y -axis, respectively. The vorticity calculated is time-averaged, assuming that the flow field is time averaged (Jamieson et al., 2013). ω_z levels are categorized as 'low' for $\omega_z \leq 3.0 \text{ s}^{-1}$ and 'high' for $\omega_z > 3.0 \text{ s}^{-1}$.

The average volumetric energy dissipation, $\bar{\varepsilon}$, in the turning pool is defined as:

$$\bar{\varepsilon} = \frac{\rho_w g Q \Delta h}{b_t l_t h} \quad (4.11)$$

where ρ_w is the density of water, g is the acceleration due to gravity, Q is the fishway's average volumetric flow rate, and h is the depth of flow. In Equation 4.11, $\rho_w g Q \Delta h$ represent the energy dissipation and $b_t l_t h$ is the volume of water in a rectangular turning pool. Note that Pools 8 and 13, and Designs 1-6 have a semi-circular back wall. Equation 4.11 over estimates the volume of water in these pools by approximately 30%. For Pool 13, $\Delta h = 0.09 \text{ m}$, $h = 2.34 \text{ m}$, $Q = 1.63 \text{ m}^3/\text{s}$; and $\bar{\varepsilon}$ is $38 \text{ W}/\text{m}^3$ (including 30% volume correction). $\bar{\varepsilon}$ is less than the calculated range, $\bar{\varepsilon} = 92 - 180 \text{ W}/\text{m}^3$ for a regular pool (Liu et al., 2006).

4.3 Results

4.3.1 Field Results and CFD Model Validation

The maximum measured slot velocity, V_{sm} , is 1.40 m/s in Pools 8 and 1.15 m/s in Pool 13. During the 2011 field study high water levels downstream of the site dam effected pool water levels. As a result fishway pool water levels increased in the downstream direction and the difference in water levels between adjacent pools decreased in the downstream direction. Accordingly, $\Delta h=0.17$ m between Pools 7 and 8, and $\Delta h=0.09$ m between Pools 12 and 13. As expressed in Equation 3.12 below, the comparatively greater Δh between Pools 7 and 8 produced a greater V_{sm} magnitude. The theoretical maximum slot velocity, V_{theor} :

$$V_{theor} = \sqrt{2g\Delta h} \quad (4.12)$$

is derived from the Bernouli equation. Assuming velocities in the pools are negligible, water elevation difference between adjacent pools produces a maximum velocity magnitude in the slot area of V_{theor} (Liu et al., 2006). In Pool 13 $V_{theor} = 1.33$ m/s is 15% greater than V_{sm} . Therefore, V_{theor} can be used to reliably estimate V_{sm} in turning pools. This agrees with results from regular pool research where V_{theor} is approximately equal to V_{sm} (Liu et al., 2006).

The mean vertical velocity, \bar{w}_{mean} , is -0.01 m/s in both pools. The maximum absolute vertical velocity, \bar{w}_{max} , is 0.15 m/s and 0.14 m/s in Pools 8 and 13, respectively, which is less than $0.1V_{sm}$ in both pools. The comparatively low vertical velocities show turning pool flows are primarily in the x, y plane as is characteristic in regular pools (Liu et al., 2006; Puertas et al., 2004).

The velocity field diagram for Pool 13 is shown in Figure 4.4. It presents the \bar{u} , \bar{v} velocity vectors in the x, y plane at an elevation of 1.74 m above the pool floor (approximately 0.50 m below the water surface). Pools 8 and 13 have a

common flow pattern. Flow enters the pool through the upstream slot as a jet, flows with high velocity towards the back wall, turns flowing along the semi-circular back wall, and flows out through the downstream slot. A large recirculation area, or vortex, forms in the centre of the pool. A second, smaller recirculation area is located in the upstream corner of the pool between the long baffle and side walls. These two areas are characterized by low velocities and recirculating flow. The large vortex is 3.0 m long, l_v , and 2.1 m wide, b_v , in Pools 8 and 13.

For scenario one the flow pattern simulated in Design 1 is consistent with the field pattern measured in Pool 13, see Figure 4.4. In both Pool 13 and Design 1 the large vortex in the centre of the pool is equal in length and width, see Table 4-2. Figure 4.4 compares the field velocity data measured in Pool 13 to the CFD simulated velocities of Design 1 at an elevation of 1.74 m above the pool floor. All 106 field measurements were used for comparison. The mean absolute error (MAE), $MAE = |CFD \text{ predicted velocity} - \text{measured mean velocity}|$, was 0.06 m/s. The value of Δh between Pools 12 and 13 is equal to 0.09 m and V_{sm} is equal to 1.15m/s for both field measurements and CFD simulated results. This demonstrates agreement between field measured and CFD simulated velocity data.

4.3.2 CFD Model Results

Velocity, turbulent kinetic energy, and vorticity results are presented for Designs 1, 3, 4, 6, and 7. Adding a 1.5 m x 0.3 m baffle wall to the centre of the pool,

perpendicular to the back wall, in Design 2 did not significantly vary from the hydraulics from Design 1; nor did a 3.5% slope of the pool floor, in Design 5. Consequently, the hydraulics of Designs 2 and 5 have been omitted. Results were simulated for depths of $z = 0.13h$, $0.5h$, and $0.8h$; where z is measured from the pool floor upwards. These three depths represent the full height of the water column (Silva et al., 2011). Note that $0.13h$ is 0.30 m above the pool floor in this study's set of simulations and represents the hydraulics a fish swimming along the bottom of the pool would encounter and was selected because sturgeon are typically considered a benthic species.

As shown in Figures 4.5 and 4.6, the slot entrance holds the maximum flow velocity for all designs. The maximum simulated jet velocity in the slot, V_0 , ranged from 1.3 – 1.4 m/s in the 7 designs tested. V_0 is consistent through the full height of the water column for all designs. This is demonstrated in Figure 4.5 for Design 1, where $V_0 = 1.35\text{-}1.4$ m/s at $z = 0.13h$, $0.5h$, and $0.8h$.

The flow pattern in Design 1 is consistent with the pattern in Pool 13. The large vortex in the centre of the pool is 3.0 m x 2.1 m. Vortex dimensions are summarized in Table 4-2 and flow patterns for all designs are shown in Figures 4.5 and 4.6. The flow pattern and vortex dimensions in Design 6 are consistent with Design 1. However, the ramping floor accelerates flow around the back wall producing comparatively larger velocities through the downstream section of the pool. The straight back wall gives Design 7 a comparatively larger pool volume, correspondingly the vortex (3.2 m x 2.5 m) in the centre of the pool is larger than in other designs. A low velocity zone forms in the upstream back corner of the

pool in Design 7. The baffle wall added to Designs 3 and 4 alters size and shape of the large recirculation area. In Design 3 jet flow is forced through the centre of the pool, inside of the centre baffle wall. A large recirculation zone (1.9 m x 2.0 m) forms between the jet flow and centre wall. Recirculation areas also form upstream (1.3 m x 4.5m) and downstream (1.8 x 1.3 m) of the centre baffle wall. In Design 4 the centre baffle wall forces high velocity flow around the back wall, and smaller recirculation zones form on both sides of the centre baffle wall. The upstream vortex is 0.9 m x 2.0 m, and the downstream vortex is 1.4 x 2.0 m.

The variation of maximum velocity, V_m , as flow travels through the pool from entrance to exit is shown in Figure 4.7, where x_m is the distance from the entrance slot along the flow path of V_m . As demonstrated by Design 1 in Figure 4.7 the patterns of V_m are nearly uniform at $z = 0.13h$, $0.5h$, and $0.8h$; this is also characteristic of the other designs tested. In Designs 1, 4, 6, and 7 V_m decays rapidly over $x_m < 2.5$ m. At $x_m \cong 2.5$ m decay stops after reaching minimum magnitudes of $0.4-0.6V_{sm}$. Through the middle of the pool, $2.50 \text{ m} < x_m \leq 9.0 \text{ m}$, V_m is nearly constant. In this section Design 4 maintains the lowest velocities, $V_m = 0.53-0.55 \text{ m/s}$, while V_m in Designs 1, 6, and 7 are $0.1-0.2 \text{ m/s}$ greater. In the downstream section ($x_m > 9.0 \text{ m}$), velocities increase linearly, reaching maximums in the downstream slot. The flow path length is approximately 11 m in these designs. The center baffle wall position in Design 3 forces V_m through the centre of the pool. As a result V_m in Design 3 follows a flow path approximately 4.0 m shorter than in other designs and has comparatively greater V_m magnitudes through the pool.

The rate of V_m decay is compared to that of a plane turbulent jet, and to a regular pool in Figure 4.8. In the designs simulated, for $x_m < 2.5$ m, V_m decays at a linear rate described as:

$$\frac{V_m}{V_j} = 1 - 0.05 \frac{x_m}{0.5b_0}. \quad (4.13)$$

The decay of a plane turbulent jet is described as (Rajaratnam, 1976):

$$\frac{V_m}{V_j} = \frac{3.5}{\sqrt{\frac{x_m}{0.5b_0}}} \quad (4.14)$$

The decay of a regular pool is described as (Liu et al., 2006):

$$\frac{V_m}{V_j} = 1 - 0.035 \frac{x_m}{0.5b_0}. \quad (4.15)$$

The decay of V_m in the turning pool does not correlate to the decay in a turbulent plane jet. This is because the potential core of a turbulent plane jet is $6b_0$; at $x_m = 6b_0$ velocity in the turning pool is no longer in decay. Therefore, before a turbulent plane jet begins to decay, turning pool decay is complete. As expressed in Equations 4.13 and 4.15 the velocity decays faster in the turning pool as compared to a regular pool. The more rapid decay is thought to be caused by the 180° turn required in the pool. The controlling factor for velocity decay stopping and reaching a minimum V_m at $x_m \cong 2.5$ m appears to be the distance from the slot entrance to the back wall. In the designs simulated this distance is 4.46 m measured in the y-direction. As shown in Figures 4.5 and 4.6 V_m decays from the slot entrance until $x, y = (2.5 \text{ m}, 3.22 \text{ m})$, approximately 1.24 m from the back wall. At this point V_m becomes constant as it turns and flows along the back wall. As the amount of velocity decay occurring in the turning pool appears to be

proportional to the distance from the slot to the back wall, further study is required investigating this relationship. Testing a variety of lengths will determine the dimensions that produce maximum velocity decay. Similar to studies completed in regular pools, assessing a variety of design dimensions is required to develop recommended geometries for turning pools (Rajaratnam et al., 1992). Similar to a regular pool, the rapid velocity decay in the turning pool is thought to be caused by the recirculating flows that surround the jet (Liu et al., 2006).

Velocity distributions were taken perpendicular to the jet trajectory to understand the structure of flow in different sections of the pool. Distributions were taken from the centre of the pool, at $(x, y, z) = (3.15, 1.31, 0.5h)$, to the outer wall at angles, θ , see Figure 4.1, of $-44^\circ, -27^\circ, 0^\circ, 22.5^\circ, 45^\circ, 67.5^\circ, 90^\circ, 112.5^\circ, 135^\circ, 157.5^\circ, 180^\circ$, and 200° . The line of $\theta = 0^\circ$ is from $(0, 1.31, 0.5h)$ to $(3.15, 1.31, 0.5h)$, is parallel to the baffle walls, θ increases in the clockwise direction, and V_m is the maximum velocity. The velocity distributions at $\theta = -22^\circ, 67.5^\circ$, and 157.5° are presented in Figure 4.9, where r is the radial distance from $(3.15, 1.31, 0.5h)$ in the direction of θ .

At $\theta = -27^\circ$, upon entering the pool through the upstream slot the velocity distribution is of Gaussian distribution similar to a plane turbulent jet, see Figure 3.10 (Rajaratnam, 1976). The velocity profile is approximately a turbulent plane jet for $-0.95b_0 < x_r < 0.95b_0$, where x_r is the radial distance from V_m . The scatter outside is caused by recirculating flows on either side of the jet. In this profile V_m ranges from 1.13-1.15 m/s at $r = 1.27$ -1.42 m; the jet width at $V = \frac{1}{2} V_m$, is 0.70 m

= $1.15 b_0$. In Designs 1, 4, 6, and 7 the velocity profile changes from a Gaussian distribution as θ increases. At $\theta = 67.5^\circ$, as shown in Figure 4.9, the maximum velocity ($V_m = 0.59 - 0.67$ m/s) is comparatively less than at $\theta = -27^\circ$ and occurs at $r = 2.49$ m. Velocity exceeds $\frac{1}{2} V_m$ over a width of 1.44 m = $2.36 b_0$, and has a range of $0.16-0.63$ m/s. Here the velocity increases radially away from the pool centre; reaching a maximum velocities in the outer portion of the pool. At $\theta = 112.5^\circ$, as shown in Figure 4.9, maximum velocity ($V_m = 0.57-0.72$ m/s) occurs at $r = 3.15$ m. Velocity ranges from $0-0.72$ m/s, and increases radially away from the pool centre reaching a maximum velocity adjacent to the side wall. This distribution is followed until high velocity flow moves off the side wall and enters the downstream slot at $\theta=200^\circ$. The centre baffle wall forces flow through the middle of the pool in Design 3 and forces flow to maintain a bell shaped distribution at $\theta = 67.5^\circ$, and 112.5° .

In all designs the pool's maximum turbulent kinetic energy is in the upstream slot, TKE_{max} , see Figure 4.10. TKE_{max} is lowest at $0.13h$ and highest at $0.8h$, increasing with elevation through the water column. In Design 1, TKE_{max} is 0.072 m^2/s^2 at $z = 0.13h$, 0.108 m^2/s^2 at $z = 0.8h$, and 0.119 m^2/s^2 at $z = 0.8h$. The rate of increase is similar in the other designs. In the 7 designs tested TKE_{max} ranged from $0.061 - 0.105$ m^2/s^2 at $z = 0.13h$, $0.099 - 0.120$ m^2/s^2 at $z = 0.5h$, and $0.110 - 0.128$ m^2/s^2 at $z = 0.8h$. Despite the increase with elevation, the pattern is consistent in all designs through the water column. Turbulent kinetic energy levels are lower in the pool than at the slot. At $z = 0.5h$ the maximum turbulent kinetic energy in the pool ranged from $0.075 - 0.078$ m^2/s^2 . Excluding the

upstream slot maximum TKE levels occurred along the upstream side wall at the beginning of the arcing back wall in Designs 1, 4, 6, and 7, and at the upstream edge of the vertical wall in Design 3. Throughout the remainder of the pool TKE levels are lower. Through the full height of the water column levels are 'high' ($TKE > 0.05 \text{ m}^2/\text{s}^2$) at TKE_{max} and at the point of maximum TKE in the pool, and 'low' ($TKE \leq 0.05 \text{ m}^2/\text{s}^2$) in the rest of the pool. Typically, $TKE < 0.02 \text{ m}^2/\text{s}^2$ in the downstream half of the pool.

For all designs vorticity in the horizontal plane, ω_z , is highest adjacent to the entrance and exits slots, see Figure 4.11. The maximum vorticity magnitudes ranged from $7.2 - 10.5 \text{ s}^{-1}$, and ω_z was uniform at the three depths evaluated. Areas where ω_z exceeds 5.0 s^{-1} are very small. Throughout the pool ω_z is typically less than 3.0 s^{-1} .

4.4 Discussion and Concluding Remarks

Velocity and turbulence results for turning pools in this study were found to be comparable to regular pools in vertical slot fishways. For Designs 1, 4, 6, and 7 flow structure is a turbulent plane jet in the upstream section of the pool. The structure changes as flow moves into the middle of the pool, where velocity increases radially from the centre to the outside of the pool. This distribution is held until flow enters the downstream slot. The rate of V_m decay is linear for $x_m < 2.5 \text{ m}$, then velocity is constant through $x_m \cong 2.5 \text{ m} - 9.0 \text{ m}$, and then V_m rapidly increases for $x_m > 9.0 \text{ m}$ until reaching the downstream slot. It appears the extent of decay is proportional to the distance between the entrance slot and the back

wall, further study is needed to determine the length which will maximize velocity decay. Extending a baffle wall into the centre of the pool from the back wall, as per Design 3, deflects high velocity flow through the centre of the pool. As a result V_m travels a shorter flow distance, with greater V_m magnitudes as compared to other designs. Extending a baffle wall into the centre of the pool from the centre wall, reduces V_m magnitudes through the pool. Consequently, V_m magnitudes in Design 4 are lower than other designs.

The maximum measured slot velocity measured in the field and the maximum jet velocities simulated in the 7 designs are within a passable range for adult lake sturgeon when adopting a prolonged swimming mode (Peake et al., 1997) and should not hinder upstream passage. Average volumetric energy dissipation ($\bar{\epsilon}$) was calculated at 29 W/m^3 in the turning pool. Volumetric energy dissipation is generally considered acceptable if $\bar{\epsilon} < 200 \text{ W/m}^3$ for salmonids, and if $\bar{\epsilon} < 150 \text{ W/m}^3$ for cyprinids (Larinier, 2008; Rodriguez et al., 2006). Kynard et al. (2011) observed successful passage of cultured lake sturgeon through a side-baffle spiral fishway when $\bar{\epsilon}$ was 196 W/m^3 . As compared to an adjacent regular pool, the width of a turning pool in the site fishway is twice the size which reduces the average volumetric energy dissipation by half.

In all simulated designs the maximum turbulent kinetic energy (TKE_{max}) was in the upstream slot and increased with elevation through the water column. Maximum turbulent kinetic energy was typically only categorised as high ($TKE > 0.05 \text{ m}^2/\text{s}^2$) in the vertical slots, and low ($TKE < 0.05 \text{ m}^2/\text{s}^2$) throughout the remainder of the pool for all designs. Comparatively, maximum turbulence levels

have been measured at $0.113 \text{ m}^2/\text{s}^2$ in a regular pools (Liu et al., 2006), $0.0676 \text{ m}^2/\text{s}^2$ in pool-type fishway (Silva et al., 2011), $0.4 - 1.2 \text{ m}^2/\text{s}^2$ in a pool with orifice fishway (Guiny et al., 2005), and $0.6 \text{ m}^2/\text{s}^2$ in a culvert retrofitted with baffles for fish passage (Morrison et al., 2008). The lower turbulence closer to the pool floor indicates that benthic species will typically incur a lower energetic cost during fishway ascension, although the threshold at which fishes are negatively affected by *TKE* may vary between species. Maximum vorticity ranged from $7.2 - 10.5 \text{ s}^{-1}$ and occurred adjacent to the entrance and exit slots. Further study is needed to identify the levels where individual species are affected by turbulent kinetic energy and vorticity.

Vortices with length and width dimensions greater than L_f of the largest fish using the site's fishway (Thiem et al., 2011; Thiem et al., In press) were present in all designs, and could potentially disorient or destabilize fish (e.g., Tritico and Cotel, 2010; Webb et al., 2010; Silva et al., 2012). The addition of a baffle wall to the centre of the pool in Designs 3 and 4 reduced the size of the large vortex by splitting it into smaller vortices. In both designs the downstream vortex has low velocities ($V \leq 0.2 \text{ m/s}$) and is hydraulically suitable to act as a resting area for migrating fish, as recommended by some authors including for sturgeon fishway passage (e.g., Webber et al., 2007). The other designs tested do not have areas suitable to act as resting areas, and Design 4 is recommended over Design 3 due to the lower pool velocities observed. In Design 4 the ratio of centre baffle wall to length of turning pool is approximately 3:5. This ratio is recommended from this study, further investigation may be required to optimize

this ratio. The addition of a baffle wall to Design 7, as per the dimensions and position of the baffle wall in Design 4, would make it a recommendable alternative to Design 4. This will reduce the size of the large vortex in the pool and provide a low velocity zone suitable for fish to rest. The straight back wall in Design 7 is less expensive to build than the semi-circular back wall in the other designs. Therefore, by adding a baffle wall to its centre Design 7 becomes a less expensive design alternative to Design 4 and is recommended for further study. To further advance the science of fish passage design, particularly for turning pools in vertical slot fishways, it is necessary to construct and field test the hydraulics and fish passage performance of the recommended designs outlined in this paper. Anecdotally, a primary function of turning pools is to provide resting areas to fish (Rajaratnam et al., 1997). However, the research conducted here in terms of field hydraulic measurements, and CFD modeling as well as observations from field studies of sturgeon passage reveals that some turning pool designs fail to provide resting opportunities and may represent confusing and challenging hydraulic features. Additional research on the biological and hydraulic aspects of turning pools is needed to improve guidelines, inform future designs, and to potentially enable the modification of existing ones.

4.5 References

- ANSYS Incorporated. 2009. ANSYS CFX-Solver Theory Guide. ANSYS Inc. Canansburg, PA.
- Brackbill, J., Kothe, D., Zemach, C., 1992. A continuum method for modeling surface tension. *J. Comput. Phys.* 100, 335-354.
- Bunt, C.M., 2001. Fishway entrance modifications enhance fish attraction. *Fish. Manag. and Ecol.* 8, 95-105.
- Bunt, C.M., Castro-Santos, T., Haro, A., 2012. Performance of fish passage structures at upstream barriers to migration. *River Res. Appl.* 28, 457-478.
- Bunt, C.M., Cooke, S.J., McKinley, R.S., 2000. Assessment of the Dunnville fishway for passage of walleyes from Lake Erie to the Grand River, Ontario. *J. Great Lakes Res.* 26, 482-488.
- Clay, C.H., 1995. Design of fishways and other fish facilities, second ed. Lewis Publishers, Ann Arbor, Michigan.
- Enders, E.C., Boisclair, D., Roy, A.G., 2003. The effect of turbulence on the cost of swimming for juvenile Atlantic salmon. *Can. J. Fish. Aquat. Sci.* 60, 1149-1160.
- Enders, E.C., Boisclair, D., Roy, A.G., 2005. A model of total swimming costs in turbulent flow for juvenile Atlantic salmon (*Salmo salar*). *Can. J. Fish. Aquat. Sci.* 62, 1079-1089.
- Fernandes, J., Lisboa, P., Simoes, P., Mota, J., Saadjan, E., 2009. Application of CFD in the study of supercritical fluid extraction with structured

- packing: wet pressure drop calculations. *J. Supercrit. Fluids*. 50(1), 61-68.
- Fernandes, J., Simoes, P., Mota, J., Saatdjian, E., 2008. Application of CFD in the study of supercritical fluid extraction with structured packing: dry pressure drop calculations. *J. Supercrit. Fluids*. 47(1), 17-24.
- Guiny, E., Ervine, D., Armstrong, J., 2005. Hydraulic and biological aspects of fish passes for atlantic salmon. *J. Hydraul. Eng.* 131(7), 542-553.
- Hatry, C., Binder, T.R., Thiem, J.D., Hasler, C.T., Smokorowski, K.E., Clarke, K.D., Katopodis, C., Cooke, S.J., In press. The status of fishways in Canada: trends identified using the national CanFishPass database. *Rev. Fish Biol. Fish.*
- Jamieson, E., Rennie, C., Townsend, R., 2013. Turbulence and vorticity in a laboratory channel bend at equilibrium clear-water scour with and without stream barbs (submerged groynes). *J. Hydraul. Eng.* 139(3), 259-268.
- Katopodis, C., Kells, J.A., Acharya, M., 2001. Nature-like and conventional fishways; alternative concepts?. *Can. Water Resour. J.* 26, 211-232.
- Katopodis, C., Williams, J.G., 2012. The development of fish passage research in a historical context. *Ecol. Eng.* 48, 8-18.
- Khan, L. A., 2006. A three-dimensional computational fluid dynamics (CFD) model analysis of free surface hydrodynamics and fish passage energetics in a vertical-slot fishway. *N. Am. J. Fish. Manag.* 26, 255-267.
- Kirkgoz, M.S., Akoz, M.S., Oner, A.A., 2009. Numerical modeling of flow over a chute spillway. *J. Hydraul. Res.* 47(6), 790-797.

- Kynard, B., Pugh, D., Parker, T., 2011. Passage and behaviour of cultured lake sturgeon in a prototype side-baffle fish ladder: I. ladder hydraulics and fish ascent. *J. Appl. Ichthyol.* 27 (Suppl. 2), 77-88.
- Larinier, M., 2008. Fish passage experience at small-scale hydro-electric power plants in France. *Hydrobiologia*, 609, 97-108.
- Lauder, B., Spalding, D., 1974. The numerical computation of turbulent flows. *Comput. Methods Appl. Mech. Eng.* 3(2), 269-289.
- Liu, M., Rajaratnam, N., Zhu, D.Z., 2006. Mean flow and turbulence structure in vertical slot fishways. *J. Hydraul. Eng.* 132(8), 765-777.
- Lupandin, A.I., 2005. Effect of flow turbulence on swimming speed of fish. *Bio. Bull.* 32(5), 461-466.
- Ma, L., Ashorth, P.I., Best, J.L., Elliott, L., Ingham, D.B., Whitcombe, L.J. 2002. Computational fluid dynamics and the physical modelling of an upland urban river. *Geomorphology.* 44, 375-391.
- Marriner, B.A., Baki, A.B., Zhu, D.Z., Thiem, J.D., Cooke, S.J., Katopodis, C. Submitted for publication. Field and numerical assessment of turning pool hydraulics in a vertical slot fishway. *Ecol. Eng.*
- Morrison, R., Hotchkiss, R., Stone, M., Thurman, D., Horner-Devine, A., 2008. Turbulence characteristics of flow in a spiral corrugated culvert fitted with baffles and implications for fish passage. *Ecol. Eng.* 35, 381-392.
- Noonan, M.J., Grant, J.W.A., Jackson, C.D., 2012. A quantitative assessment of fish passage efficiency. *Fish Fish.* 13, 450-464.

- Nortek AS. 2009. Vectrino velocimeter user guide. Nortek AS, Vangkroken, Norway.
- Pavlov, D.S., Lupandin A.I., Skorobogatov M.A., 2000. The effects of flow turbulence on the behaviour and distribution of fish. *J. Ichthyol.* 40(2), S232-S261.
- Peake, S., Beamish, F.W.H., McKinley, R.S., Scruton, D.A., Katopodis, C., 1997. Relating swimming performance of lake sturgeon, *Acipenser fulvescens*, to fishway design. *Can. J. Fish. Aquat. Sci.* 54: 1361-1366.
- Pon, L.B., Hinch, S.G., Cooke, S.J., Patterson, D.A., Farrell, A.P., 2009. Physiological, energetic and behavioural correlates of successful fishway passage of adult sockeye salmon *Oncorhynchus nerka* in the Seton River, British Columbia. *J. Fish Biol.* 74, 1323-1336.
- Puertas, J., Pena, L., Teijeiro, T., 2004. Experimental approach to the hydraulics of vertical slot fishways. *ASCE J. Hydraul. Eng.* 130, 10-23.
- Rajaratnam, N., 1976. *Turbulent Jets*, Amersterdam, The Netherlands.
- Rajaratnam, N., Katopodis, C., Solanki, S., 1992. New designs for vertical slot fishways. *Can. J. Civ. Eng.* 19, 402-414.
- Rajaratnam, N., Katopodis, C., Wu, S., Saburm M.A., 1997. Hydraulics of resting pools for denil fishways. *ASCE J. Hydraul. Eng.* 123 (7), 632-638.
- Rodriguez, T.T., Agydo, J.P., Mosquera, L.P., 2006. Evaluating vertical-slot fishway designs in terms of swimming capabilities. *Ecol. Eng.* 27, 37-48.

- Roscoe, D.W, Hinch, S.G., 2010. Effectiveness monitoring of fish passage facilities: historical trends, geographic patterns and future directions. *Fish Fish.* 11, 12-33.
- Schlumberger Water Services. 2011. Mini-Diver product manual. Schlumberger Water Services, Delft, The Netherlands.
- Silva, A., Katopodis, C., Santos, J., Ferreira, M., Pinheiro., 2012. Cyprinid swimming behaviour in response to turbulent flow. *Ecol. Eng.* 44, 314-328.
- Silva, A.T., Santos, J.M., Ferreira, M.T., Pinheiro, A.N., Katopodis, C., 2011. Effects of water velocity and turbulence on the behaviour of Iberian barbell (*Luciobarbus bocagei*, Steindachner 1864) in an experimental pool-type fishway. *River Res. Appl.* 27, 360-373.
- Thiem, J., Binder, T., Dawson, J., Dumont, P., Hatin, D., Katopodis, C., Zhu, D.Z., Cooke, S., 2011. Behaviour and passage success of upriver-migrating lake sturgeon *Acipenser fulvencens* in a vertical slot fishway on the Richelieu River, Quebec, Canada. *Endanger. Species Res.* 15, 1-11.
- Thiem, J.D., Binder, T.R., Dumont, P., Hatin, D., Hatry, C., Katopodis, C., Stamplecoskie, K.M., Cooke, S.J., In press. Multispecies fish passage behaviour in a vertical slot fishway on the Richelieu River, Quebec Canada. *River Res. Appl.*
- Tritico, H.M., Cotel, A.J., 2010. The effects of turbulent eddies on the stability and critical swimming speed of creek chub (*Semotilus Atromaculatus*). *J. Exp. Bio.* 213, 2284-2293.

- Webb, P.W., Cotel, A.J., 2010. Turbulence: does vorticity affect the structure and shape of body and fin propulsors?. *Integrative and comparative biology*, 50(6), 1155-1166.
- Webber, J.D., Chun, S.N., Maccoll, T.R., Mirise, L.T., Kawabata, A., Anderson, E.K., Sung Cheong, T., Kavvas, L., Mcgee Rotondo, M., Hochgraf, K.L., Churchwell, R., Cech Jr., J.J., 2007. Upstream swimming performance of adult white sturgeon: effects of partial baffles and a ramp. *Transactions of the American Fisheries Society* 136, 402–408.
- White, L.J., Harris, J.H., Keller, R.J., 2011. Movement of three non-salmonid fish species through a low-gradient vertical slot-fishway. *River Res. Appl.* 27, 499-510.
- Williams, J.G., Armstrong, G., Katopodis, C., Larinier, M., Travade, F. 2012. Thinking like a fish: a key ingredient for development of effective fish passage facilities at river obstructions. *River Res. Appl.* 28, 407–417.
- Wu, S., Rajaratnam, N., Katopodis, C., 1999. Structure of flow in vertical slot fishway. *J. Hydraul. Eng.* 125(4), 351-360.

Table 4-1 Summary of mesh properties as tested to assess the effect of mesh size on numerical modelling results.

Mesh	1	2	3
Size (m)	0.14	0.12	0.11
Nodes	171,399	271,974	352,082
Elements	927,754	1,485,274	1,932,418

Table 4-2 Summary of turning pool vortex lengths and widths for Pools 8 and 13, and Designs 1, 3 4, 6, and 7.

Design	l_v (m)	b_v (m)
	x - dir.	y - dir.
Pools 8 and 13	3.0	2.1
1	3.0	2.1
3 (centre)	1.9	1.2
3 (upstream)	1.3	4.5
3 (downstream)	1.8	1.3
4 (upstream)	0.9	2.0
4 (downstream)	1.4	2
6	3.0	2.1
7	3.2	2.5

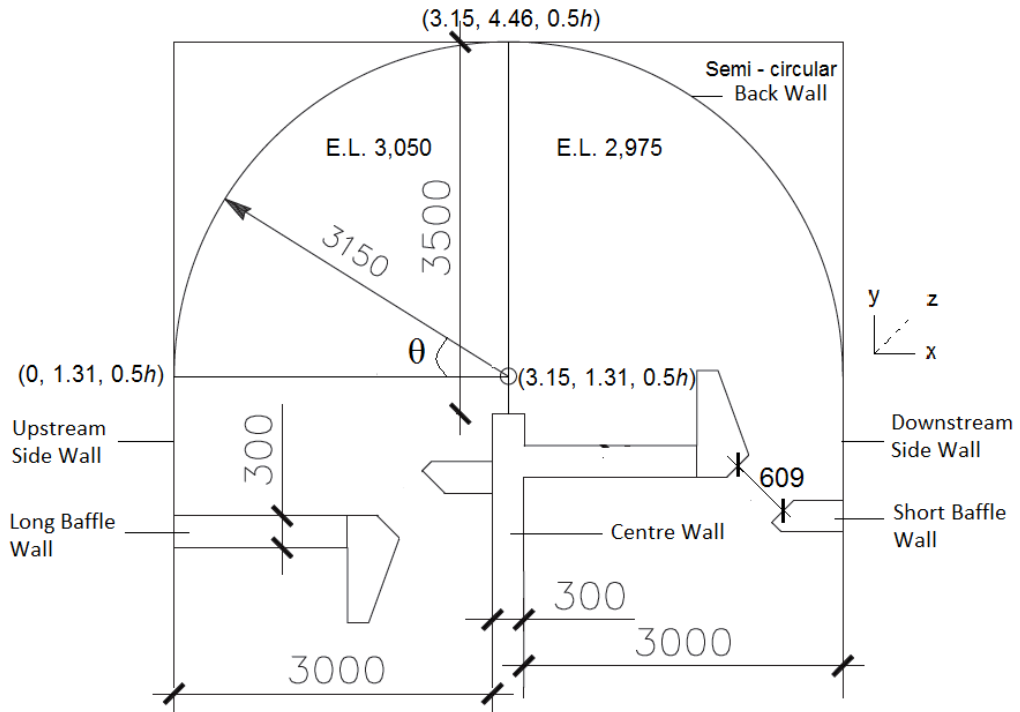


Figure 4.1 Plan view schematic diagram of a turning pool, Pool 13, in the Vianney-Legendre vertical slot fishway; this geometry is simulated using CFD modelling in Design 1.

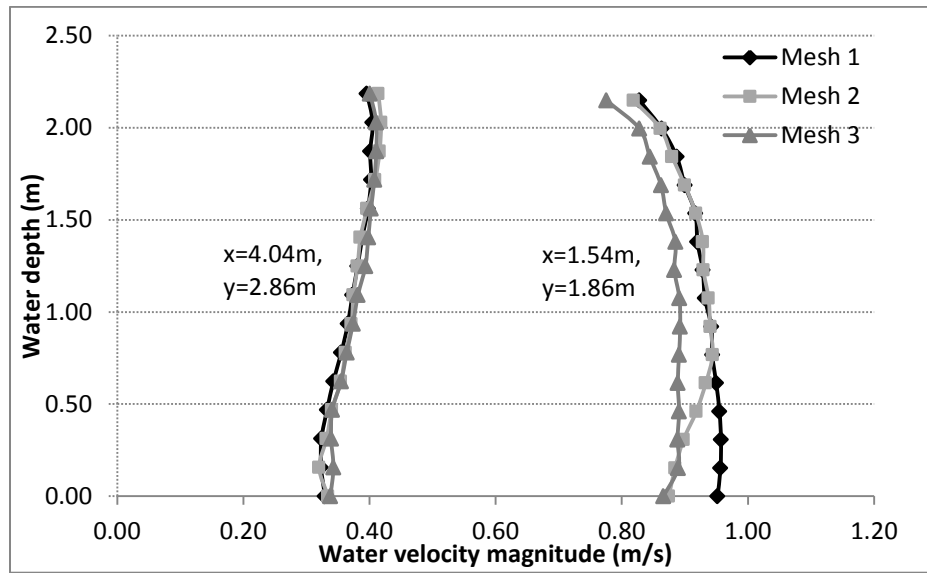


Figure 4.2 Results of the mesh independency test completed to determine the sensitivity of grid size on numerical results of Design 1.

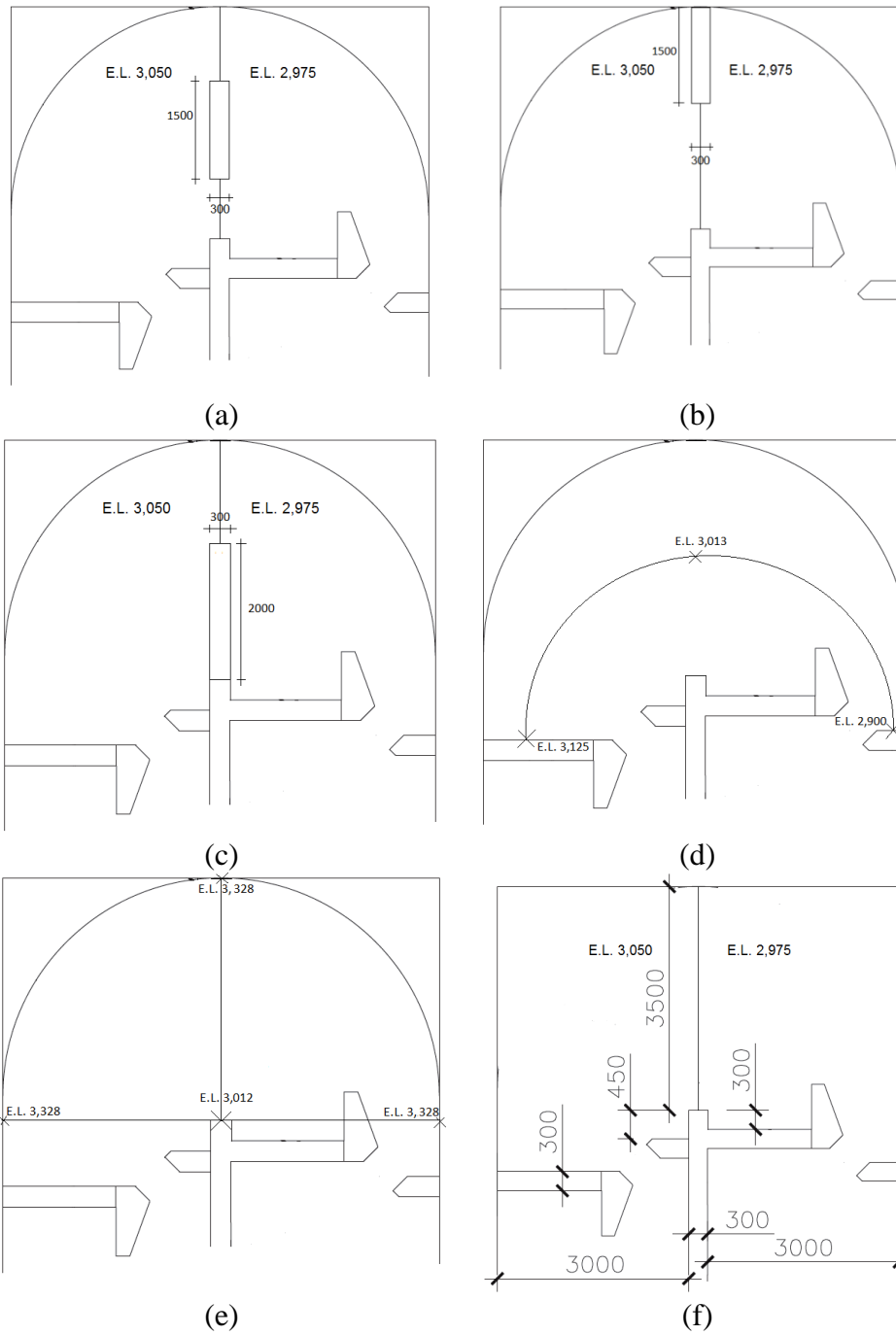


Figure 4.3 Plan view schematic diagrams of vertical slot turning pool designs:
 (a) Design 2, (b) Design 3, (c) Design 4, (d) Design 5, (e) Design 6, (f) Design 7.

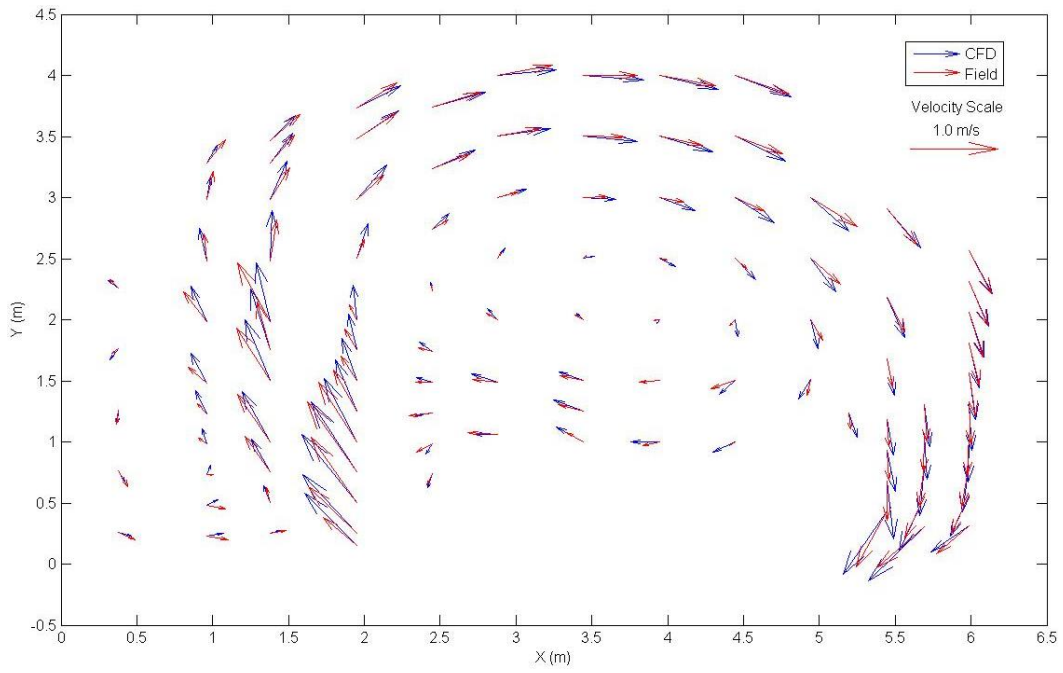


Figure 4.4 Velocity data points comparison between field measurements taken in Pool 13 of the Vianney-Legendre vertical slot fishway and results simulated in Design 1 for scenario 1 with CFD modelling.

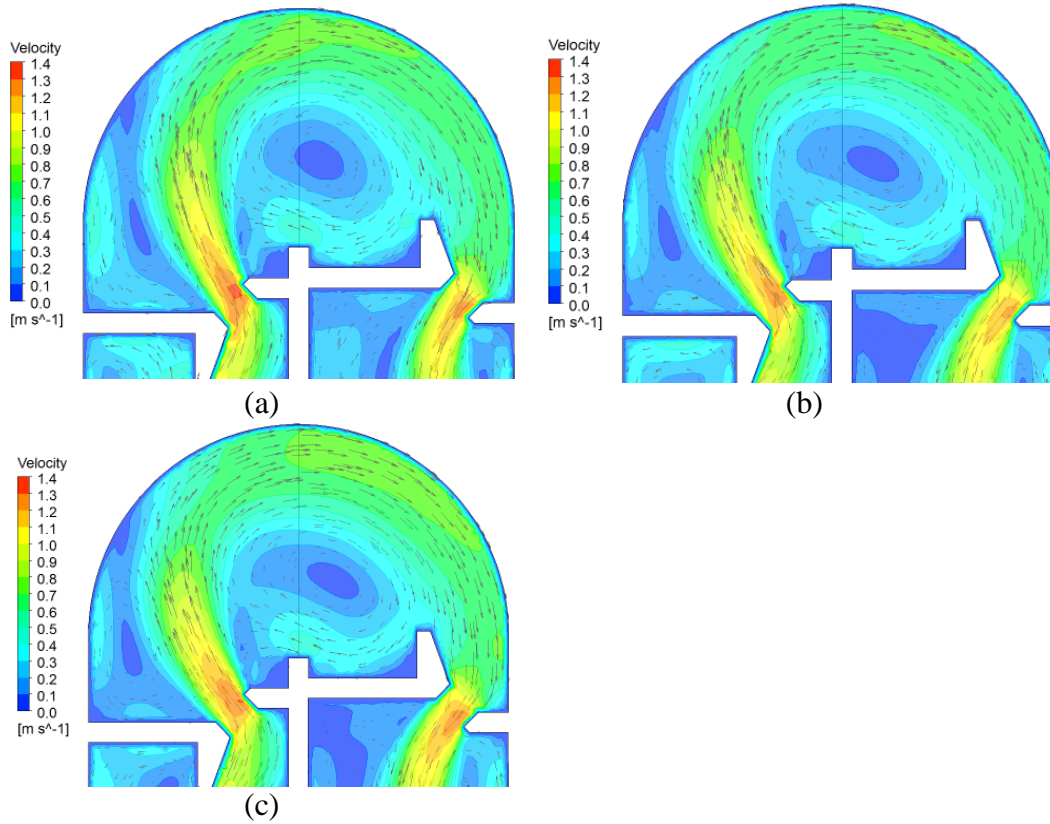


Figure 4.5 Velocity magnitudes and directions in turning pool Design 1: (a) at depth $z = 0.13h$, (b) at depth $z = 0.5h$, (c) at depth $z = 0.8h$.

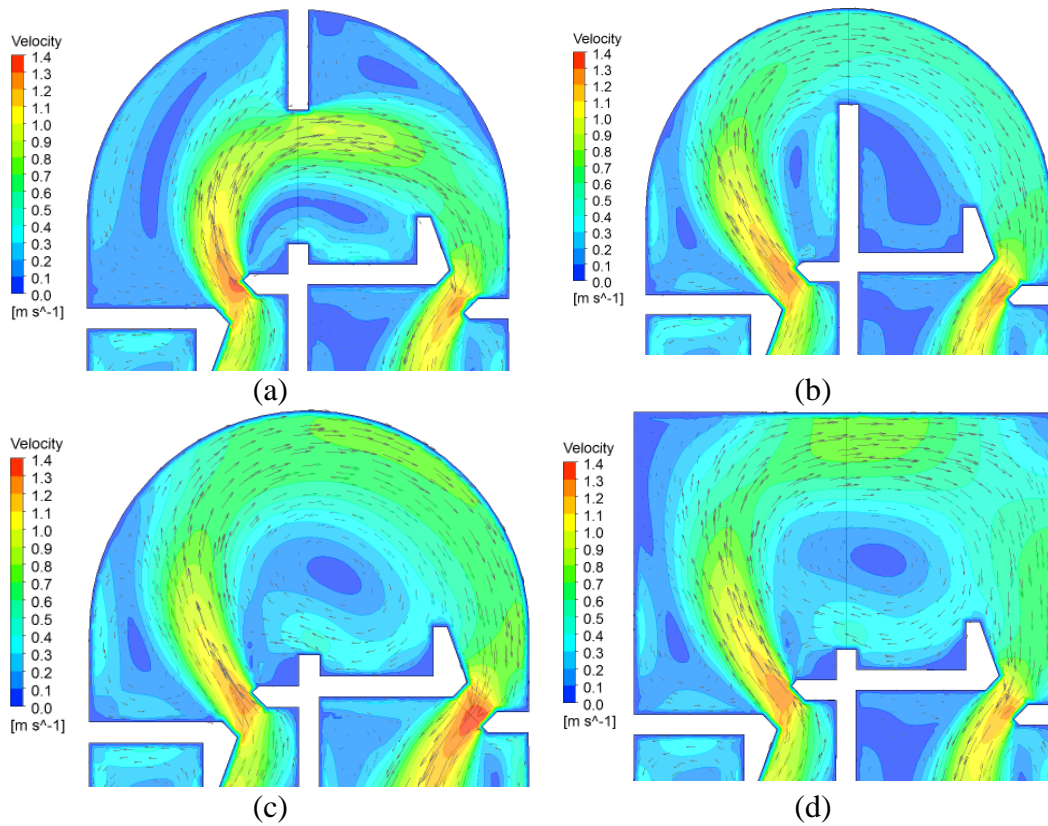
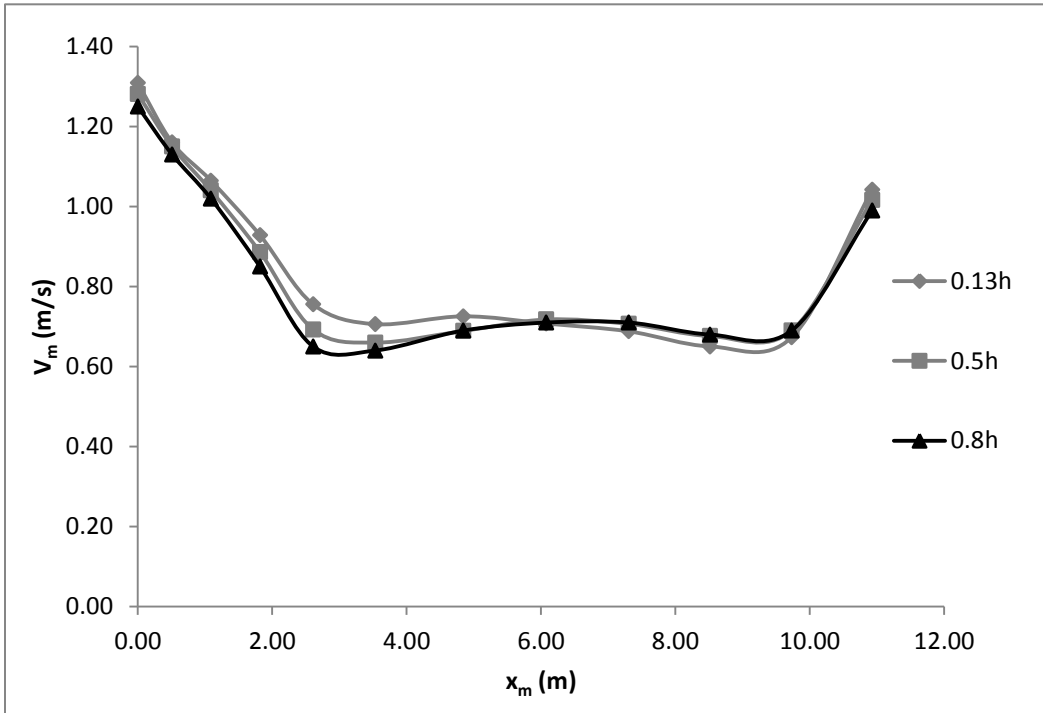
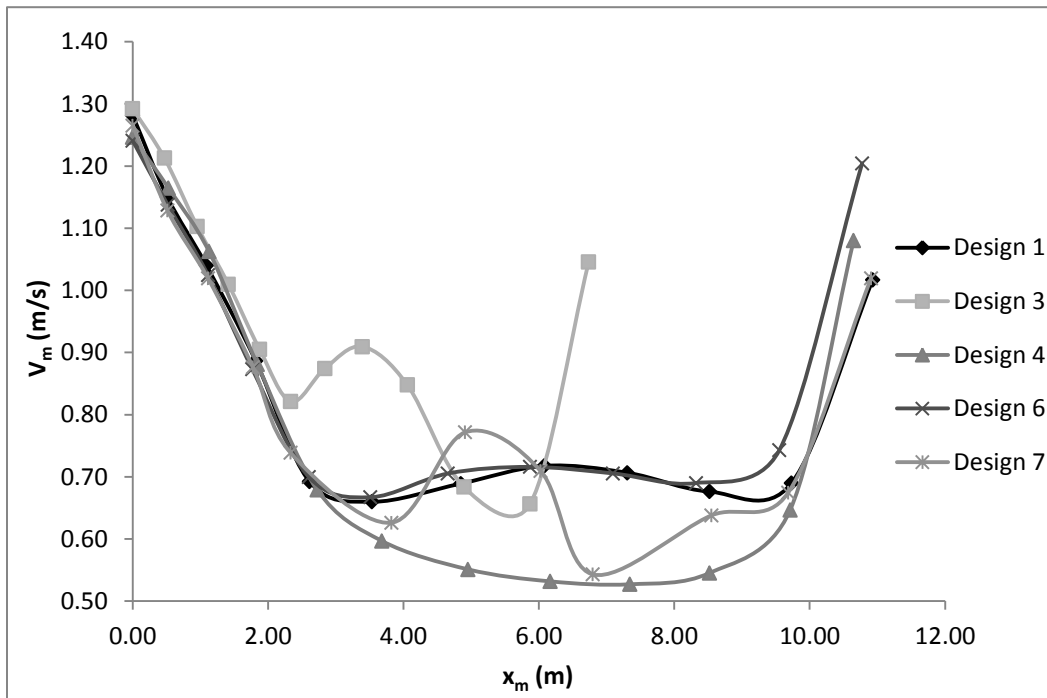


Figure 4.6 Velocity magnitudes and directions at depth $z = 0.5h$ in turning pool designs: (a) Design 3, (b) Design 4, (c) Design 6, (d) Design 7.



(a)



(b)

Figure 4.7 Variation of maximum velocity, V_m , through the turning pool; where x_m is the path of V_m from the slot entrance to the slot exit: (a) Design 1 at depths of $z = 0.13h$, $z = 0.5h$, and $z = 0.8h$; (b) Designs 3, 4, 6, and 7 at depth of $z = 0.5h$.

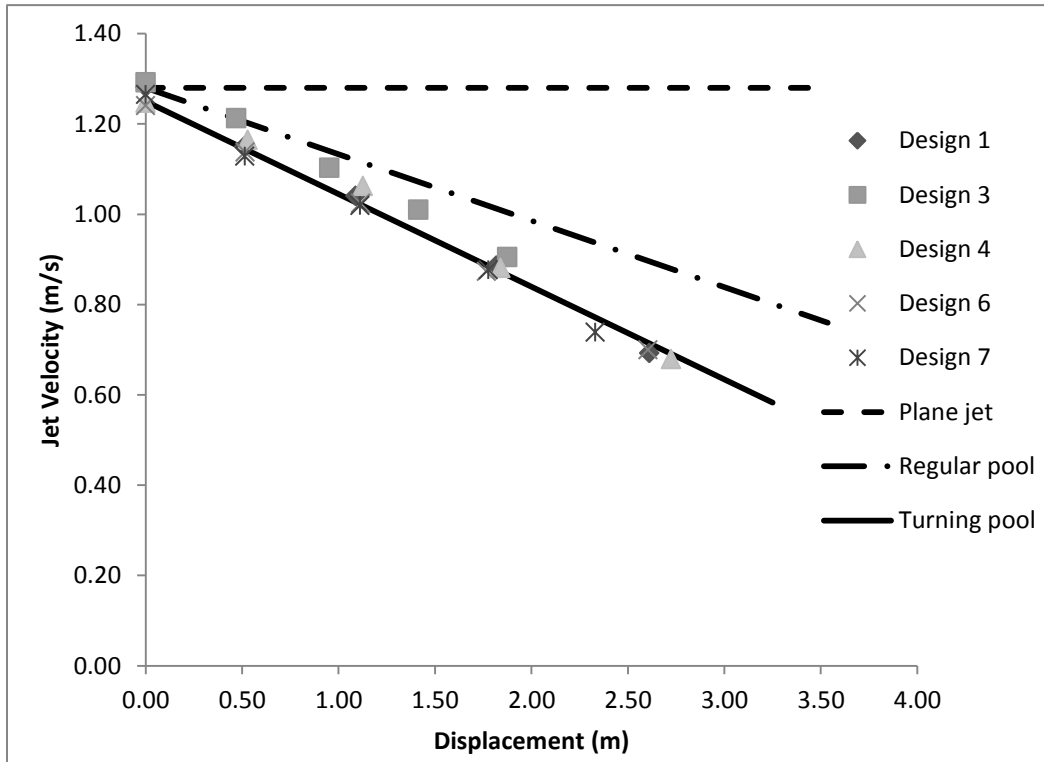
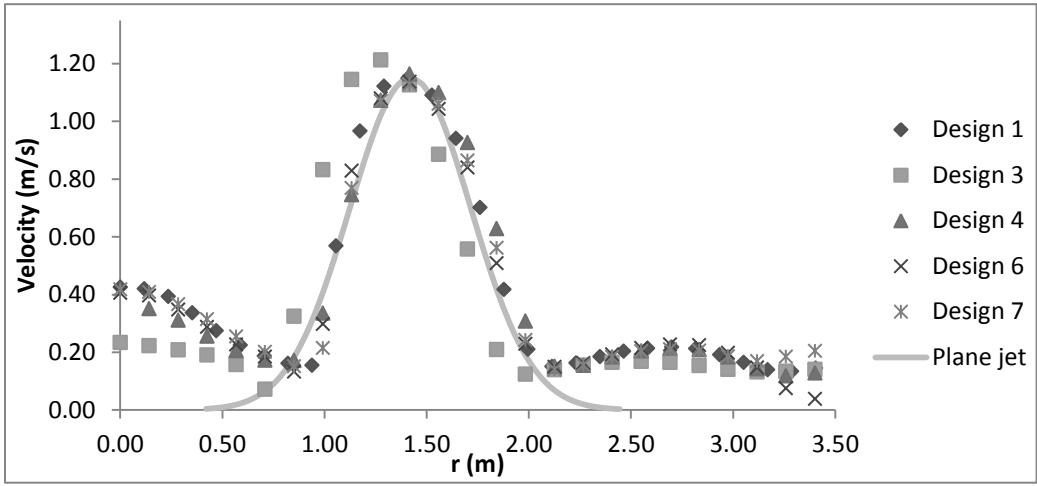
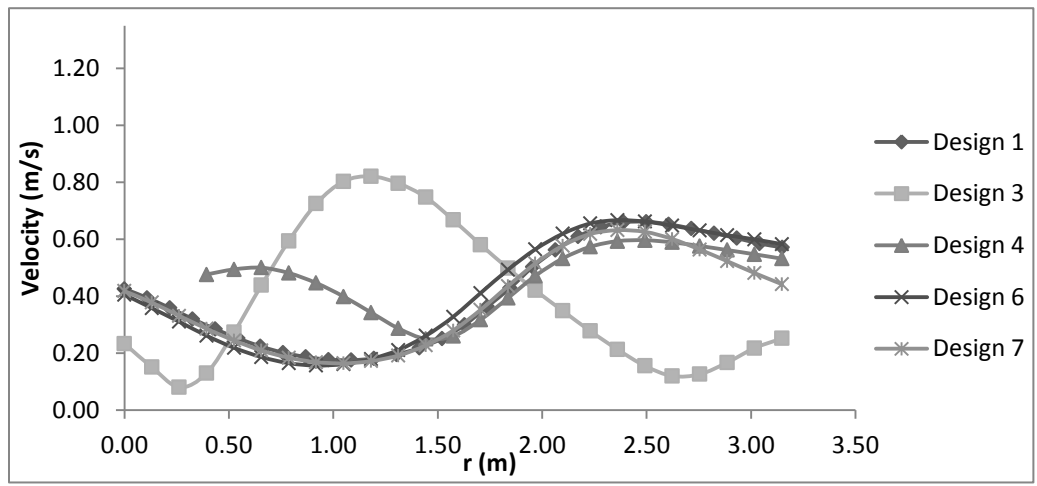


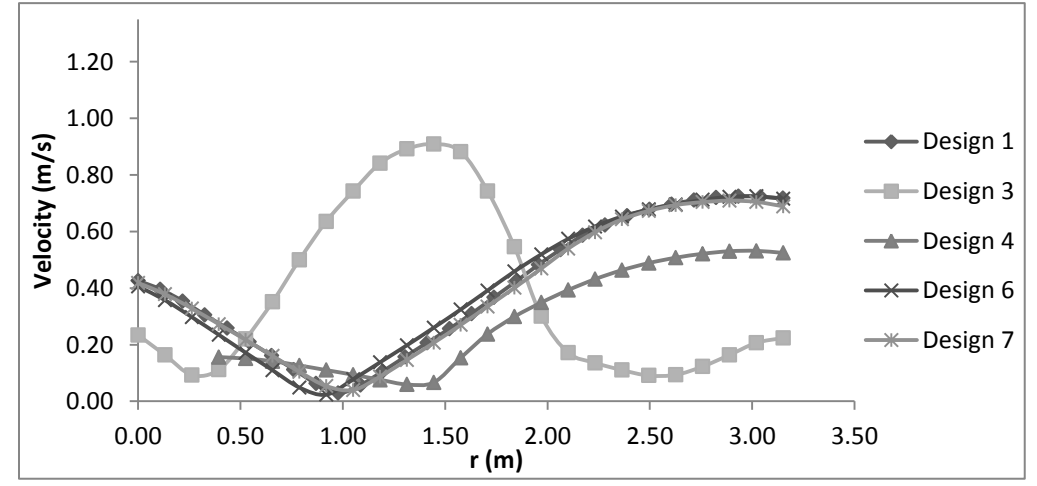
Figure 4.8 Maximum velocity, V_m , decay comparison of a single slot pool, a plane jet, and turning pool Designs 1, 3, 4, 6, and 7 at a depth of $z = 0.5h$.



(a)



(b)



(c)

Figure 4.9 Radial velocity distributions of Designs 1, 3, 4, 6, and 7 at $z = 0.5h$: (a) $\theta = -27^\circ$, (b) $\theta = 67.5^\circ$, (c) $\theta = 112.5^\circ$.

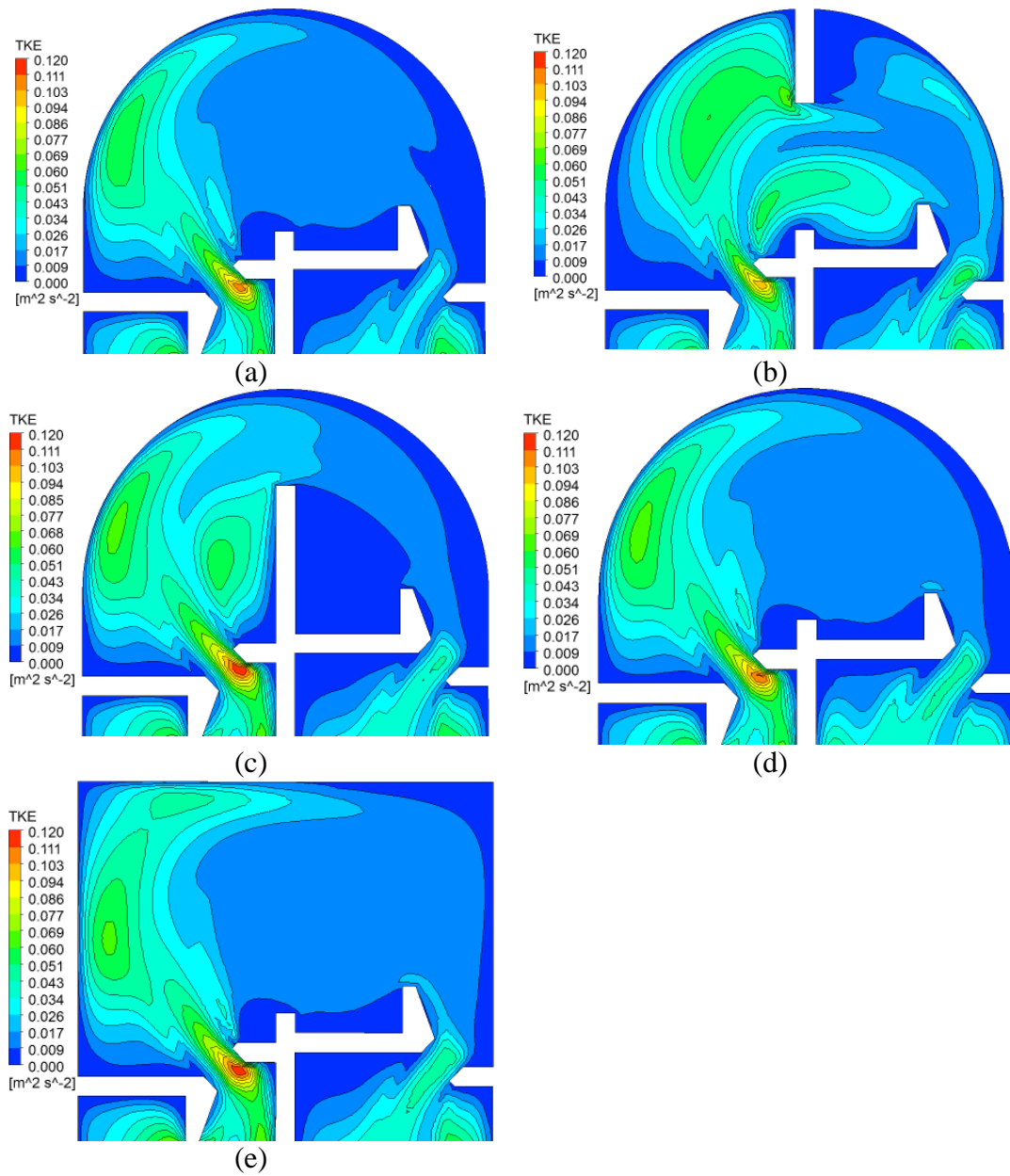


Figure 4.10 Turbulent kinetic energy levels at depth $z = 0.5h$ in turning pool designs: (a) Design 1, (b) Design 3, (c) Design 4, (d) Design 6, (e) Design 7.

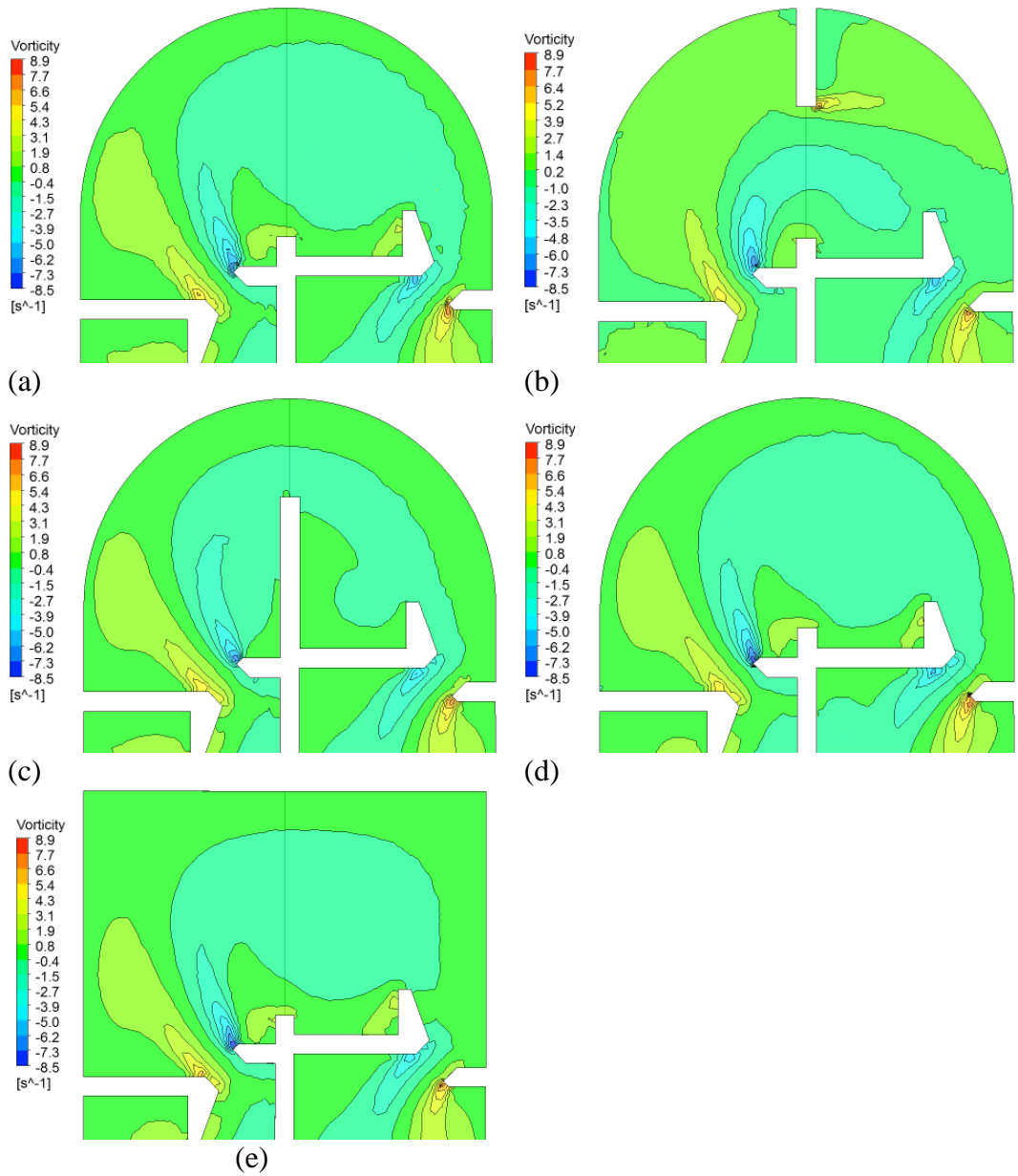


Figure 4.11 Vorticity levels at depth $z = 0.5h$ in turning pool designs: (a) Design 1, (b) Design 3, (c) Design 4, (d) Design 6, (e) Design 7.

CHAPTER 5

Conclusions and Recommendations

5.1 Overall Conclusions

This is a hydraulics case study of the Vianney-Legendre vertical slot fishway in Quebec, Canada. Included are a detailed account of the study site and fishway, an overall assessment of hydraulics gained through field measurements, and a numerical model study assessing the flow characteristics of turning pools.

--The site fishway was found to have non-uniform flow, characterized by depth increasing towards the downstream end of the fishway. As a result, the change in water levels between adjacent pools is highest at the upstream end and lowest at the downstream end of the fishway. This produces higher maximum velocities at the upstream end of the fishway.

The site fishway's regular pools dimensions are shorter and narrower than recommended. This results in less jet velocity decay, causing to higher velocities through the pool. Despite the regular pools not following the recommended design guidelines the fishway still passes multiple species of fish.

The design of turning pools at the site fishway is closely linked to regular pools. Turning pool widths are equal to the total width of the attaching two regular pools and the length is equal to that of regular pools. The hydraulics in a turning pool with a semi-circular back wall are not significantly different than an equivalent pool with a square back wall. Consequently, a square back wall can

serve as an alternative design to the semi-circular back wall used at the site fishway.

The turning pools hydraulics are highlighted by a large recirculation area, or vortex, in the centre of the pool, which have been shown to negatively impact the swimming capabilities fish. Additionally, the hydraulics in the site fishway's turning pools do not provide any areas suitable to act as resting spaces for ascending fish. Adding a long baffle wall, extending from the inside centre wall into the pool, reduced the size of the large vortex by dividing it into two smaller flow recirculation areas. The downstream recirculation area is characterized by relatively low velocities and appears to be hydraulically suitable to act as a resting zone for ascending fish.

It is thought that this fishway was initially designed to follow the recommended regular pool design guidelines, having a slot width of approximately 0.35 m. However, the slot width may have been increased to its constructed width as an afterthought when it was determined that adult lake sturgeons would likely have difficulty ascending through a 0.35 m slot because of their large body sizes. The author is of this opinion because recommended regular pool design dimensions were established more than 10 years prior to the construction of this fishway. The other fish species using this fishway are generally much smaller than adult lake sturgeons and would not be negatively affected by a smaller slot width.

It is hoped that results emanating from this study can be used alongside concurrent ichthyology studies to assist engineers and biologists to evaluate the

site fishway's performance in terms of hydraulics and fish passage. This study may also serve as reference of a case study on the hydraulics of a successful multi-species passing fishway. The flow characteristics presented on turning pools provide a hydraulic understanding and hopefully will act as a foundation from which turning pool hydraulics and design can be developed.

5.2 Recommendations for Future Study

To date little study has focused on the hydraulics and fish recruitment of fishway attraction flow. As an essential aspect of passage is fish recruitment, attraction flows study is needed to maximize recruitment of fish to the downstream entrance of fishways. This area of fishways research requires advancement in knowledge.

Results of this study can serve as a foundation for the development of turning pool design guidelines. Further study is needed in many areas in to fully understand the hydraulics and fish passage performance of turning pools. Testing and evaluation of a variety of lengths will help determine the length to slot width ratio that will maximize jet velocity decay in turning pools. Field testing is required to complete analysis on the effects of adding a baffle wall to the pool centre, as per Design 4, on both the hydraulics and fish passage rates within turning pools. Various baffle wall lengths should be investigated to develop a ratio of baffle wall length to turning pool length which produces the hydraulics most suitable to fish passage. More field study of fish behaviour and passage rates through turning pools is needed to improve the knowledge of how fish perform in the hydraulic conditions of turning pools. This is a very important

aspect to increasing our knowledge of turning pools and advancing the science of their design.